Modeling Phosphorus Cycling in a Seasonally Stratified Reservoir (Fanshawe Reservoir, Ontario, Canada)

by

Shengde Yu

A thesis

presented to the University of Waterloo

in fulfillment of the

thesis requirements for the degree of

Master of Science

in

Earth Sciences (Water)

Waterloo, Ontario, Canada, 2020

Author's Declaration

I hereby declare that I am the sole author of this thesis. This is a true copy of the thesis, including any required final revisions, as accepted by examiners.

I understand that my thesis may be made electronically available to the public.

Abstract

Human activities, such as mining, sewage discharge, fertilizer usage and dam construction for electricity and flood controll, have significantly disturbed the biogeochemical cycling of nutrients, such as carbon, phosphorus, and nitrogen, in atmospheric, terrestrial, and aquatic systems. Globally, negative effects of the excess inputs of nutrients have been observed in freshwater and saline surface water environments. Phosphorus (P) is an essential nutrient for primary production, and due to intensive anthropogenic activities, including rapid agricultural intensification and urban development, excess P has been loaded into the Thames River Watershed (TRW), Ontario, Canada for around 45 years. Water quality in the TRW has been significantly affected by inputs of P and other nutrients. These eutrophic waters could have significant and chronic negative effects on the downstream and nearby aquatic environment, such as Lake St. Clair and Lake Erie. This thesis focuses on Fanshawe Reservoir, located in the Northern TRW, where Fanshawe Dam has been built to control potential flood events that may damage the City of London. However, excess nutrients could accumulate in the reservoir sediments and slowly release over a long period, posing significant difficulties for water quality management. During summertime, blue-green algae and elevated bacterial concentrations have been frequently observed by the Upper Thames River Conservation Authority (UTRCA). However, the existing field data cannot explain the seasonal variation of the algal blooms or the long-term scale interaction between the external loading of P and internal loading of P. To provide a computational framework to analyse existing field data and relate P availability in Fanshawe Reservoir to external and internal P loading, I developed a two-dimensional model for Fanshawe Reservoir using the CE-QUAL-W2 software. The model combines hydrodynamic, water quality, and sediment diagenesis modules. The simulation results imply a major role of internal P loading during the summer when the reservoir stratifies. Retention of P mainly occurs during wintertime, while the reservoir is a source of P during summertime. In a scenario where external P input to the reservoir is instantaneously reduced by 40%, the annual downstream export of P from the reservoir only decreases by 22%, because of continued internal P loading from the sediments. Due to the legacy P stored in the sediments, it would take on the order of 22 years for P export from Fanshawe Reservoir to drop to 36.5% of its current value. In another biomass scenario, the sediment P loading has 40.1% larger effects on algal growth than the external loading of P during summertime. Furthermore, to provide feasible and fast water

quality modeling applications, a back propagation artificial neural network (BP-ANN) model was successful developed and calibrated for the future modeling works.

Keywords: Phosphorus cycling, retention efficiency, water quality and sediment model

Acknowledgements

Firstly, I would love to express my sincere gratitude to my supervisor Dr. Philippe Van Cappellen for teaching me by his invaluable and expert modeling skills, and comprehensive scientific viewpoints. He always shares his experiences and knowledge to me, and his continued support and encouragements make me feel like home during my study and growth in our Ecohydrology Research Group. Thank you!

I am also grateful to my other committee members Dr. Chris Parsons and Dr. Nandita Basu for their continued support and their detailed advice during my research work. They always welcome me to ask them some questions. Dr. Parsons always provides professional nutrients knowledge, perspectives and insightful comments to me.

I am also indebted to Amanda Niederkorn and Nady Kao and UTRCA's colleagues who provided lots of measurement data of Fanshawe Reservoir and laboratory efforts for me. Thank your Amanda and Nady, you always

I would like to thank Tamara Van Staden, thank you for sharing your research experiences, writing skills and language skills with me. Thank you for your support during my research writing. You always quickly response my questions in details and thank you so much for your patience and encouragement.

Thanks to Dr. Shuhuan Li, Tatjana, and Erin for their great assistant and guidance during my Master study. In addition, I would like to thank Zahra Akbarzadeh, Mahyar Shafii, and all my friends in the Ecohydrology Family group for sharing their own research and study experiences.

Thanks to Bhaleka and Linden, your support during my master study are selfless. Bhaleka, you always provide inspiring support to our group. Thank you for saving my lost backpack! Linden, thank you for your detailed support in my writing skills and language skills in my master life.

As an international student, I feel like home in our Ecohydrology Research Group. We are both friend and mentor. We support each other and improve ourselves together. Thanks for our excellent group providing pleasant research environment for students. Thanks to Philippe let me join our group in that beautiful fall term!

In the last, I would like to thank my parents (Guojun Yu, Meili Wang) for their unconditional support during my undergraduate and graduate study and my whole life. Your moral quality and kindness always accompany with me.

Table of Contents

List of Figures

List of Tables

List of Abbreviations

ANN	Artificial Neural Network
BP-ANN	Back Propagation Artificial Neural Network
C	Calibration Values
CBOD	Carbonaceous Biochemical Oxygen Demand
cHABs	Harmful Cyanobacterial Algal Blooms
D	Default Values
DO	Dissolved Oxygen
DOM	Dissolved Organic Matter
DRP	Dissolved Reactive Phosphorus
DNRP	Dissolved Non-reactive Phosphorus
F	Fitting Values
LIO	Land Information Ontario
N	Nitrogen
L	Literature Values
LDOM	Labile Dissolved Organic Matter
LPOM	Labile Particulate Organic Matter
P	Phosphorus
PRP	Particulate Reactive Phosphorus
PNRP	Particulate Non-Reactive Phosphorus
QGIS	Quantum Geographic Information System
RDOM	Refractory Dissolved Organic Matter
RPOM	Refractory Particulate Organic Matter
RMSE	Root Mean Square Error
NW	Northwest
TP	Total Phosphorus
TRW	Thames River Watershed
UTRCA	Upper Thames River Conservation Authority
2-D model	Two-dimensional model

Chapter 1 General Introduction

1.1 Summary of Thesis Structure

This thesis has 5 chapters with supporting materials in the appendix. The first chapter is the introduction of the research issues, research background, and research objectives. Chapter 2 gives detailed information about the research area, which was studied in Chapter 3 and Chapter 4. In Chapter 2, the CE-QUAL-W2 modeling governing equations, a schematic of the modeling equations and items are discussed and listed for future reference. A simple introduction of the BP-ANN model is also provided in Chapter 2. In Chapter 3, CE-QUAL-W2 modeling method, modeling results and scenarios were demonstrated and summarized. In Chapter 4, BP-ANN modeling step, modeling results were discussed. Chapter 4 is the first step for the development of the CE-QUAL-W2 model and BP-ANN model. Chapter 5 was the conclusion and perspective chapter. Detailed assumptions, research findings, and research perspectives were discussed in this chapter.

1.2 The Biogeochemical Cycling of Phosphorus (P)

The cycling of P has four major components. Firstly, in the terrestrial systems, phosphorus-bearing rocks may be weathered during the tectonic uplift event and other exposure conditions (Figure 1-1). In addition, the physical erosion, chemical weathering and biological metabolism could generate inorganic P and organic P to the sediment, groundwater, surface water systems (Figure 1-1). The subsurface (groundwater) and surface (riverine, watershed and estuaries) systems then transport P into lakes and oceans (Figure 1-1). Finally, P sedimentation buries particulate, organic and inorganic P into sediments and this sediment P may be chronic released into aquatic systems under different conditions at the sediment water interface. For example, P may be released from the sediment of aquatic systems under reducing environment (Filippelli, 2008; Jarvie et al., 2013; Ruttenberg, 2014).

In lake and river systems, P and its chemical compounds is the dominant nutrient that causes eutrophication (Schindler, 1974; Schindler et al., 2008; Smith and Schindler, 2009). The accumulation of P in waterbody sediments is an important source that related to the retention efficiency of P and the legacy of P. According to Maavara et al. (2015), river damming plays an important role in the retention of global P. The global modeling results in their study illustrated that nearly 17% of the global river loading of total phosphorus could be reserved in dam reservoir until 2030. Although dam reservoirs could be P sink around the world, the retention capacity of

those reservoirs is not clearly, and intensive input of P may cause more algae blooms in the downstream area. Meanwhile, the legacy of P in reservoir sediments may become a severe challenge for the effectiveness of management strategies. For instance, the reduction of external loading of P may not have timely reduction of P in the reservoirs and their downstream area.

In the oceanic systems, the cycling of P is controlled by floating marine algae which influence the cycling of carbon and nitrogen. In general, dissolved phosphate is an important limiting nutrient for biological productivity in marine systems and the concentration of dissolved phosphate is highly related to the photosynthetic organisms and water age (Filippelli, 2008; Ruttenberg, 2014). Ocean surface water typically has a very low concentration of dissolved phosphate because the phytoplankton use up the P as they grow (Figure 1-2). P concentration also increases with the water age. For example, Atlantic Ocean has the youngest water and has a P concentration nearly 40% smaller than the Indian and Pacific Ocean (Filippelli, 2008; Paytan and McLaughlin, 2007; Ruttenberg, 2014).

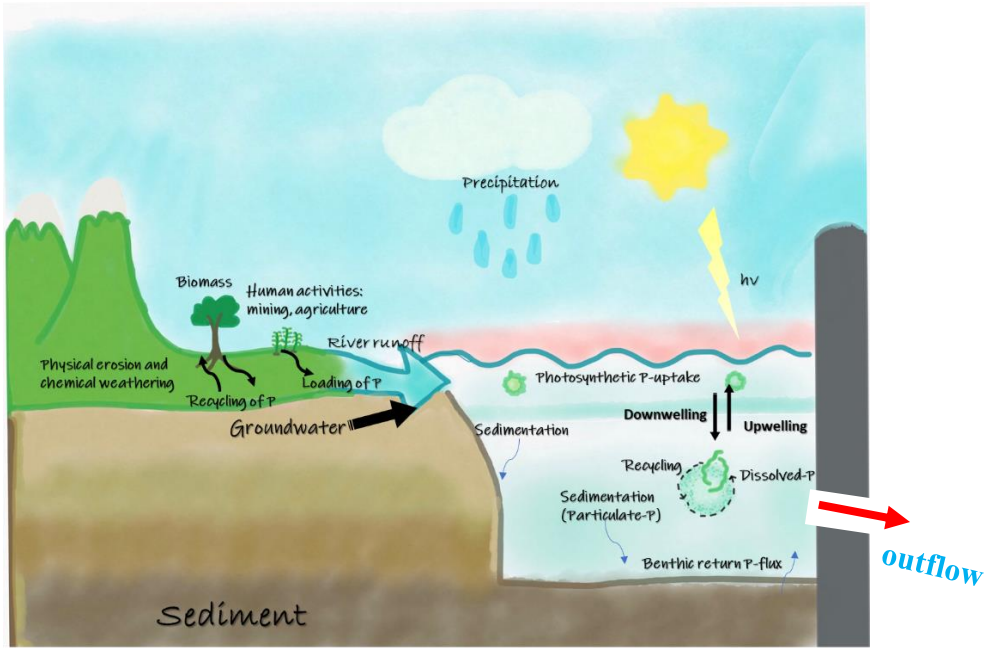

Figure 1-1. Major processes of P cycle in the terrestrial and aquatic system. The red area represents the surface heat exchange. Modified from Ruttenberg, (2014) and Van Cappellen and Maavara, (2016).

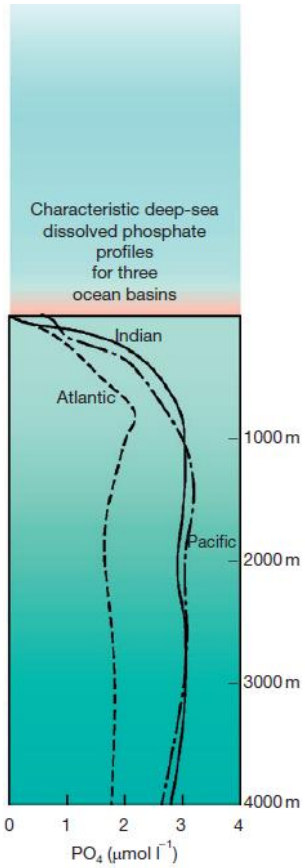

Figure 1-2. Dissolved phosphate concentrations in three ocean basins (After Ruttenberg, 2014).

1.3 Global Human Perturbation and P cycling

The natural P cycle is assumed to be at steady state during the natural physical and chemical cycling, however, human activities have significantly disturbed the natural biogeochemical cycling of P (Bennett et al., 2001; Elser and Bennett, 2011). Human perturbations in the P cycle include lots of ways, such as phosphate mineral extraction, food consumption and sewage production, fertilizer application and livestock production (Bennett et al., 2001; Filippelli, 2002, 2008; Maavara et al., 2015; Yuan et al., 2018).

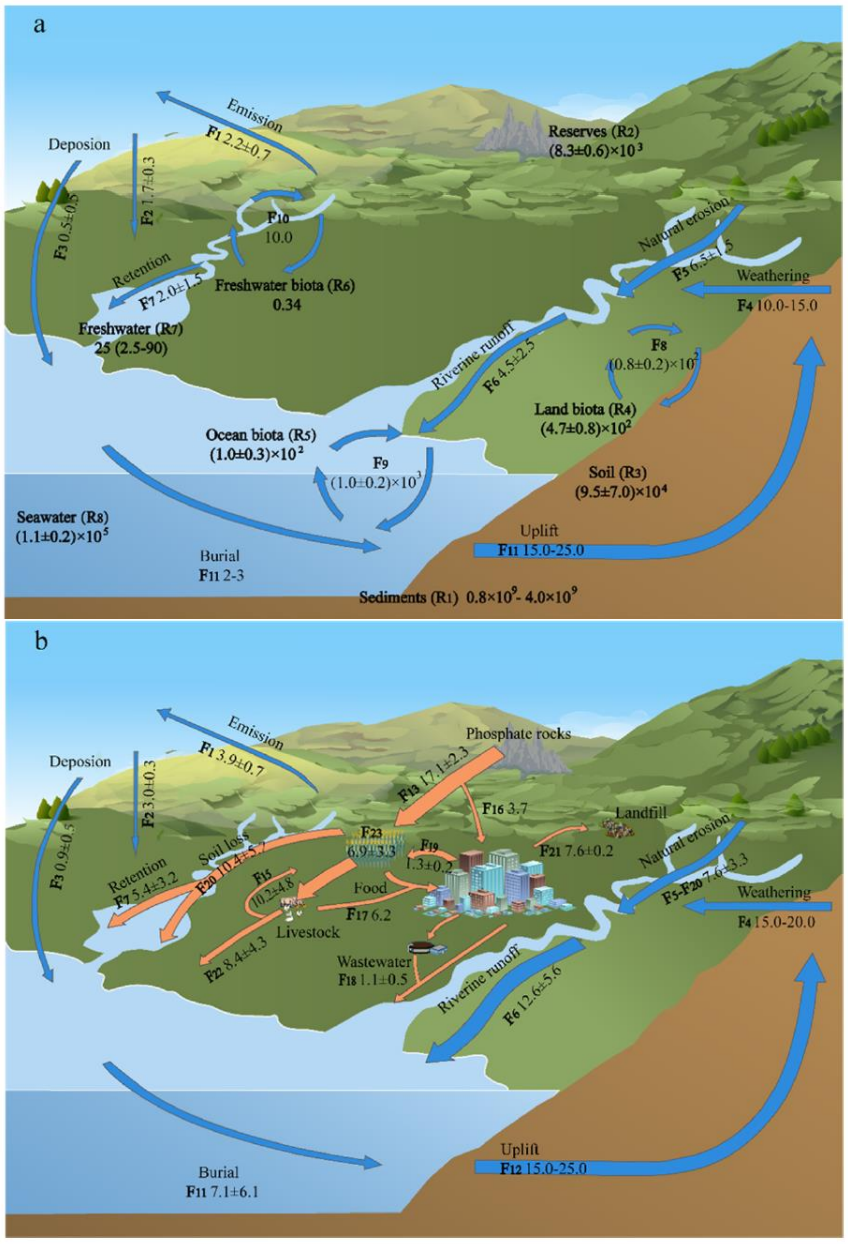

Figure 1-3. Schematic graphs of the global P cycling processes with the stocks and fluxes of P for a) the steady state of global P in the past and b) the global P after human perturbations. (The blue arrows represent P fluxes in natural land and ocean systems and the orange arrows represent P fluxes that created by human activities. The bold black texts indicate the fluxes between different reservoirs. The units of P fluxes and stocks are Tg P yr^{-1} and Tg P). Modified from Yuan et al., (2018).

Rock extraction is the primary source of P and a total of 1.1x 102 Tg P in phosphate minerals has been mined since P production technology was created and applied in the UK in the 1840s (Ashley et al., 2011). Due to the sharp increase of population size, the total P consumption that is related to human activities has tripled since the 1960s (Cordell et al., 2009) (9.9 Tg P yr-1, F_{16} and F_{17} in

Figure 1-3b), and the sewage production is around 1.3 ± 0.2 Tg P yr-1 (F_{19} in Figure 1-3b). In addition, P fertilizer use for crops has increased from 2.0 Tg P yr-1 to 17.1± 2.3 Tg P yr-1 since the 1940s, whereas the crop P uptake has only increased to 12.3 ± 0.3 Tg P yr-1 (F_{13} and F_{14} in Figure 1-3b) (Yuan et al., 2018). Livestock manure production and fertilizer application exceed crop P needs, and this excess P may prove difficult to manage, eventually becoming non-point sources of P pollution(Ashley et al., 2011; Cordell et al., 2009). The F_{22} flux in Figure 1-3 showed the livestock annual P flux to aquatic systems is about 8.3 ± 4.3 Tg P yr-1 (Yuan et al., 2018). Most agricultural P and urban P are stored in and carried by river watersheds, which become significant sources of nutrients for lakes and oceans. Although an increasing number of countries have begun regulating P consumption through their policies, human activities still have significant negative effects on global P cycle. Redundant P has been discharged and stored in aquatic systems and now pose a threat to water quality. Previous studies have clearly demonstrated that river damming in watersheds could retain nutrients in the reservoirs, which may subsequently pose a water quality threat to downstream aquatic systems. For example, the amount of nutrients retained in the dammed reservoirs may increase in the decades to come and may become a chronic nutrient source pool for future release events (Jarvie et al., 2013; Maavara et al., 2015; Maavara et al., 2020).

1.4 Phosphorus Cycling and Pollution in Watersheds and Lakes

1.4.1 Thermal Stratification in Lakes and Reservoirs

Thermal Stratification significantly influences water quality through modifying the dissolved oxygen and vertical water temperature, and informs water management strategies in freshwater systems, such as dammed reservoirs and lakes (Elçi, 2008; Kirillin and Shatwell, 2016; Nowlin et al., 2004; Søndergaard et al., 2003). Different factors have several different effects on the thermal stratification in the waterbody. For instance, the depth and shape of reservoirs and lakes have important effects on the thermal stratifications; Wind-induced currents and air temperature are major factors that may alter the stratification in the shallow lakes and reservoirs (Elçi, 2008; Kirillin and Shatwell, 2016). The density of the water is majorly affected by temperature and cold water is denser than warm water, therefore, water stratification mainly occurs in summer and winter (Figure 1-4). Stratification influences water quality because it affects nutrient cycling, and nutrient retention or release in the bottom sediments of the waterbodies in freshwater systems (Elçi, 2008; Kirillin and Shatwell, 2016; Nowlin et al., 2004). Due to climate change and human

modification of the inflow and outflow in reservoirs, the duration of the stratification in reservoirs and the distribution of the substances could vary year to year (Elçi, 2008; Kirillin and Shatwell, 2016). Thermal stratification may not happen in some reservoirs and lakes due to the depth, shape (such as surface area) and other environmental conditions(Gorham & Boyce, 1989; Kirillin & Shatwell, 2016).

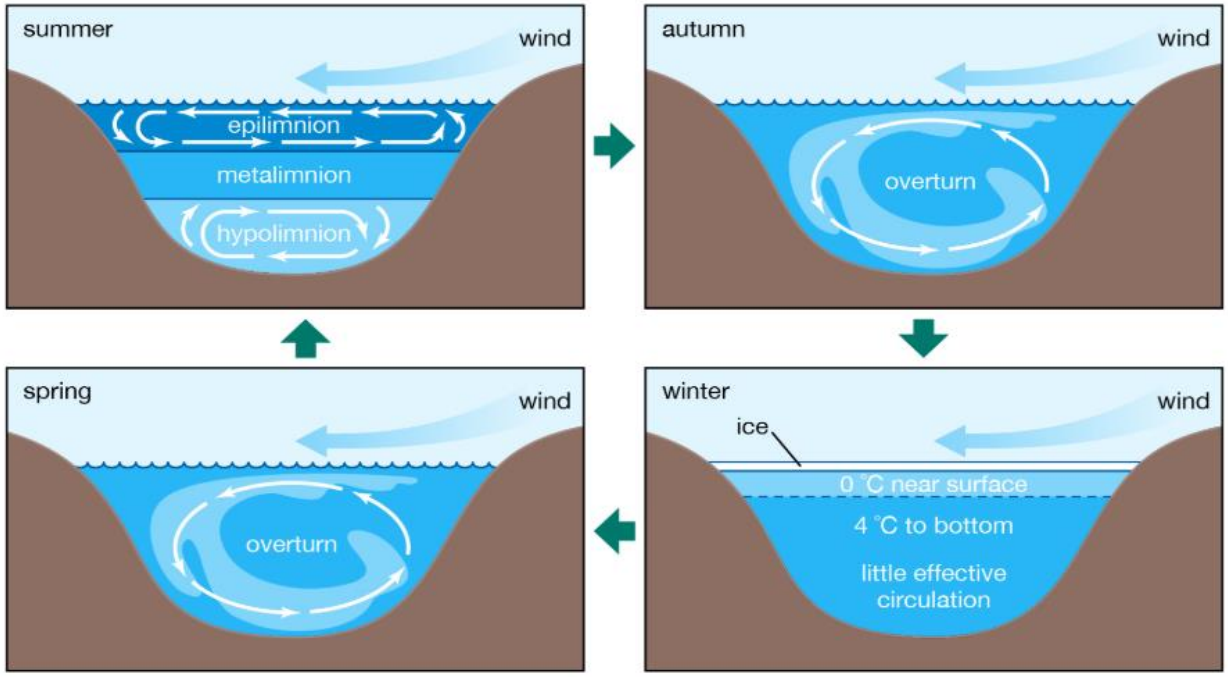

Figure 1-4. General schematic of thermal stratification of lakes (Britannica.com).

In the current study, Fanshawe Reservoir is a shallow reservoir in southern Ontario which has a maximum depth of 12.1m (Nürnberg and Lazerte, 2005). In shallow reservoirs, water stratification is very sensitive to wind speed and wind direction, which can easily mix water and alter the water temperature (Kirillin and Shatwell, 2016). However, pervious water quality studies and observation data only estimated the sediment releasing in summer season through a mass balance model, and did not fully illustrate the effects of sediments on P retention or release processes in shallow stratified reservoirs at different season (Nürnberg and Lazerte, 2015). There are multiple factors that influence external and internal P loading in dammed reservoirs, and it is still not fully clear which is important for future watershed management.

1.4.2 Phosphorus Cycling and Pollutions

Eutrophication refers to the algal blooms and anoxic events caused by excess inputs of nutrients in aquatic systems (Smith and Schindler, 2009). Understanding the P cycle in watersheds and

lakes plays an important role for informing the water quality improvements in our aquatic systems (Correll, 1998; Filippelli, 2008; Goyette et al., 2018; Maavara et al., 2015; Ruttenberg, 2014). In general, the anthropogenic sources of nutrients can be divided into two parts. The first source is the regulated point sources which are related to the municipal and industrial inputs that could be recorded. The second source is the non-point sources which are important and are complex to observe and manage. For example, intensive agricultural areas are very common primary non-point sources (Carpenter, 2005). A lot of evidence indicates that these inputs of P can be accumulated in aquatic systems, such as rivers, lakes over a long period(Carpenter et al., 1998; Carpenter, 2005; Jarvie et al., 2012, 2013; L. H. Kim et al., 2003; Maavara et al., 2015; A. Sharpley et al., 2013). In general, particulate P could occur as P adsorbed to suspended solids, and P could be trapped by solid oxyhydroxides under oxidizing environment and P could be released from sediments into the water under the reducing conditions (Katsev et al., 2006; Orihel et al., 2017; Ruttenberg, 2014). Previous studies have demonstrated the estimated time scale for the retention P in different water pools (Figure 1-5). The chronic release of P refers to the impacts of "legacy P", which may cause delays in reaching the water quality management goals (Jarvie et al., 2012; Jarvie et al., 2013; Meals et al., 2010; Sharpley et al., 2013).

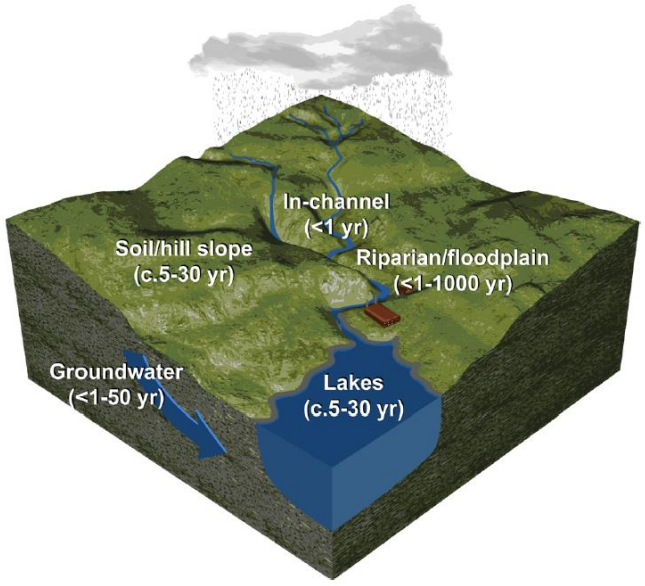

Figure 1-5. Residence time of P retention and recycling in different reservoirs (Jarvie et al., 2013).

The main reason of persistence of the legacy P is that watersheds and their dammed reservoirs retain nutrients in the water-sediment systems (Goyette et al., 2018; Maavara et al., 2015; Powers

et al., 2016). P retention can create a buffer for the excess nutrient transport, initially delaying its movement in aquatic systems (Powers et al., 2016). However, the threshold of this buffer in different watersheds is variable, complex and vulnerable to change. If the P retention threshold value in watersheds is reached and excess P is continually inputted to the aquatic systems, the P pollution could be accelerated, and P sinks could become P sources, and these sources could persist for decades (Goyette et al., 2018; Jarvie et al., 2012; Jarvie et al., 2013; Powers et al., 2016). One previous study illustrated that the threshold of P retention in 23 watersheds in North America is very low and unreliable. The threshold value is between 0.03-8.7 t P km^{-2} (Goyette et al., 2018), a small value when compared with the inputs P by human activities. Therefore, retention of P and its impact factors in watersheds, dammed reservoirs and lakes become important research issues for integrated water quality management.

1.5 External and Internal Loading of Phosphorus

The accumulation of P in watersheds, dammed reservoirs and lake sediments is related to external and internal loading of P. Here, the definition of external and internal loading is explained and reviewed for better understanding of the current work. External and internal loading of P are the two main processes of P transport aquatic systems. The external loading of P refers to the total P in the river or lake inflows coming from outside sources. These types of P inputs are relatively easy to monitor and manage because we can directly decrease P inputs in our runoff. The internal loading of P has units of mass per area per time and is defined as the gross benthic P flux (L_{gross}) and net internal P loading rate (L_{net}) (Figure 1-6). The time scale for gross benthic P flux is hours-to-days and it usually researched in core incubation (small-scale) (Orihel et al., 2017). Additionally, net internal P loading rate has a larger scale (for example, reservoirs, lakes and oceans etc.), and an annual time scale. The current study focuses on net internal loading of P that may significantly delay the improvements of the original water management strategies (Orihel et al., 2017; Søndergaard et al., 2003). According to previous studies, internal loading of P in shallow lakes is also strongly connected to seasonal variations, bioactivities and the turbidity of the waterbody (Søndergaard et al., 2003; Søndergaard et al.,2013). Therefore, internal loading of P is a very complex process that varies with time and the characteristics of the surrounding environment, such as water and sediment temperature, sediment porosity, and sediment depthetc.

Due to the accumulation of nutrients in watersheds and lake sediments, the legacy of nutrients will affect the water quality and remediation methods on a long-term scale (Carpenter et al., 1998;

Stephen R. Carpenter, 2005; Van Meter et al., 2018). Furthermore, the efflux mechanisms of P from sediments are related to multi-factors, such as pH, water temperature (seasonal change), redox reaction (the main factor is iron speciation and redox environment), external loading of P and the bioactivities (Katsev et al., 2006; Orihel et al., 2017). In the current study, the external P loading and internal P loading were simulated using the CE-QUAL-W2 model, which combined a sediment diagenesis model with a hydrodynamic water quality model. It may be used to identify long-term solutions for the water quality in the Fanshawe Reservoir and Thames River Watershed.

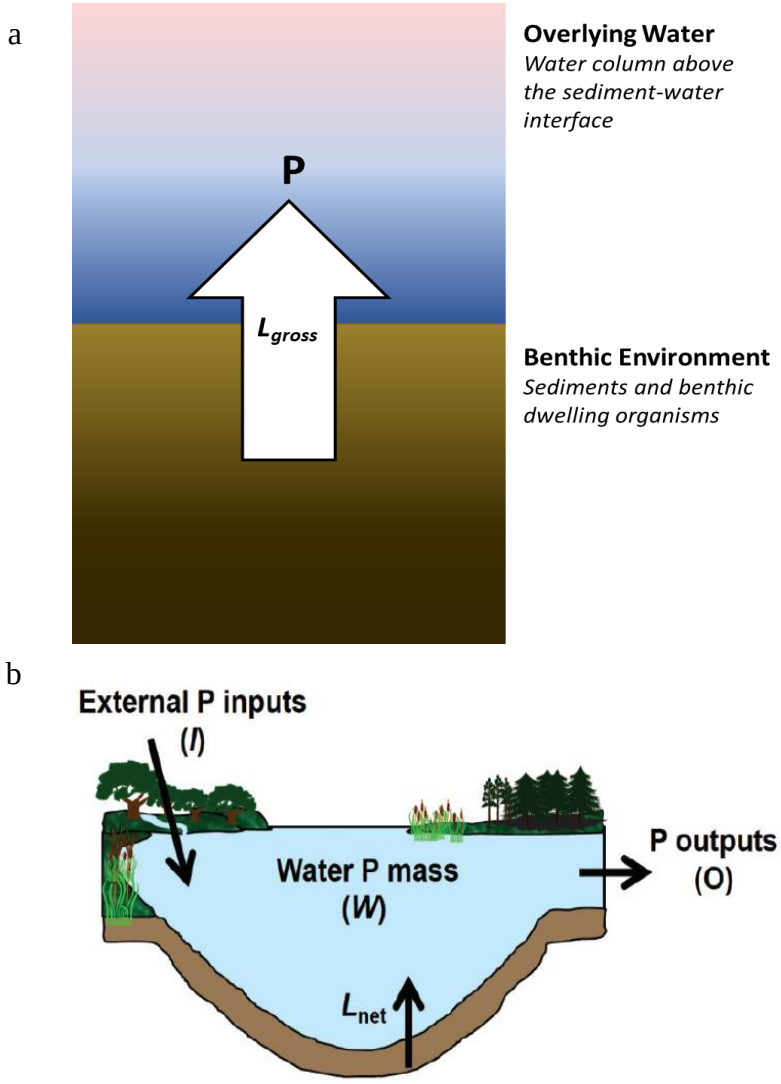

Figure 1-6. Schematic of internal P loading. (a) Gross benthic P flux (Lgross); (b) Net internal P loading rate (L_{net}). Modified from Orihel et al., (2017).

1.6 Research Objectives

The current study area, Fanshawe Reservoir, is affected by legacy P, which can lead to an unpredictable release of P in the aquatic and sediment systems. According to Nürnberg and Lazerte (2005, 2015), the internal loading of the Fanshawe Reservoir during the summertime may have a very high release rate of P (range from 24 to 56 $mg/m^2/d$), and they also argued the annual average total phosphorus loading of upstream Fanshawe Reservoir is higher than the annual average total phosphorus loading of downstream Fanshawe Reservoir or not. The sediment effects and retention efficiency of P in Fanshawe Reservoir during the whole year period is still not clear. These legacies of P may become excess nutrients for algae in the reservoir. In addition, according to UTRCA's report, although nearly three decades pollution management has been applied in the watershed, the water quality in Fanshawe Reservoir is still poor (Nürnberg and Lazerte, 2015; Nürnberg and Lazerte, 2005). Therefore, more advanced modeling and controlling methods should be considered for evaluating and understanding the water quality in both the aquatic and reservoir sediment systems.

To have a more advanced understanding of the biogeochemical cycling of nutrients, such as the fate of P in Fanshawe Reservoir, the impact factors for internal and external loading of P, and sediment effects on P seasonal variation and biomass accumulation, modeling methods have been built for understanding the complex transport processes of nutrients (P) in the Fanshawe Reservoir.

The current research objectives can be described in five parts:

1. Previous studies illustrated that legacy P is an urgent issue for water quality management, however, the focus has not been on the retention of P in watersheds consideration to their hydrodynamic characteristics. To have comprehensive understanding of the fate of P in the reservoir and reservoir sediment, a hydrodynamic model, which includes the water level, water flow and water temperature for the Fanshawe Reservoir, will be built to test and predict the physical properties of Fanshawe Reservoir, such as the variations of thermal structure in Fanshawe Reservoir.
2. After building the 2-D hydrodynamic model for Fanshawe Reservoir, the water quality model that focused on P, oxygen and biomass will be developed into previous hydrodynamic model to understand the biogeochemical processes of P in the water column. Different scenarios will be addressed to examine the relationship between different

constituents. For example, the effects of internal loading of P on the dissolved oxygen and algal growth.

3. Due to low winter temperatures in Canada, there is often a bias in field measurements towards warmer seasons. Therefore, the ice events and seasonal variation of P concentration will be simulated and analyzed through the 2-D model produced in this study to attempt to compensate for the lack of direct field measurements. In addition, during the long-time scale (months to years) simulation, the fate of P can be identified in Fanshawe Reservoir through this 2-D model. For example, the variation of P concentrations in different depths and location will be estimated from the modeling results. These modeling results may support future water quality analyses in a variety of spatial locations in the waterbody.
4. To examine detailed sediment P information, such as the relationship between internal loading and external loading, and P retention efficiency during different season, the sediment diagenesis model coupled with the hydrodynamic and water quality model will be developed and applied into current study for quantitative analysis of the relationship between internal P loading and external P loading. A 40% reduction of external P loading will be examined for testing the effects of the sediment P loading and feasibility of the government regulation (*Canada-Ontario Lake Erie Action Plan*, 2018).
5. Globally, watershed and reservoirs are affected by factors that differ from location to location, including the temperature, wind, the size of dams and the sediment characteristics. Water quality in these watersheds may be overwhelmed by legacy nutrients or other contaminants. To have easily feasible and predictable modeling application for other dammed area, this 2-D water-sediment model will be coupled with BP-ANN model, which is a type of data driving model. The hybrid model may be applied to other lakes or whole watersheds with similar issues, to simulate and predict the seasonal variation and spatial distribution of nutrients and contaminants in a long period time.

Chapter 2 Research Materials and Research Methods

2.1 Overview

The Fanshawe Reservoir study, which involves building CE-QUAL-W2 water quality model and BP-ANN model and implementing comprehensive topographical data, hydrogeological data and meteorological data into the current CE-QUAL-W2 and BP-ANN model, focuses on the seasonal variation of the stratification in the lake (such as ice cover events, temperature variations and hydrodynamic effects), the impact factors of the external and internal P loading (such as water temperature, algal effects, sediments and other nutrients effects, and oxygen effects) as well as the transport mechanisms of nutrients (P) in the whole aquatic system. In this chapter, the characteristics of the research area and data sources are reviewed and discussed based on previous report and study. To provide easily accessible model for future users, detailed introduction of research methods and CE-QUAL-W2 model is described and demonstrated.

2.2 Research Area and Characteristics

The TRW is located in the most important and intensive agricultural area in southwestern Ontario(Nürnberg and Lazerte, 2005). This watershed has three parts: The North Thames River, the South Thames River and the Thames River (Figure 2-1) (Nürnberg and Lazerte, 2015; Nürnberg and Lazerte 2005; Quinlan, 2013). Fanshawe Reservoir, which is created by Fanshawe Dam, is the last reservoir in the downstream area of the North TRW. The latitude of Fanshawe Reservoir is 43°03’29’’ and the longitude of Fanshawe Reservoir is 81°10’29’’ (Figure 2-1 A). The latitude and longitude are inputs for the surface heat exchange calculation (internal short-wave solar calculation and shading calculations) in the CE-QUAL-W2 2-D model (Cole and Wells, 2017).

There are two branches that flow into the Fanshawe Reservoir. The main branch has the potential to carry about 95% of the external loading of TP to the Fanshawe Reservoir, and the other 5% external loading of TP comes from either the secondary branch, Wye Creek, or precipitation (Nürnberg and Lazerte, 2005). The outflow of Fanshawe Reservoir is controlled by Fanshawe Dam, for which, hydrogeological and meteorological data is available from Environment and Climate Change Canada.

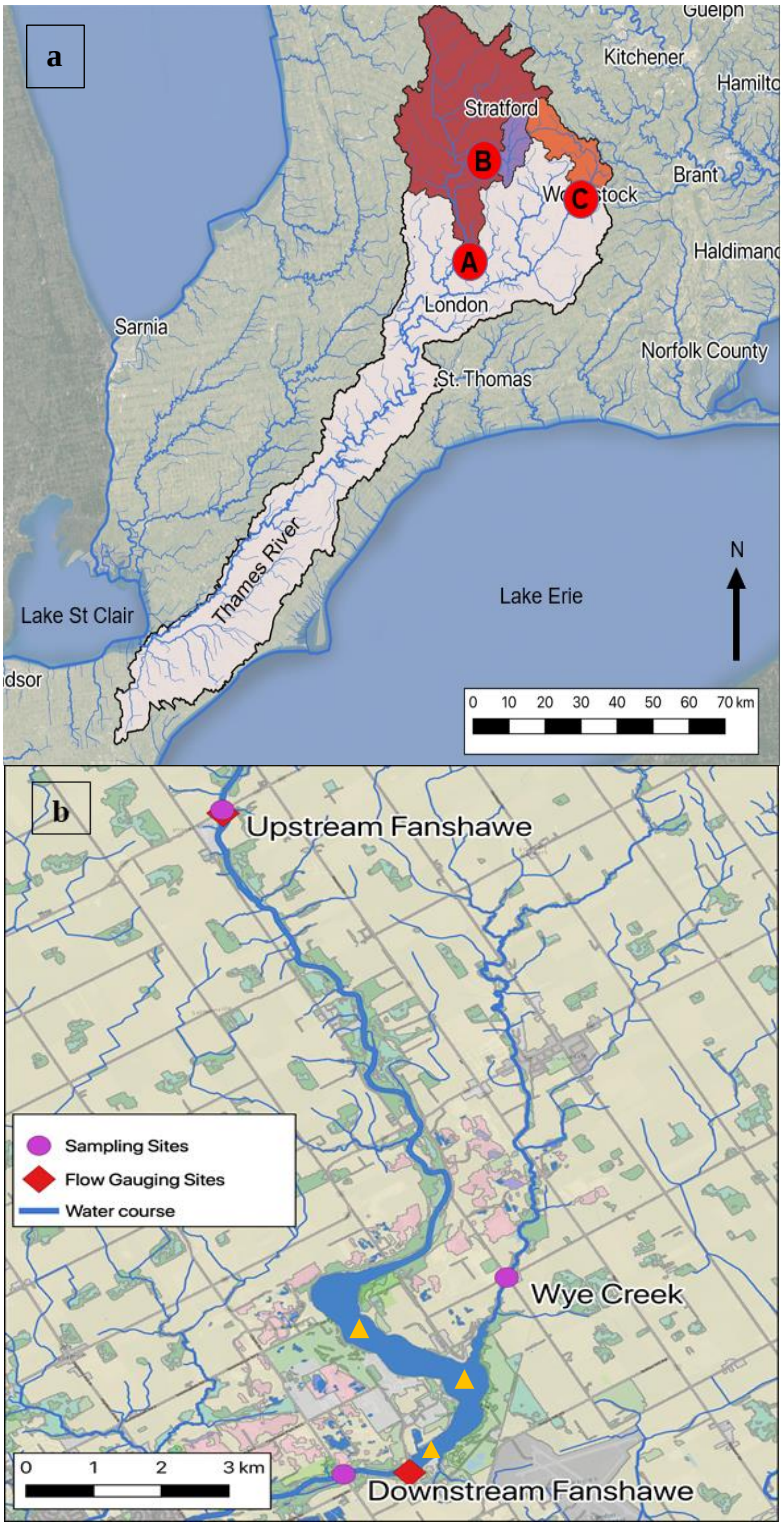

Figure 2-1. The overview map of (a) the Thames River Watershed and (b) Fanshawe Reservoir. (A is Fanshawe Reservoir, B is Wildwood Reservoir and C is Pittock Reservoir. Red Diamonds are the Water Survey of Canada (WSC) flow gauging stations, the purple circles are water samping locations (UW samples), the orange triangles are measuring sites.

The satellite maps and contour data contain the depth and topographical information of Fanshawe Reservoir (Figure 2-2a) and modified in Google Earth Pro. The contour line data are obtained from Bathymetry lines, Bathymetry index, and Bathymetry points, Land Information Ontario (LIO).

There are several characteristics of Fanshawe Reservoir which have been described by the UTRCA (2005): The average volume of Fanshawe Reservoir is about 13.146 × 106 m^3, and the water residence time ranges from 5 to 20 days during 1954 to 2004 : average water residence time is about 9.5 days(Table 2-1). The Fanshawe Reservoir bathymetry and sampling sites are shown in Figure 2-2b. There are three outlets for Fanshawe Reservoir: The first outlet is the high flow surface outlet and another two outlets, which have same elevations, are the bottom outlets. One bottom outlet is for the hydroelectrical power generation and another one is a low flow valve (Nürnberg and Lazerte, 2005). Thus, the Fanshawe Reservoir can be a sink for the nutrients from upstream as well as a source for the downstream area. In addition, the assessment of the water quality suggests that the water is eutrophic to hypereutrophic in Fanshawe Reservoir(Nürnberg and Lazerte, 2005). Algal blooms are observed in the waterbody during the summertime and fall time, and the oxygen depletion occur during the thermal stratification in the deep layer of Fanshawe Reservoir (Nürnberg and Lazerte, 2005). However, the reason for the observation of elevated total phosphorus (TP) concentrations, blooms of algae, and the relationship between the P sinks and P sources are still not clear in the Fanshawe Reservoir.

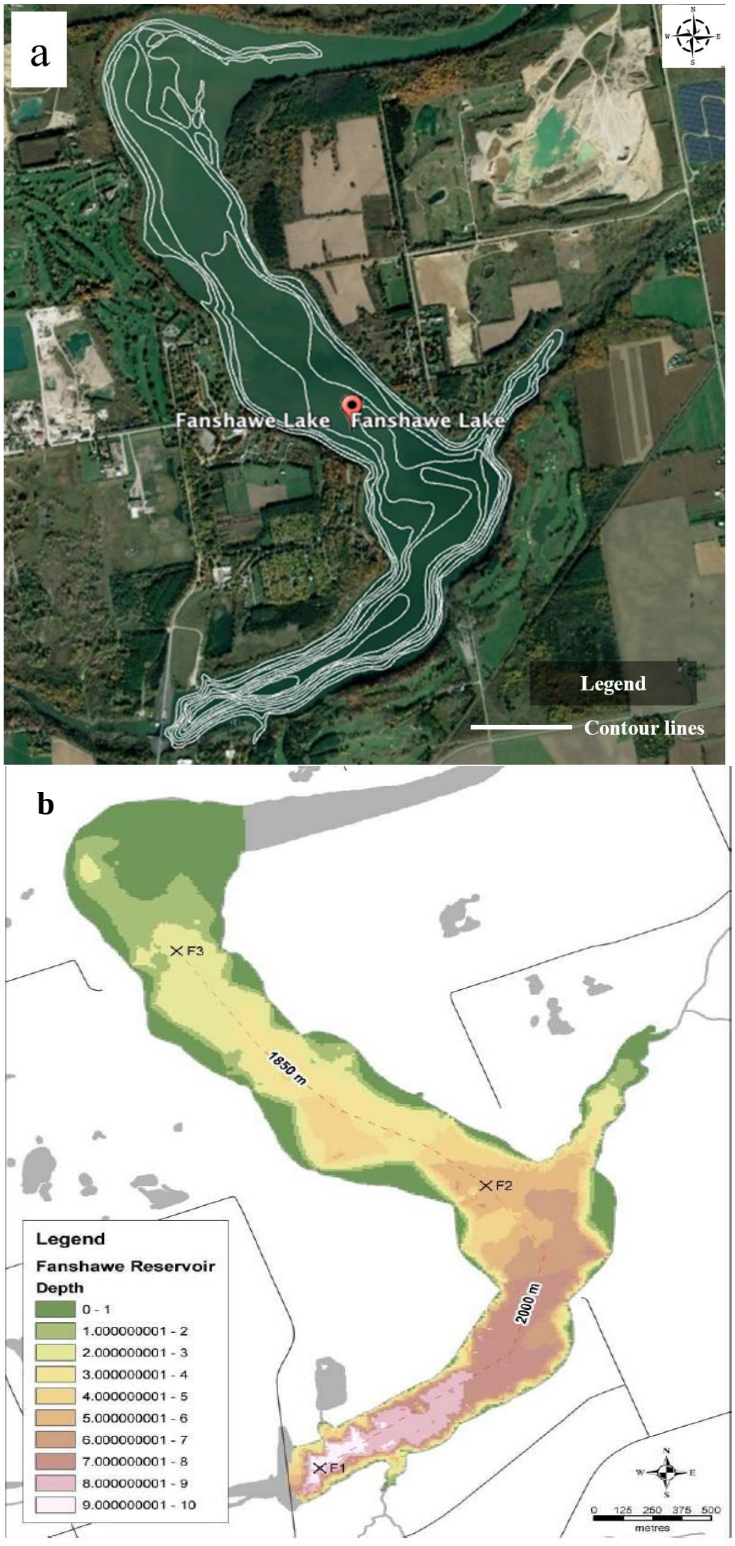

Figure 2-2. a) Satellite map of Fanshawe Lake with contour line (white lines, depth information), and b) Sampling sites of Fanshawe Reservoir (XF1-XF3). Satellite map obtained from Google Earth Pro and contour line data obtained from LIO tools; Modified from Nürnberg and Lazerte, (2005).

Table 2-1. Long-term average hydrological data for Fanshawe Lake (1954 - 2004). Data from Nürnberg and Lazerte, (2005).

Parameter	Values
Altitude at average pool (m above sea level)	262.4
Watershed area (km^2)	1447.4
Surface area (km^2)	2.726
Maximum Depth (m)	12.1
Mean Depth (m)	4.82
Volume (m^3)	13.146×10^6
Outflow Volume (m^3 per year)	560×10^6
Water Residence Time	9.5 days

2.3 Research Data and Data Sources

Field measurement data were used for the calibration and validation processes of the model. The bathymetry row data and the contour lines were obtained from LIO. There are 8 contour lines with depth information (Table 2-2). The topographic data and depth information were used in the development of the modeling bathymetry file.

Table 2-2. Contour lines with depth information (Land Information Ontario).

Contour line Number	Depth(m)
1	0.9
2	1.5
3	3
4	4.6
5	6.1
6	7.6
7	9.1
8	10.7

The water inflow daily data, and climate data, such as temperature, wind speed and wind direction and daily cloud information, were obtained from ECCC (*Canadian Weather - Environment Canada*, n.d.; *Water Level and Flow - Environment Canada*, n.d.). The water outflow daily data and water level data were obtained from UTRCA (*Fanshawe Reservoir Water Levels | UTRCA: Inspiring A Healthy Environment*, n.d.). Additional water quality, water temperature, and sediment

data were measured by Amanda Niederkorn and Nady Kao, which obtained under the Thames River Phosphorus speciation project funded under the Canada-Ontario Agreement through the Ontario Ministry of Environment Conservation and Parks.

2.4 Research Methods

2.4.1 Modeling Methods

In the current research study, CE-QUAL-W2 (Version 4.1), which is a finite difference, 2-D laterally averaged hydrodynamic and water quality model, are applied in simulating the hydrodynamic characteristics of the research area, the seasonal variations of different constituents and the impact factors of nutrients (P is the main nutrient that simulated in the current model) at different location in Fanshawe Reservoir. The CE-QUAL-W2 model is open source and was designed by US Army Engineer Waterways Experiment Station and Portland State University. The model can be used to predict hydrodynamic information for multiple waterbodies with different branches, including water elevations, flow velocities and water temperature. In addition, CE-QUAL-W2 model can simulate over 100 constituents, such as nutrient concentrations, bacteria, and algae. The latest version of CE-QUAL-W2 combined these modules with a sediment diagenesis model (Cole and Wells, 2017). In addition, to have comprehensive understanding and integrated feasible applications of CE-QUAL-W2 model, a BP-ANN model was developed and coupled with CE-QUAL-W2 model in the current Fanshawe study.

The magnitude of legacy P in reservoirs is unclear but it is important to know for future water management. Previous water quality models have not simulated and specified the retention and releasing effects of reservoir bottom sediments on P regulations. The current Fanshawe Reservoir model aims to quantify the effects of sediment P, and it contains four main parts: hydrodynamic model, water quality model, sediment diagenesis model and BP-ANN model.

2.4.2 CE-QUAL-W2 Model

The governing equations of hydrodynamic model and water quality model in CE-QUAL-W2 can be summarized as the following several equations (Cole and Wells, 2017):

(1) Momentum Equations:

The momentum equations including longitudinal and vertical equations. The lateral direction is averaged:

X-momentum (longitudinal):

$$\frac{\partial UB}{\partial t} + \frac{\partial UUB}{\partial x} + \frac{\partial WUB}{\partial z} = gB \sin\alpha + g\cos\alpha B \frac{\partial \eta}{\partial x} - \frac{g\cos\alpha B}{\rho}\int_{\eta}^{z} \frac{\partial \rho}{\partial x} dz + \frac{1}{\rho}\frac{\partial B\tau_{xx}}{\partial x} + \frac{1}{\rho}\frac{\partial B\tau_{xz}}{\partial z} + qBU_x$$

Z-momentum (vertical):

$$\frac{\partial W}{\partial t} + U\frac{\partial W}{\partial x} + V\frac{\partial W}{\partial y} + W\frac{\partial W}{\partial z} = g\cos\alpha - \frac{1}{\rho}\frac{\partial P}{\partial z} + \frac{1}{\rho}\left(\frac{\partial \tau_{zx}}{\partial x} + \frac{\partial \tau_{zy}}{\partial y} + \frac{\partial \tau_{zz}}{\partial z}\right)$$

where U is the horizontal velocity (m s^{-1}), W is the vertical velocity (m s^{-1}), g is the gravitational acceleration (m s^{-2}), B is the channel width (m), τ_x is the lateral average shear stress at x-direction (kg m^{-1} s^{-2}), τ_y is the y direction shear stress (kg m^{-1} s^{-2}), τ_z is the z direction lateral average shear stress (kg m^{-1} s^{-2}), ρ is the density (kg m^{-3}), P is the pressure, and α is the channel slop (radian).

Here, the Z-momentum equation can be simplified as:

$$g\cos\alpha - \frac{1}{\rho}\frac{\partial P}{\partial z} = 0$$

The reason is the lateral direction is averaged and the longitudinal length scale is much larger than the vertical length scale. Therefore, the W (vertical velocities) is much smaller than the U (horizontal velocities) and cancels out of the equation (Cole and Wells, 2017).

(2) Continuity Equation:

$$\frac{\partial UB}{\partial x} + \frac{\partial WB}{\partial z} = qB$$

Where U is the horizontal velocity, (m s^{-1}), W is the vertical velocity (m s^{-1}), B is the channel width (m), q is the net lateral inflow per unit volume of cell (s^{-1}) (Cole and Wells, 2017).

(3) State Equation:

$$\rho = f(T_w, \phi_{TDS}, \phi_{ISS}) = \rho_T + \Delta\rho_s$$

Where ρ is the density (kg m^{-3}), which is a function of temperature (ρ_T), the concentration of total dissolved solids (ϕ_{TDS}), and the concentration of inorganic suspended solids (ϕ_{ISS}). Here, $\Delta\rho_s$ represents the density increment due to solids.

The following relationship is applied in the model to represent the water temperature and density:

$$\rho_{T_w} = 999.84 + 6.79 \times 10^{-2} T_w - 9.10 \times 10^{-3} T_w^2 + 1.00 \times 10^{-4} T_w^3 - 1.12 \times 10^{-6} T_w^4 + 6.54 \times 10^{-9} T_w^5$$

where ρ is density (kg m^{-3}) and T_w is water temperature (°C)(Cole and Wells, 2017).

(4) Free surface Equation:

This equation is related to the water surface elevation:

$$B_\eta \frac{\partial \eta}{\partial t} = \frac{\partial}{\partial x} \int_\eta^h UB \, dz - \int_\eta^h qB \, dz$$

where η is water surface depth (m), h is the depth (m), U is the horizontal velocity (m s^{-1}), B is the channel width (m), q is the net lateral inflow per unit volume of cell (s^{-1}) (Cole and Wells, 2017).

(5) Advection and Diffusion Equations:

$$\frac{\partial B\phi}{\partial t} + \frac{\partial UB\phi}{\partial x} + \frac{\partial WB\phi}{\partial z} - \frac{\partial \left(BD_x \frac{\partial \phi}{\partial x} \right)}{\partial x} - \frac{\partial \left(BD_z \frac{\partial \phi}{\partial z} \right)}{\partial z} = q_\phi B + S_\phi B$$

Where U is the horizontal velocity (m s^{-1}), W is the vertical velocity (m s^{-1}), B is the channel width (m), ϕ is the laterally averaged constituent concentration (g m^{-3}) D_x is the longitudinal temperature and constituent dispersion coefficient (m^2 s^{-1}) D_z is the vertical temperature and constituent dispersion coefficient (m^2 s^{-1}) q_ϕ is the lateral inflow or outflow mass flow rate of constituent per unit volume (g m^{-3} s^{-1}) S_ϕ lateral averaged source and sink term (g m^{-3} s^{-1}) (Cole and Wells, 2017).

These six equations are the governing equations in this 2-D model and the finite difference method is used to solve the equations.

(6) Ice Formation:

In Fanshawe Reservoir, ice covering events are important for understanding the seasonal variation of P retention and release because of the low temperature season in the research area. During the winter season, the internal loading of P cannot be observed due to the limitation of the current measured data because field measurement is not available. The ice cover is a complex formation

process which is related to air-water surface heat exchange, air-water temperature, and absorption of the solar radiation (Figure 2-3). Here, the Fanshawe Reservoir model only applies a sample ice cover model based on the temperature and meteorological data. The following ice covering, water quality and sediment diagenesis model equations are applied in the current stud. The overall ice growth and melt (at the ice-water interface) equation is:

$$\Delta\theta_{iw}^{n} = \frac{1}{\rho_i L_f}\left[K_i \frac{T_f - T_s^n}{\theta^{n-1}} - h_{wi}\left(T_w^n - T_f\right)\right]$$

where $\Delta\theta_{iw}^{n}$ is the change of the thickness of ice, (m), ρ_i is density of ice, (kg m^{-3}), L_f is the latent heat of fusion, (J kg^{-1}), K_i is the thermal conductivity of ice, (W m^{-1} °C^{-1}), T_f is freezing point temperature, (°C), T_s^n is the ice surface temperature, (°C), $h_{wi}$is the coefficient of water to ice heat exchange through the melt layer, (W m^{-2} °C^{-1}). T_w^n is the water temperature in the uppermost layer under the ice, (°C) (Cole and Wells, 2017).

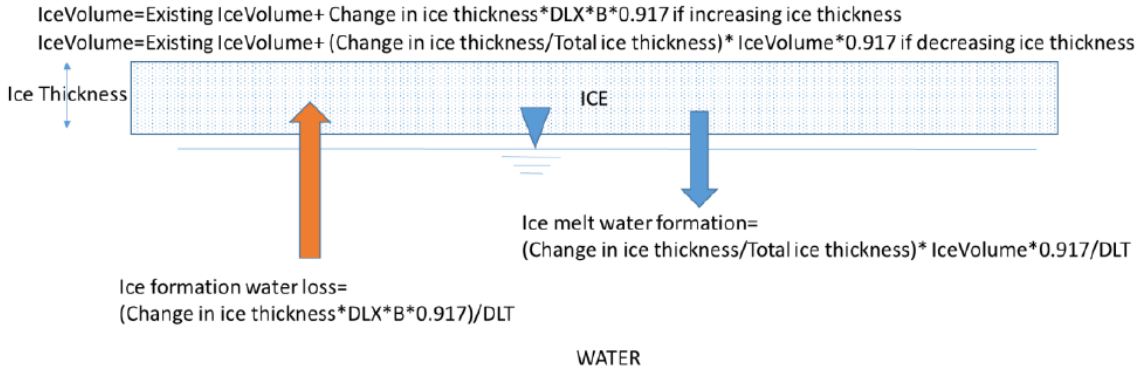

Figure 2-3. Schematic diagram of ice formation and the water balance. Modified from Cole and Wells, (2017).

(7) Generic constituents and P Equations:

In the CE-QUAL-W2 model, any number of generic constituents can be defined in the water quality model for modeling the research issues (Figure 2-4). The generic constituents are also necessary in order to develop the sediment diagenesis model. For example, the sediment P is built for sediment diagenesis model in the current study.

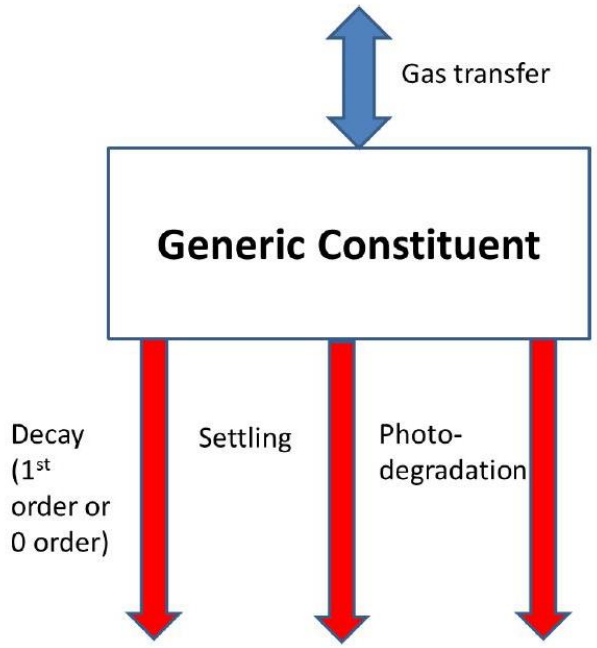

Figure 2-4. Schematic diagram of source and sink terms of generic constituents. Modified from Cole and Wells, (2017).

The summary equation of the source and sink term of generic constituent can be described as:

$$S_g = -K_0\theta_g{}^{(T-20)} - K_1\theta_g{}^{(T-20)}\Phi_g - \omega_g\frac{\partial\Phi_g}{\partial_Z} - \alpha I_o(1-\beta)e^{-\lambda z}\Phi_g + \frac{A_{sur}}{V_{sur}}K_L(\Phi_s - \Phi_g)$$

0-order decay | 1st-order decay | settling | photodegradation | gas transfer

where θ_g is the temperature rate multiplier (-), T is the water temperature (℃), α is the photodegradation parameter ($m^2\ J^{-1}$), I_o is the radiation at surface ($W\ m^{-2}$), λ is the light extinction coefficient, (m^{-1}), β is the fraction of short wave solar absorbed on the surface (-), ω_g is the settling velocity ($m\ s^{-1}$), K_0 is the zero order decay coefficient ($g\ m^{-3}\ s^{-1}$), K_1 is the first order decay coefficient (s^{-1}), Φ_g is the generic constituent concentration ($g\ m^{-3}$), Φ_s is the gas saturation in the atmosphere ($g\ m^{-3}$) A_{sur} is the surface area (m^2), V_{sur} is the surface volume (m^3), and $K_L$is the surface gas transfer coefficient ($m\ s^{-1}$) (Cole and Wells, 2017).

P is considered as the primary limiting nutrient of phytoplankton biomass in the freshwater systems (Cole and Wells, 2017; Schindler, 1974; Schindler et al., 2008). In CE-QUAL-W2 model, P is assumed to be fully available as ortho-phosphate (PO_4^{3-}). Field measured data of dissolved reactive phosphorus (DRP) are closest to the form simulated in the model (Cole and Wells, 2017). PO_4^{3-}

sources and sinks terms showed in figure 2-5. In this water quality model, the 1st-order sediment release and 0-order sediment release are simulated for PO_4^{3-} (Cole and Wells, 2017).

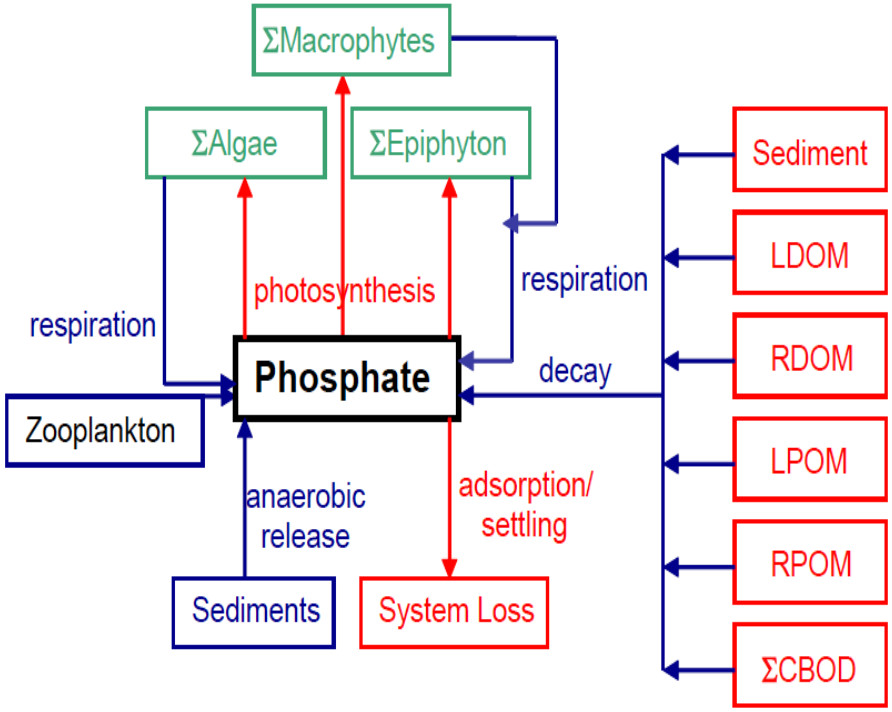

Figure 2-5. Schematic diagram of source and sink terms of phosphate (LDOM is labile dissolved organic matter, RDOM is refractory dissolved organic matter, LPOM is labile particulate organic matter, RPOM is refractory particulate organic matter, CBOD is carbonaceous biochemical oxygen demand). Modified from After Cole and Wells, (2017).

The summary equation of source and sink term of phosphate can be described as:

$$S_p = \underbrace{\sum (K_{ar} - K_{ag})\delta_{Pa}\Phi_a}_{\text{algal net growth}} + \underbrace{\sum (K_{er} - K_{eg})\delta_{Pe}\Phi_e}_{\text{epiphyton net growth}} + \underbrace{K_{LDOM}\delta_{POM}\gamma_{OM}\Phi_{LDOM}}_{\text{labile DOM decay}}$$

$$+ \underbrace{K_{RDOM}\delta_{POM}\gamma_{OM}\Phi_{RDOM}}_{\text{refractory DOM decay}} + \underbrace{K_{LPOM}\delta_{POM}\gamma_{OM}\Phi_{LPOM}}_{\text{labile POM decay}} + \underbrace{K_{RPOM}\delta_{POM}\gamma_{OM}\Phi_{RPOM}}_{\text{refractory POM decay}}$$

$$+ \underbrace{\sum K_{CBOD}\, R_{CBOD}\delta_{P-CBOD}\Theta^{T-20}\Phi_{CBOD}}_{\text{CBOD decay}} + \underbrace{K_s\delta_{POM}\gamma_{OM}\Phi_s}_{\text{1st-order sediment release}} + \underbrace{SOD\gamma_{OM}\frac{A_{sed}}{V}}_{\text{0-order sediment release}}$$

$$- \underbrace{\frac{(\sum \varpi_{ISS}\Phi_{ISS} + \omega_{Fe}\Phi_{Fe})P_P}{\Delta z}\Phi_P}_{\text{inorganic solids adsorption}} + \underbrace{\sum (K_{mr} - (1 - f_{psed})K_{mg})\delta_{Pm}\Phi_{macro}}_{\text{macrophyte net growth}}$$

$$+ \underbrace{\sum K_{zr}\,\delta_{Pz}\Phi_{zoo}}_{\text{zooplankton respiration}}$$

where Δz is the model cell thickness (m), A_{sed} is the sediment surface area (m^2), V is cell volume, (m^3), P_P is the adsorption coefficient ($m^3\ g^{-1}$), K_g and K_r are growth rate and dark respiration rate (unit is s^{-1}) (algal and epiphyton), K_{LDOM}, K_{RDOM}, K_{LPOM}, K_{RPOM}, K_{CBOD}, and K_s are decay rates for different species (s^{-1}),(LDOM and LPOM are for labile dissolved and particulate organic matter; RDOM and RPOM are for refractory dissolved and particulate organic matter), δ_P is the stoichiometric coefficient for different P species (plants and organisms), Φ is the concentration for different species ($g\ m^{-3}$), f_{psed} is the fraction of macrophyte phosphorus uptake from sediments (-); γ_{OM} is the temperature rate multiplier for organic matter decay (-), Θ is the temperature rate multiplier for CBOD decay (-), ϖ is the settling velocity ($m\ s^{-1}$) (Cole and Wells, 2017).

(8) Sediment Equations:

In the current study, the sediment diagenesis model was coupled with the hydrodynamic and water quality model for understanding P retention and release processes in Fanshawe Reservoir. The original sediment diagenesis model was built for the gas transfer and oil sand research(Berger and Wells, 2014; Cole and Wells, 2017; Prakash et al., 2015; Vandenberg et al., 2015). The update version (version 4.1) of CE-QUAL-W2 includes the fate of P(Berger and Wells, 2014).

Figure 2-6 is the schematic diagram of sediment diagenesis model of $PO_4^{3-}$and Figure 2-7 is the schematic diagram of sediment diagenesis model of iron species.

Sediment Heat Exchange:

$$H_{sw} = -K_{sw}(T_W - T_S)$$

where H_{sw} is the rate of sediment and water heat exchange ($W\ m^{-2}$), K_{sw} is the coefficient of sediment and water heat exchange ($W\ m^{-2}\ °C^{-1}$), T_W is the water temperature and T_S is the sediment temperature (°C) (Cole and Wells, 2017).

Sediment P concentration is related to organic matter, biomass, and redox reaction. In the current sediment model, P concentrations were simulated by particulate organic matter (POM) decay processes, biomass sedimentation processes and sediment diagenesis processes. In the current sediment diagenesis model, two layers are simulated for sediment P species. Figure 2-6 to Figure 2-8 illustrate the sediment diagenesis model results for P and iron. Phosphate in the sediment diagenesis model exists in dissolved and particulate forms. The first modeling layer (Layer 1) is aerobic layer which is assumed to be a very thin layer. Therefore, the source and rate equation of

phosphate in this layer was assumed to be 0. Another layer (Layer 2) is an anaerobic layer that has a first order rate equation for PO_4^{3-}. Within the layer 1, phosphate will absorb to iron oxyhydroxide. In layer 2, the class **i** from 1 to 3 represent labile, refractory and slow refractory particulate organic phosphorus (POP) The absorption and releasing extent of phosphate from iron oxyhydroxide are dependent on the dissolved oxygen concentrations in the water-sediment surface (Cole and Wells, 2017).

Sediment Phosphorus Equation:

$$S_{Psed} = \frac{\varpi_{RPOM} A_{bottom}}{V} \Phi_{RPOM-P} + \frac{\varpi_{LPOM} A_{bottom}}{V} \Phi_{LPOM-P} + \sum \frac{\varpi_a A_{bottom}}{V} \delta_{Pa} \Phi_a$$
$$- K_s \Phi_{s-P} + \sum K_{epom} K_{em} \delta_{Pe} \Phi_e - \frac{\varpi_{SED} A_{bottom}}{V} \Phi_{s-P}$$

where ϖ is settling velocity (m s^{-1}), δ is the stoichiometric coefficient for P (-), A is the bottom area (m^2), V is the volume of computational cell (m^3), K is decay rate and mortality rate (s^{-1}), K_{epom} is the fraction of epiphyton that form particulate organic matter (-) (Cole and Wells, 2017).

Sediment Diagenesis Model

Layer 1 rate equation:

$$S_{po41} = 0$$

Layer 2 rate equation:

$$S_{po42} = \sum_{i=1}^{3} k_{POPi} \Upsilon_{POPi} \Phi_{POPi}$$

where S_{po4} is the rate of phosphate in layer 1 or layer 2 (g m^{-3} s^{-1}); K_{POPi} is the particulate organic phosphorus class i mineralization rate (s^{-1}), Υ_{POPi} is the particulate organic phosphorus temperature rate multiplier (-), $\Phi_{POPi}$is the POP class i concentration, unit is g m^{-3}.

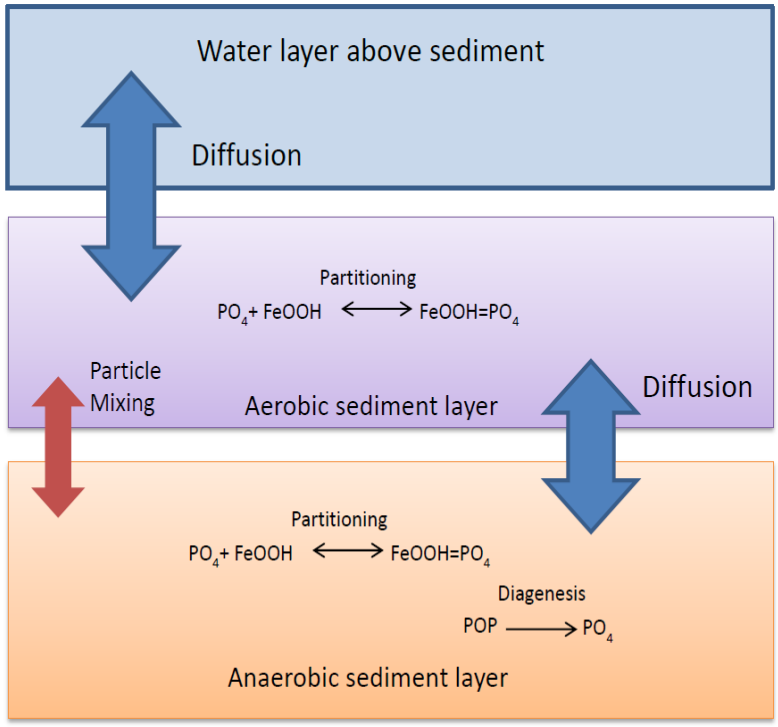

Figure 2-6. Schematic diagram of sediment diagenesis model of phosphate. Modified from After Cole and Wells, (2017).

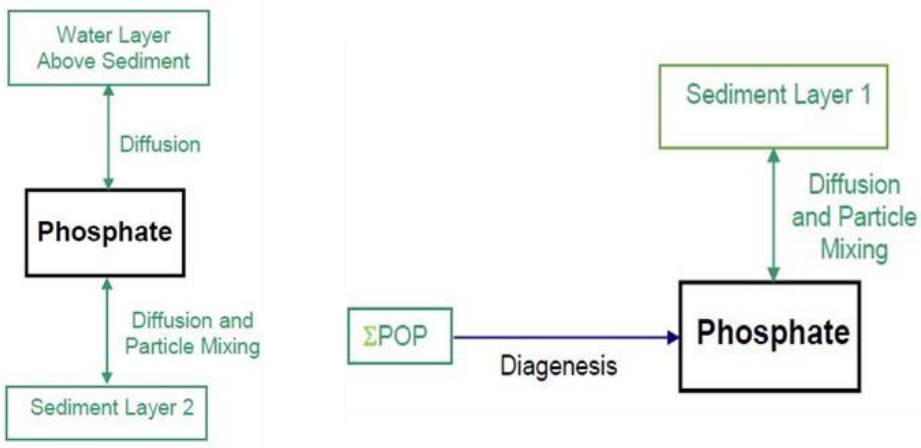

Figure 2-7. Phosphate internal flux of sediment diagenesis model in layer 1 (aerobic layer) and layer 2 (anaerobic layer) . Modified from Cole and Wells, (2017).

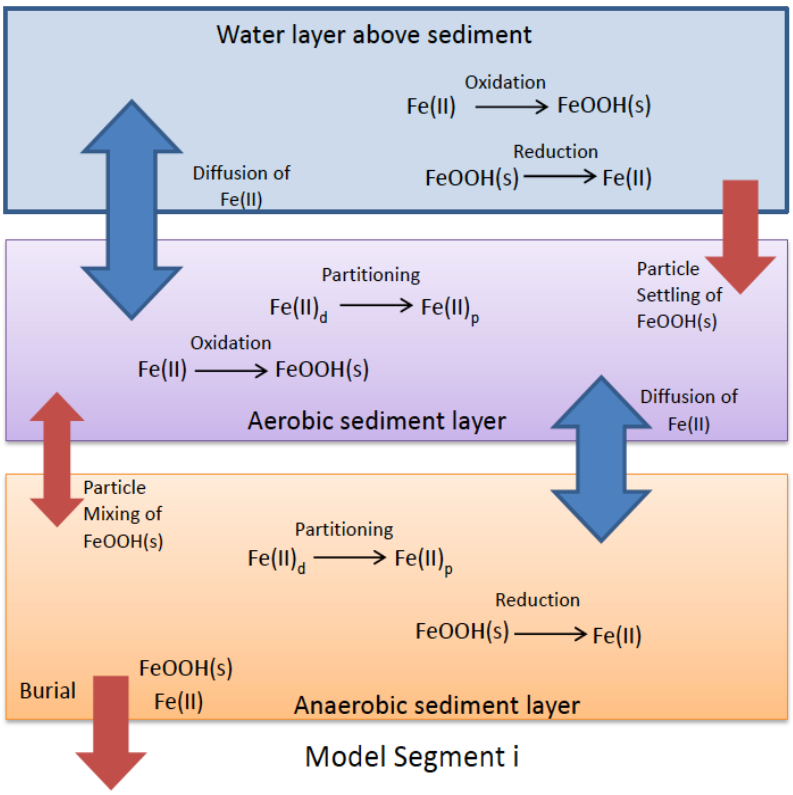

Figure 2-8. Schematic diagram of sediment diagenesis model for iron. Modified from Cole and Wells, (2017).

Iron oxyhydroxide rate equation in water column:

$$s_{FeOOH} = k_{Fe(II)0}\Phi_{DO}10^{2(pH-7)}\Phi_{Fe(II)} - k_{FeOOH}\left(\frac{K_{FeOOH}}{K_{FeOOH}+\Phi_{DO}}\right)\Phi_{FeOOH}$$

Iron oxyhydroxide rate equation in aerobic layer 1:

$$s_{FeOOH1} = k_{Fe(II)1}\Phi_{DO}10^{2(pH-7)}f_d\Phi_{Fe(II)1}$$

Iron oxyhydroxide rate equation in aerobic layer 1:

$$s_{FeOOH2} = -k_{FeOOH2}\Phi_{FeOOH}$$

where $k_{Fe(II)}$ is the ferrous iron oxdidation rate in each layer (s^{-1}), k_{FeOOH} is the iron oxyhydroxide reduction rate in each layer (s^{-1}); K_{FeOOH} is the half saturation constant for this reaction (g m^{-3}), f_d is the dissolved fraction of ferrous iron(-); pH is the pH values in water column, layer 1, or layer 2 (Cole and Wells, 2017).

2.4.3 BP-ANN Model

In the current modeling study, a BP-ANN model was developed and calibrated through CE-QUAL-W2 modeling results. The original code was developed in MATLAB software. The ANN models have been widely implemented into different research area, such as rainfall-runoff forecasting, water temperature and water quality forecasting etc. (Demirel et al., 2009; Kişi, 2008; Maier and Dandy, 2000; Ömer Faruk, 2010; Singh et al., 2009). The BP-ANN model has been extensively and commonly used in the data driven modeling works (Kişi, 2008; Maier and Dandy, 2000; Ömer Faruk, 2010; Yang et al., 2018). The current modeling work is the first time that combine the CE-QUAL-W2 modeling results with a BP-ANN model. The combination of these two methods provides high-efficiency and reliable model for future prediction and application. For example, the CE-QUAL-W2 model need lots of parameters and measured data for simulating biomass in different year. After calibrating BP-ANN model with validated CE-QUAL-W2 modeling results, BP-ANN model could forecast algal blooms only through changing the inflow or climate data. It may not be an accurate or perfect way to obtain water quality information, however, it would be a very fast way to predict water quality information.

In the BP-ANN model, the modeling signal is feedforward and the modeling errors are back propagation. The BP-ANN model adjusts the weight values and threshold values through the comparison between the modeling results and input data until the errors of the whole network are minimized (Demirel et al., 2009; Maier & Dandy, 2000; Yang et al., 2018). The BP-ANN model in the current Fanshawe Reservoir study used the sigmoid transfer functions which have been developed in MATLAB software, and the Levenberg-Marquardt BP method was applied as the training algorithm. The detailed schematic was discussed in Chapter 4 and the parameters was in Appendix C.

Chapter 3 Fanshawe Reservoir Water Quality Assessment and Prediction

3.1 Summary

In this chapter, 2-D water quality and sediment model was developed and implemented based on our field data. Hydrodynamic, physical, and chemical modeling results, and modeling applications were detailed demonstrated and discussed through different scenarios. In modeling calibration and validation sections, the simulation results well reproduced and predicted the topographical and hydrodynamic characteristics, such as the variation of water temperature, and ice cover events etc., the DRP and TP loading information of the Fanshawe Reservoir also well captured through the current modeling results. In diagnostic scenarios, dissolved oxygen and algal growth information were simulated with different scenarios. The internal loading of P has major effects on algal growth from late April to late September. In the prognostic scenarios, the relationship between internal P loading and external P loading was predicted and simulated. Furthermore, in the modeling application scenarios, the current water quality and sediment model provided reliable algae, DRP and TP simulation results for the water outflow control management.

3.2 Introduction

Eutrophication is an important global issue which has negative effects on global aquatic systems and human living conditions, including oxygen depletion, fish death, and degradation of surface and ground water quality(Carpenter et al., 1998; Correll, 1998; Orihel et al., 2017).The main reason for eutrophication is the excess loading of different nutrients, such as phosphorus (P) and nitrogen (N). Understanding the P cycle in watersheds and lakes plays an important role for informing the water quality improvements in our aquatic systems (Correll, 1998; Filippelli, 2008; Goyette et al., 2018; Maavara et al., 2015; Ruttenberg, 2014). A lot of evidence indicates that these inputs of P can be accumulated in aquatic systems, such as rivers, lakes over a long period(Carpenter et al., 1998; Carpenter, 2005; Jarvie et al., 2012, 2013; L. H. Kim et al., 2003; Maavara et al., 2015; A. Sharpley et al., 2013). Previous studies have demonstrated the chronic release of P may cause delays in reaching the water quality management goals (Jarvie et al., 2012; Jarvie et al., 2013; Meals et al., 2010; Sharpley et al., 2013)

Fanshawe Reservoir is last big reservoir in the North Thames River Watershed (TRW), Ontario, Canada. The TRW is an important source of nutrients for Lake St. Clair, and the Thames River is

the largest Canadian tributary input of P for the western basin of Lake Erie (Nürnberg and Lazerte, 2005; Nürnberg and Lazerte 2006; Nürnberg and Lazerte, 2015). Intensive agriculture and other human activities have led to the input of excess nutrients into the TRW (Nürnberg and Lazerte, 2005). Most of these inputs of nutrients come from non-point sources, which are difficult to monitor and manage in the whole watershed, especially considering the nutrient retention capabilities of river and reservoir sediments. During the seasonal variation, especially in summertime and fall time, blue-green algae and elevated bacterial concentrations have been frequently observed in Fanshawe Reservoir by the Upper Thames River Conservation Authority (UTRCA) (Nürnberg & Lazerte, 2005; Nürnberg and Lazerte, 2006). However, the existing field data cannot explain the seasonal variation of reservoir water quality, the long-term scale interaction between the external loading of P and internal loading of P, and the effects of P retention on the downstream area. Therefore, the systematic modeling methods would be useful for simulating and observing these types water systems with complex geological, hydrogeological characters and meteorological data, and will contribute to the comprehensive understanding of the fate of P and other nutrients in the Fanshawe Reservoir. The current modeling study is aided by the CE-QUAL-W2 model.

3.3 Modeling Methods and Modeling Conditions

3.3.1 CE-QUAL-W2 Model

In the current research study, CE-QUAL-W2 (Version 4.1), which is a finite difference, 2-D laterally averaged hydrodynamic and water quality model, are applied in simulating the hydrodynamic characteristics of the research area, the seasonal variations of different constituents and the impact factors of nutrients (P is the main nutrient that simulated in the current model) at different location in Fanshawe Reservoir. The CE-QUAL-W2 model is open source and was designed by US Army Engineer Waterways Experiment Station and Portland State University. The model can be used to predict hydrodynamic information for multiple waterbodies with different branches, including water elevations, flow velocities and water temperature. In the newest version of CE-QUAL-W2 model, sediment diagenesis module has been coupled with original hydrodynamic and water quality model (Cole and Wells, 2017). The sediment diagenesis model need user to modify the input file by themselves and some assumptions were made into the current sediment model, such as the aerobic layer is assumed to be zero. In addition, CE-QUAL-W2 model can simulate over 100 constituents, such as nutrient

concentrations, bacteria, and algae. Previous studies well demonstrated that CE-QUAL-W2 model has advantages on the modeling of narrow rivers, reservoirs, and lakes (Cole & Wells, 2017; Gelda et al., 2009; Kim et al., 2009). For example, CE-QUAL-W2 model was successfully implemented as DO and thermal stratification model in DeGray Reservoir(Martin, 1988); CE-QUAL-W2 model was also well implemented to Lake Erie as nutrients loading and zebra mussels testing tool (Boegman et al., 2001); The dam outflow elevation impacts on water quality were also simulated and predicted through CE-QUAL-W2 model (Lindenschmidt et al., 2019). However, these applications of CE-QUAL-W2 model did not consider or fully implement sediment module into CE-QUAL-W2 model, and the complex relationship between water column model and sediment model was not fully demonstrated. The current Fanshawe Reservoir Study was implemented Sediment Diagenesis Model into the current water quality model.

3.3.2 Research Data and Conditions

The current modeling study is supported through different data sources. To have a better understanding on the modeling processes, data types were summarized (Table 3-1). There are several different data sources: Environment and Climate Change Canada (ECCC), Upper Thames River Conservation Authority (UTRCA), Calibration values (C), and measurement values (M). Calibration values were modified and verified from modeling results and measurement data. Measurement data were field measurement data that provided by Amanda Niederkorn and Nady Kao. The measured data were measured once per two weeks (Bi-weekly). Field measured data were used for the calibration and validation processes of the model. The bathymetry row data and the contour lines were obtained from Land Information Ontario. There are 8 contour lines with depth information (Figure 3-1 blue lines and Table 3-2 listed the depth information). The topographic data and depth information were used in the development of the modeling bathymetry file.

Table 3-1. Summary of data types.

Data Types	Resolution	Units	Maximum	Minimum	Sources	Comments
Air Temperature	Hourly	℃	32.3	-24.7	ECCC	2018-2019
Dewpoint Temperature	Hourly	℃	25.9	-30	ECCC	2018-2019
Wind Speed	Hourly	m/s	16.1	0	ECCC	2018-2019

Cloud	Hourly	-	10	0	ECCC	2018-2019
Branch1 Inflow	Daily	m^3/s	608	1.01	ECCC	2018-2019
Branch2 Inflow	Daily	m^3/s	33	0	ECCC	2018-2019
Branch Inflow Temperature	Bi-weekly	℃	29.3	0	M	
DRP	Bi-weekly	mgP/l	0.24	8E-04	M	
DNRP	Bi-weekly	mgP/l	0.06	0.003	C	TDP-DRP
PRP	Bi-weekly	mgP/l	0.43	0.002	C	TP-TDP
PNRP	Bi-weekly	mgP/l	0.23	0.002	C	
DO	Bi-weekly	mg/l	16.5	6.2	M	
Algae	Bi-weekly	mg/l dry weight OM	2.3	0.6	M	Estimated small input values and Derived from Chlorophyll a data
Dam Outflow	Daily	m^3/s	496	0	UTRCA	2018-2019

The water inflow daily data, and climate data, such as temperature, wind speed and wind direction and daily cloud information, were obtained from ECCC (*Canadian Weather - Environment Canada*, n.d.; *Water Level and Flow - Environment Canada*, n.d.). The water outflow daily data and water level data were obtained from UTRCA (*Fanshawe Reservoir Water Levels | UTRCA: Inspiring A Healthy Environment*, n.d.). Additional water quality, water temperature, and sediment data were measured by Amanda Niederkorn and Nady Kao. Dissolved reactive phosphorus (DRP) or soluble reactive phosphorus (SRP) was directly extracted from measured data and converted the unit in mgP/l. Dissolved non-reactive phosphorus (DNRP) was calculated from total dissolved phosphorus (TDP) and DRP. Particulate phosphorus (PP) was divided into particulate reactive phosphorus (PRP) and particulate non-reactive phosphorus (PNRP), PP were calculated from total phosphorus (TP) and total dissolved phosphorus (TDP). Previous study illustrated the bioavailable phosphorus in the total PP ranges from 6% to 69%(Petticrew & Gregor, 1982; A. N. Sharpley et al., 1992). An input assumption made in the current study for PRP and PNRP: PRP accounts for 50% of the PP, and PNRP accounts for the rest of PP.

Before developing the physical model of Fanshawe Reservoir through CE-QUAL-W2 model, a topographical conceptual grid model was built to obtain a better understand of the whole system. Based on the geological and hydrogeological data (contour lines and topographic data) from LIO, the Fanshawe Reservoir bathymetry data were collected and created in the Quantum Geographic Information System (QGIS). 39 segments, including four boundary segments, were applied in the Fanshawe Reservoir and each segment was separated into 19 vertical layers (Table 3-2). The first top layer and bottom layer of each segments are boundary layers. The Fanshawe Reservoir has two branches which account for the inflow in modeling processes. Branch 1 is main inflow from North Thames River, and branch 2 is inflow from Wye Creek which has very small water flow compared with the main inflow (Figure 3-1). The black rectangles represent the segments, rotated to indicate the direction of flow (Cole and Wells, 2017). The segment length and layer width, which were created from QGIS, are listed in Appendix A. The rotation of the segments was applied as radian in CE-QUAL-W2 model and are listed in Appendix A.

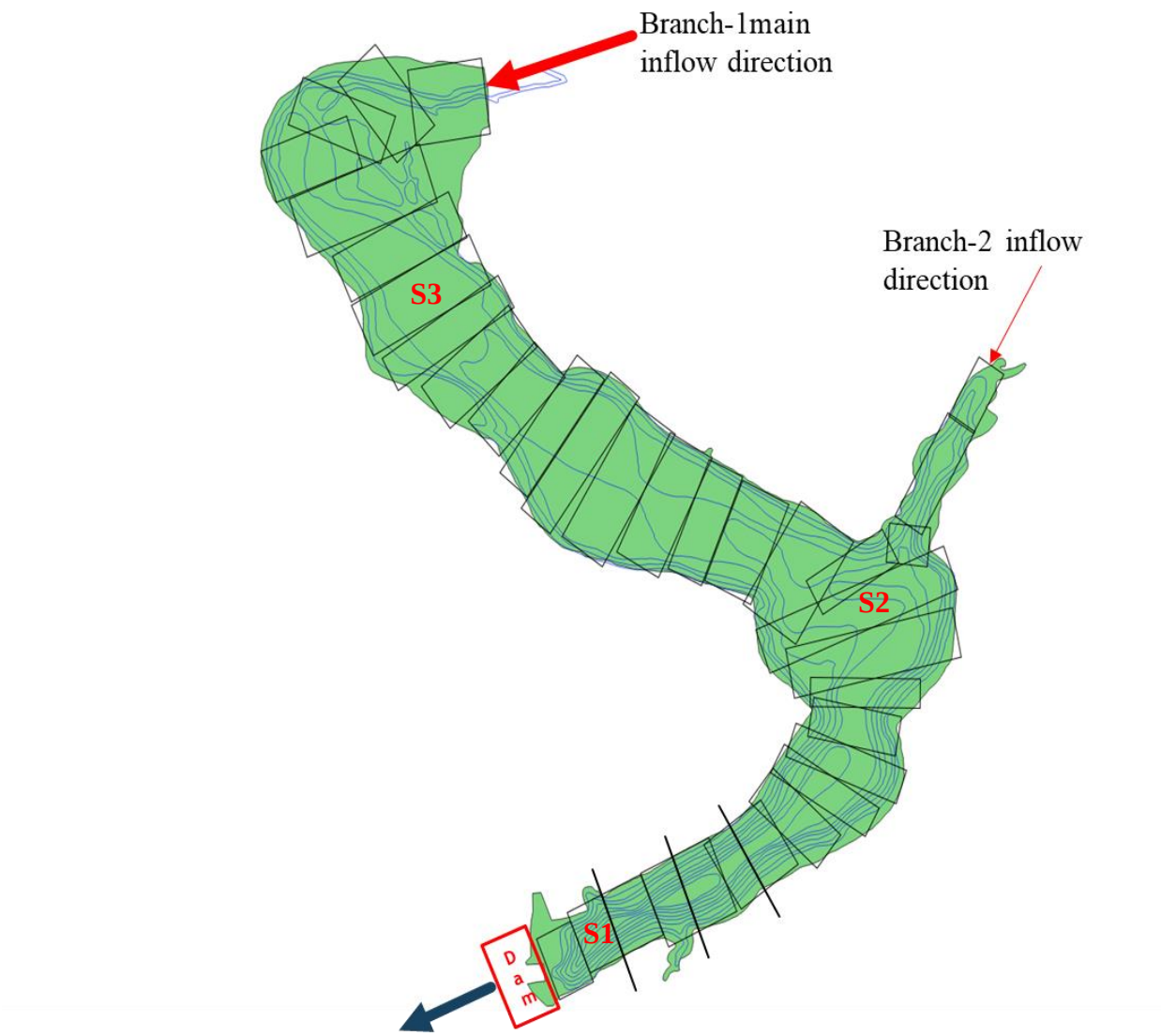

Figure 3-1. Conceptual grid diagram of Fanshawe Reservoir (Measurement sites is S1 to S3; Inflow has two branches, which indicated as red arrow; Dam outflow is located in the downstream area, which represents as dark blue arrow; Blue contour lines represents the depth information within the reservoir).

Table 3-2. Layer numbers and layer height in CE-QUAL-W2 bathymetry file (Layer 1 and Layer 19 are boundary layer).

Layer Number	Layer Height(m)
1	0.45
2	0.45
3	0.45
4	0.3
5	0.3
6	0.75
7	0.75
8	0.8
9	0.8
10	0.75
11	0.75
12	0.75
13	0.75
14	0.75
15	0.75
16	0.8
17	0.8
18	0.8
19	0.8

3.3.3 Model Domain Discretization

CE-QUAL-W2 is a two-dimensional model which need to convert the measured topographic data to the rectangular grids in the modeling file as the first modeling process. The physical grid model of the Fanshawe Reservoir was generated and calibrated through implementing the bathymetry data, creating the water inflow, water temperature and meteorological initial and boundary conditions modeling files, and creating the modeling control file in the CE-QUAL-W2 model. The topographical modeling results are crucial to the following modeling progress. For example, topographical modeling results highly affect the volume of the waterbody, which has essential effects on the water residence time, water flow direction and hydrodynamic characteristics in Fanshawe Reservoir. The following figures (Figure 3-2. a, b, c) demonstrated the top view, side view, and end view of the physical grid modeling results for Fanshawe reservoir. The 1, 34, 35, and 39 segments are boundary segments, which have zero width, and the lengths of these segments are same as the connective segments. In the physical grid model, Segment 2 - Segment 33 represent the main branch of Fanshawe Reservoir in the model. Segment 36, segment 37, and Segment 38 belong to the branch 2, which accounts for the water inflow from Wye Creek. Different segments have different segment lengths and widths, which obtained from the Land Information Ontario Metadata Management tool and edited with QGIS (Appendix A). Layer 1 and Layer 19 are boundary layers which have 0m as the layer height. The heights of layers in CE-QUAL-W2 model are usually from 0.2m to 5m (Cole and Wells, 2017), and the width of different layers are based on topographic data. In the current Fanshawe model, variable heights were applied to layer 2 – layer 18. The rotation of each segment was based on the average of the inflow direction of the water pathway (Appendix A). The water outflow structures were developed in the segment 33 based on the Fanshawe Dam information, such as water outflow elevation and daily discharge data. The main inflow (Branch 1) entered the waterbody from the Segment 2 and the minor inflow (Branch 2) entered the waterbody from the Segment 36. The modeling volume of the whole waterbody was 13,072,506 m^3. According to Nürnberg and Lazerte's study (2005), the morphometric volume of Fanshawe Reservoir is about 13,146,000 m^3, which is obtained from the hypsographic database of UTRCA. This measured volume was organized based on the observed data from year 1954 to year 2004. The volumetric variables may differ from previous studies because of the measurement errors of the hypsographic data. Comparing the current waterbody modeling volume with the morphometric

volume, the absolute error was only 0.56%. Therefore, the physical gird model of Fanshawe Reservoir well reproduced the volumetric characteristics and it is suitable for the calibration of the hydrodynamic and water temperature model.

Table 3-3. Modeling waterbody volume.

Name and Units	**Values**	**Description**
Hypsographic volume (m^3)	13,146,000	Differences: 0.56%
Waterbody volume (m^3)	13,072,506	
Branch 1 volume (m^3)	12,735,543	Modeling Results
Branch 1 volume (m^3)	336,963	Modeling Results

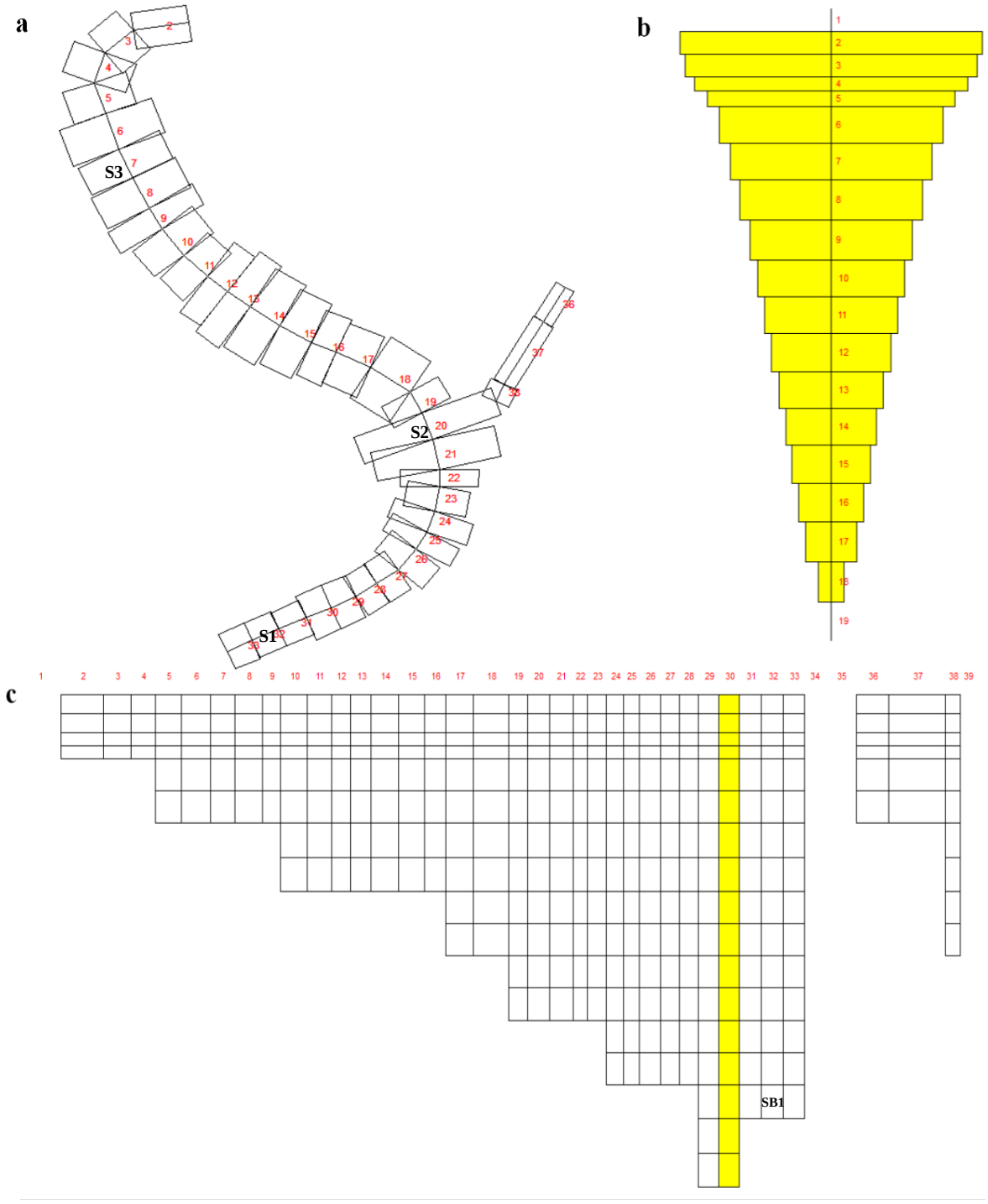

Figure 3-2. Grid modeling results: Top view(a), End view(b), and Side view (c) of the Fanshawe Reservoir (The yellow segment is the active segment for showing the side and end view, and measurement site 1 is at segment 32, measurement site 2 is at segment 20, and measurement site 3 is at segment 7; S1 to S3 are the measurement sites, and the SB1 is the bottom measurement stie).

3.3.4 Modeling Calibration and Validation

Hydrodynamic and water temperature results play significant roles in the water quality and sediment model because the variations of waterflow, water residence time, and water temperature have multiple effects on the transport of water constituents in the model. To obtain more reliable water quality modeling results, the calibrations and validations of hydrodynamic model are necessary for building the water quality and sediment model in the Fanshawe Reservoir. The 2018 flow data, meteorological data, and nutrients data were used to calibrate the parameters in the current model. The 2019 observed data were used to validate the water temperature, DO, biomass, and P in the Fanshawe Reservoir model. Bias or average error, Mean Absolute Error (MAE), and Root Mean Square Error (RMSE) were used in the assessment of modeling performance. These test methods are commonly used in the evaluation between the modeling work and field data (Afshar et al., 2011; Cole & Wells, 2017; J.Berger & Wells, 2008; Y. Kim et al., 2009; Shabani et al., 2017). The equations for Bias, AME, and RMSE are:

$$Bias = \frac{\sum_{i=1}^{n} X_{iobs} - X_{imod}}{n}$$

$$MAE = \frac{\sum_{i=1}^{n} |X_{iobs} - X_{imod}|}{n}$$

$$RMSE = \sqrt{\frac{\sum_{i=1}^{n} (X_{iobs} - X_{imod})^2}{n}}$$

Where n is the number of observations or modeling results; X_{iobs} is the observed data; X_{imod} is the modeling results. The high values of Bias, MAE, and RMSE illustrated the differences between modeling results and measured data. When the Bias, MAE, and RMSE close to 0, it indicated that the modeling results perfectly reproduce the field data.

The Fanshawe Reservoir simulation results were able to reasonably reproduce following characteristics in the Fanshawe Reservoir. The water level (Figure 3-3), water residence time, and water temperature (Figure 3-4 to Figure 3-5) are well simulated and feasible for applying in other scenarios. The Bias, MAE and RMSE of original water flow model were 7.65m, 7.68m, and 8.25m, respectively, which may be caused by multiple reasons. For example, the inflow stage may have some incorrect measured data, and the upstream inflow measured stage is 15km away from the

Fanshawe Reservoir. Exploring the water level is beyond the scope of the current study. The current research goal was to focus on reservoir water quality (such as P and DO dynamics). Therefore, the daily adjustment of water level was implemented into the water level model for promoting an accurate hydrodynamic system and minimizing the error that caused through water budget. After calculating the water difference between observed data and modeling results, the distributed tributary inflows were implemented into the model. The distributed tributary inflows, which represent non-point sources loading of water, are useful in accounting for missing flows for the water budget (Cole and Wells, 2017). The differences between the theoretical modeling water level results and measured data were less than 1%. The Bias, MAE and RMSE are -0.04m, 0.04m, and 0.05m, respectively. The average modeling water residence time is about 10 days, consistent with the long-term report data from Nürnberg and Lazerte's study. Water temperature data are required for the water quality and sediment model because temperature has essential effects on the chemical reaction and bioactivities. The fate of biomass, water column nutrients, and sediment nutrients is significantly affected by the variation in water temperature. The surface water temperature simulation results reasonably fit the variation of the observed water temperature in Fanshawe Reservoir (Figure 3-4). The measured data were measured once every two weeks and obtained from using two methods: the first measured method is RBR XR-620 profile data. Another measured method is YSI method. These two measurement methods both measured the temperature of water samples in the field. The vertical variables of profile data(RBR XR-620), such as vertical temperature and vertical dissolved oxygen (DO) are more accurate than YSI measured data because YSI measured water sample were pumped from the bottom reservoir, which may have caused some errors in the final measurement results. For instance, the pumped water may be heated before the measurement.

The modeling results reasonable reproduced the 2018-2019 surface water temperature in the Fanshawe Reservoir. Some outliers occurred, such as the surface water temperature at September 5th 2018, which may be caused by the limitations in the CE-QUAL-W2 model the measurement errors mentioned above. The absolute errors of surface water temperature range from 0.036 ℃ to 3.29 ℃. The Bias of surface water temperature is 0.74℃. The MAE and RMSE of surface water temperature are 1.04℃ and 1.39℃, respectively. The highest error is 3.29℃ on June 19th 2019, which may be caused by the assumptions in the CE-QUAL-W2 model. For example, the cloud in the meteorological data was assumed by the order of number from 1 to 10. The surface temperature

may be not very accurate represented at this day. To sum up, although there are some uncertainties of the current modeling results, such as, the surface water temperature at September 5th 2018, and June 19th 2019, the Bias, MAE and RMSE assessment of the current water temperature modeling results illustrated that the surface water temperature profiles of Fanshawe Reservoir were very well reproduced. The simulation results also provided reliable and valid surface water temperature for following research objectives.

Thermal stratification of Fanshawe Reservoir has significant effects on the dynamic systems of DO and bioactivities. To evaluate the water temperature in the whole reservoir at different depth, The vertical water temperature were also simulated and output for Fanshawe Reservoir during 2018 to 2019 modeling year (Figure 3-5 and Figure 3-6). The measured data are also measured once every two weeks and some measured data are not available due to the weather limitations. For example, the vertical water temperature is not available in the wintertime. The modeling results reasonably reproduced the vertical water temperature for Fanshawe Reservoir and was able to estimate the vertical water temperature during different seasons in the Fanshawe Reservoir. The differences of vertical water temperature range from -3.0 ℃ to 2.6 ℃. The bias between observed data and modeling results ranges from -0.7℃ to 2.0℃. The MAE ranges from 0.1℃ to 2.0℃. The RMSE ranges from 0.1℃ to 2.1℃. There are still some errors displayed between modeling results and measured data. The modeling results underestimated the vertical temperature on April 10th 2018 and April 10th 2019 (Figure 3-5 and Figure 3-6). The vertical water temperature on May 29th 2018 (Day 149) is underestimated at the top of the water and overestimated from 2m to 6m. The differences may be caused by the assumptions in the model and measurement errors. For example, the WSC input file control the wind effects on the whole system. Wind induced current has significant effects on the shallow reservoir. The low values in WSC file may underestimate the thermal stratification in the reservoir. The measured vertical water temperature may be also limited by the measured errors. For example, measured equipment has small oscillation at the measured depth; The vertical water temperature profile may not accurately perpendicular to the bottom of the reservoir, and the measured equipment may also influence by aquatic plants.

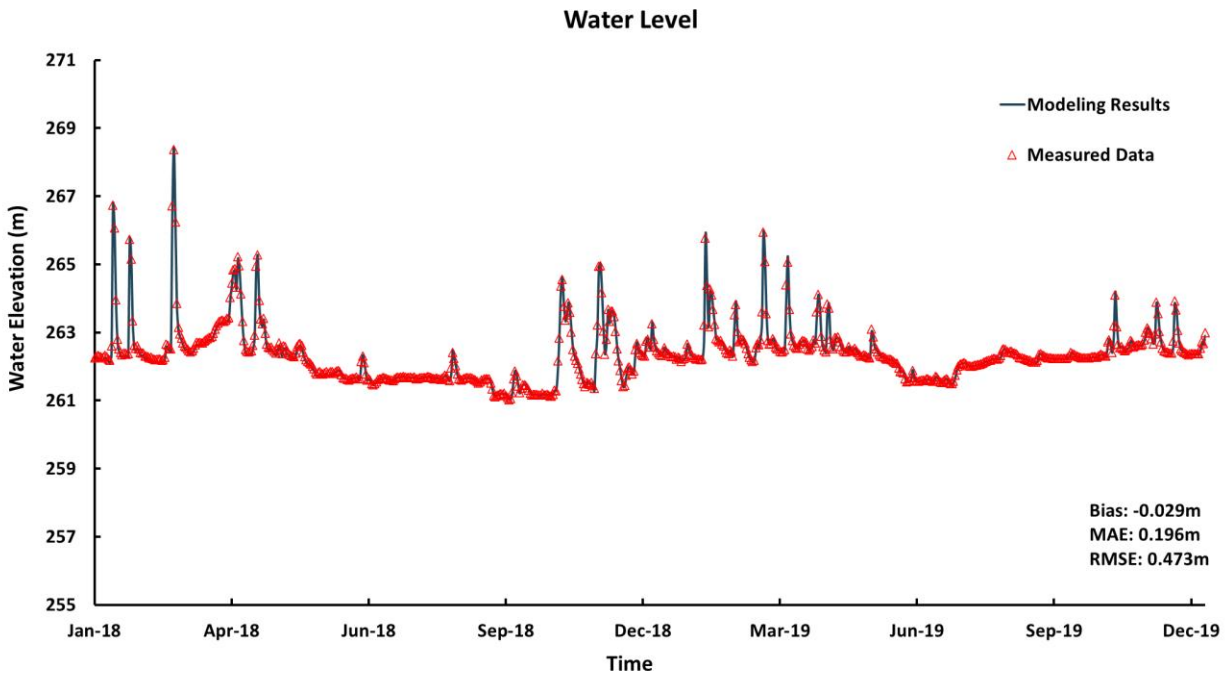

Figure 3-3. Comparison of the theoretical water surface elevation simulation results with measured data in Fanshawe Reservoir from 2018 to 2019.

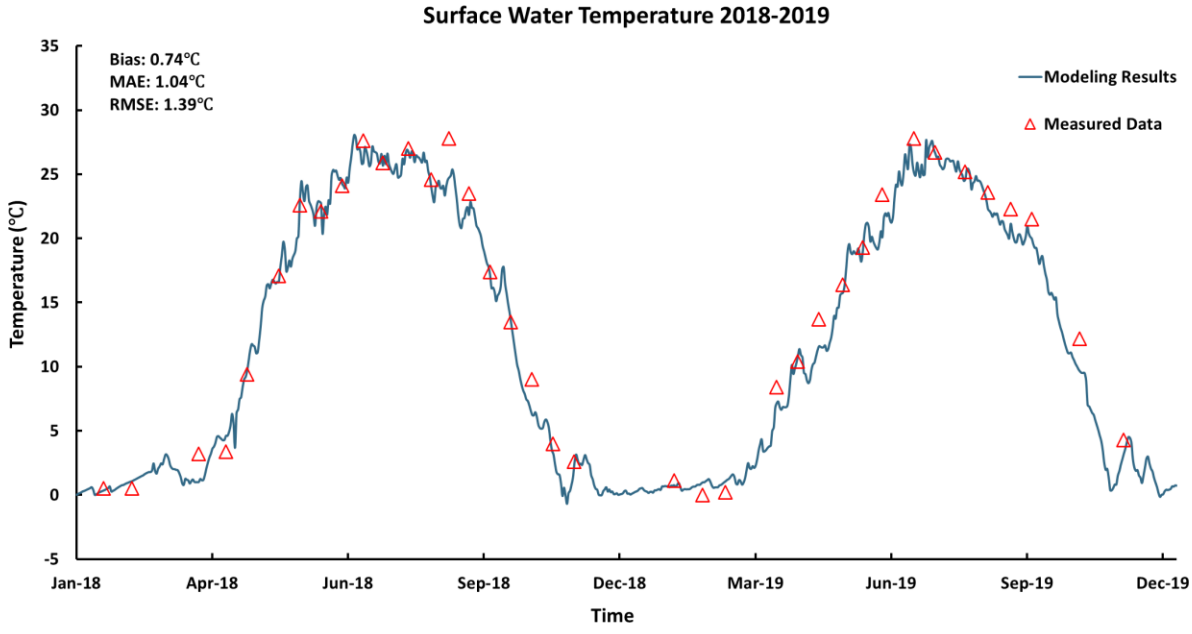

Figure 3-4. Comparison of surface water temperature simulation results with measured data in Fanshawe Reservoir.

To have a better view of the whole reservoir thermal structures, the seasonal spatial distributions of water temperature were generated for Fanshawe Reservoir (Figure 3-7 to Figure 3-8). Thermal structures of Fanshawe Reservoir were displayed well from 2018 to 2019 in the current modeling work : the Fanshawe Reservoir was well mixed during spring and fall season; Stratifications of Fanshawe Reservoir occurred during summertime, and low-temperature water with minor stratifications appeared in winter season. Due to the shallow depth of Fanshawe Reservoir, the variation of thermal structures in wintertime is very small: The largest differences between bottom water temperature and top water temperature are 1.1 ℃ at 2018 and 1.3℃ at 2019. In addition, the hydrodynamic and water temperature modeling results were not only able to simulated in the measured sites but also extended to the entire waterbody (Figure 3-7 and Figure 3-8).

In summary, the topographical, hydrodynamic, and water temperature CE-QUAL-W2 modeling results are highly similar with previous report data and measured data. Reasonable and feasible water level was produced and was extended across the whole Fanshawe Reservoir. Reasonable water temperature modeling results was reproduced and was able to predict the water temperature in the whole reservoir system. Thermal structures occurred in the summertime during 2018 to 2019 modeling year. Wintertime and these thermal structures were simulated for all seasons.

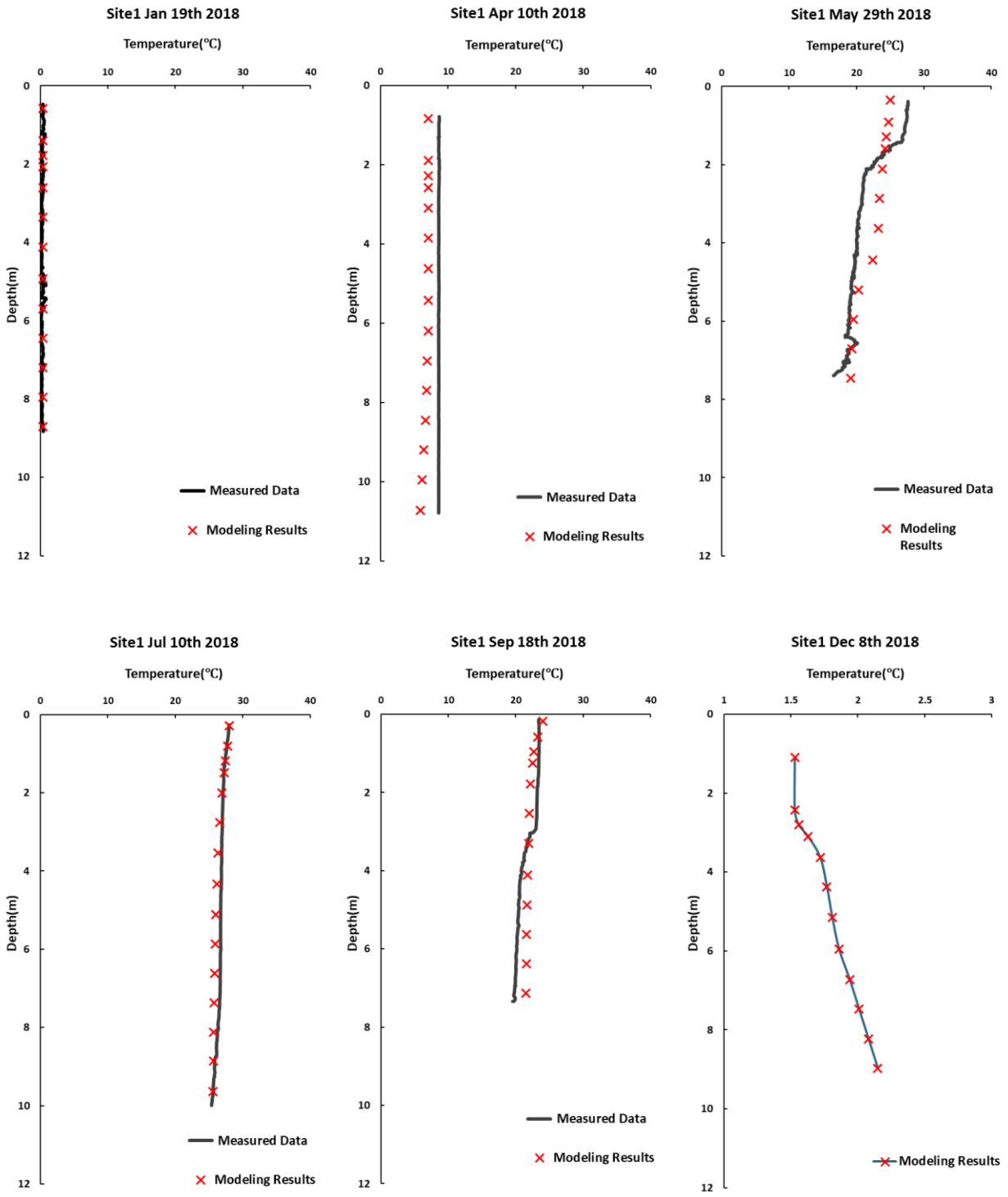

Figure 3-5. Vertical water temperature simulation results versus measured data in Fanshawe Reservoir at 2018 year (Black lines are measured data; Red crosses are modeling results).

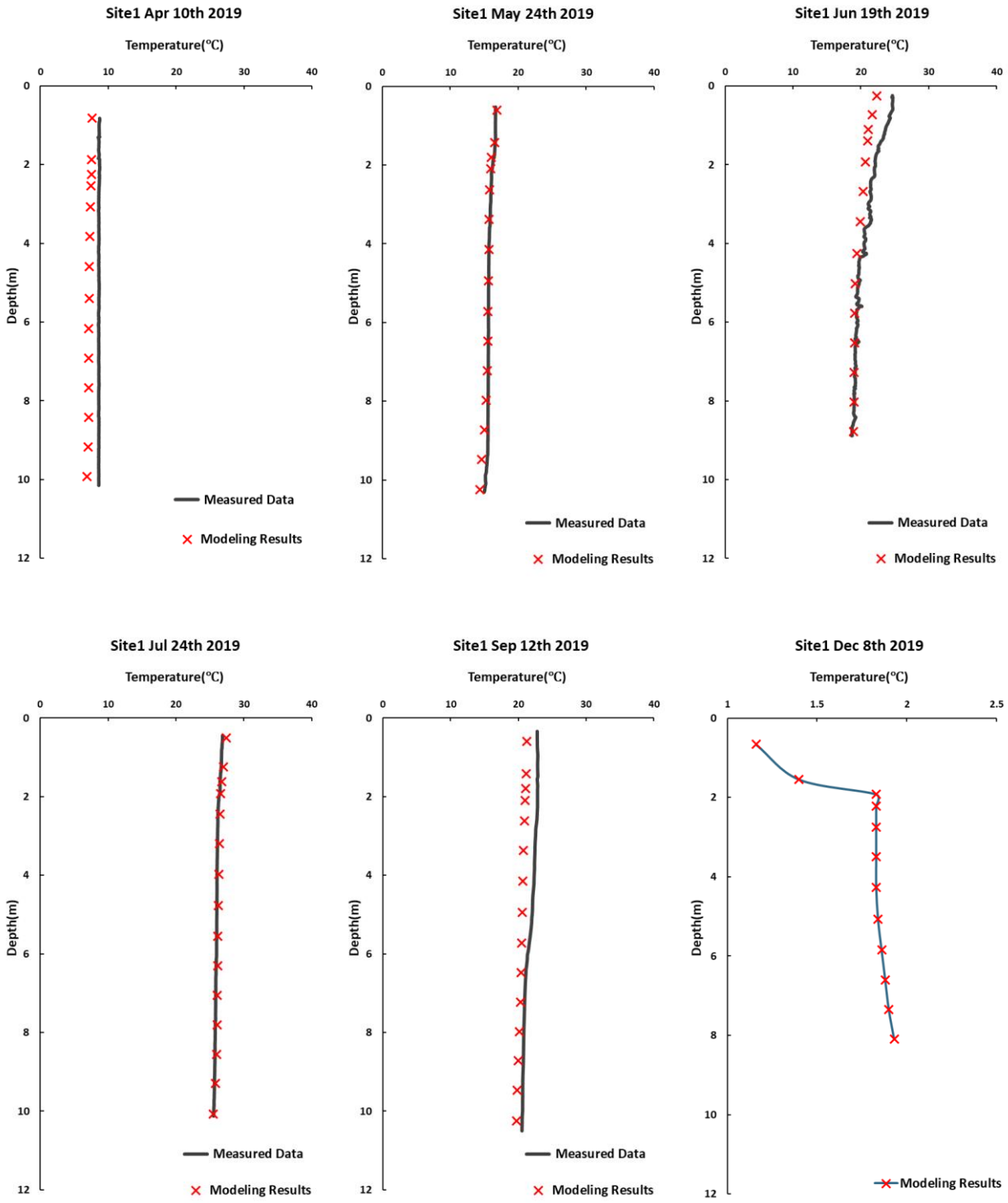

Figure 3-6. Vertical water temperature simulation results versus measured data in Fanshawe Reservoir at 2019 year (Black lines are measured data; Red crosses are modeling results).

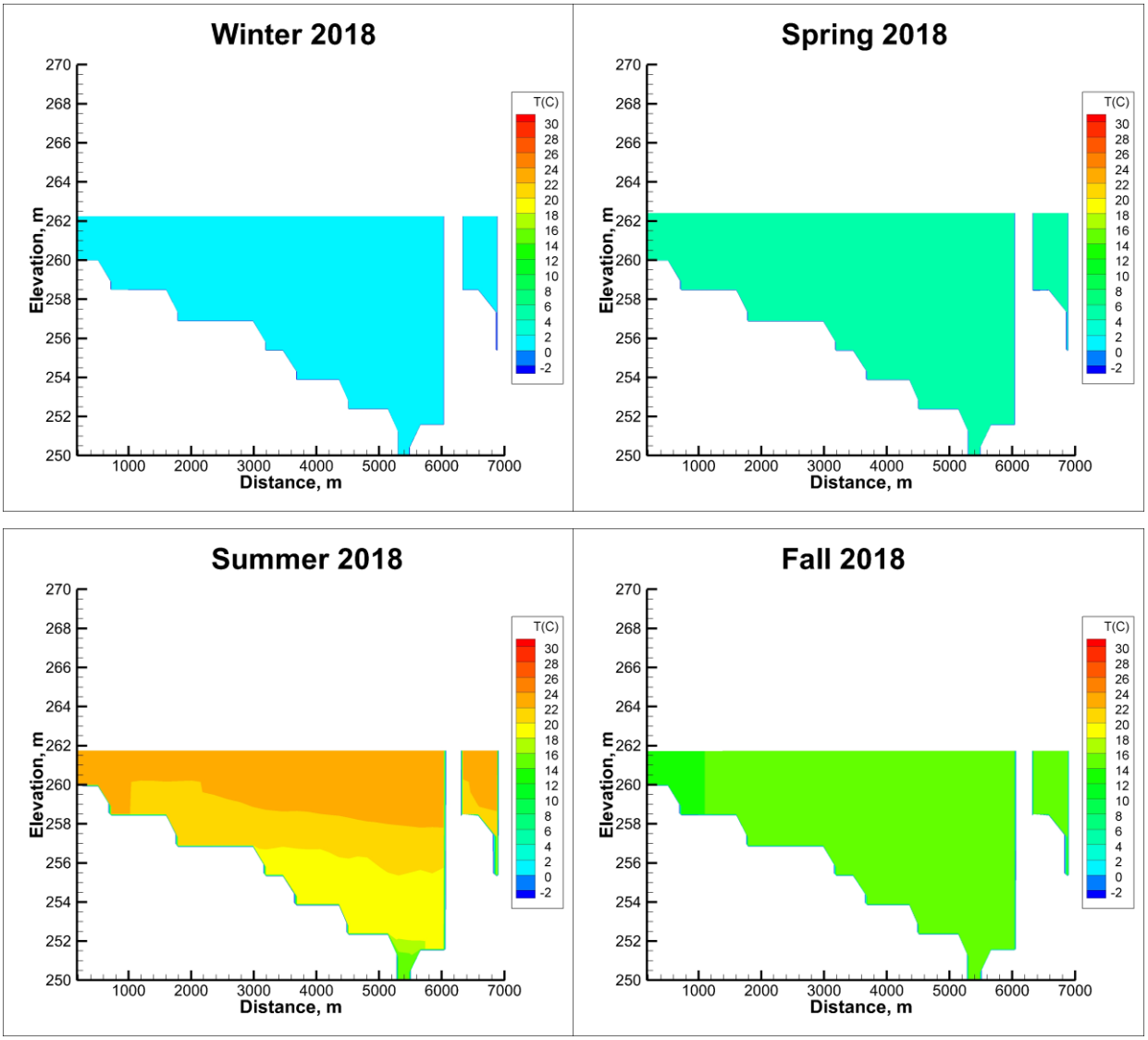

Figure 3-7. Spatial distribution of water temperature for whole Fanshawe Reservoir in different season at 2018 (Segments 2-33 were plotted from 0m to 6000m; Segments 36-38 were plotted from 6300m-7000m).

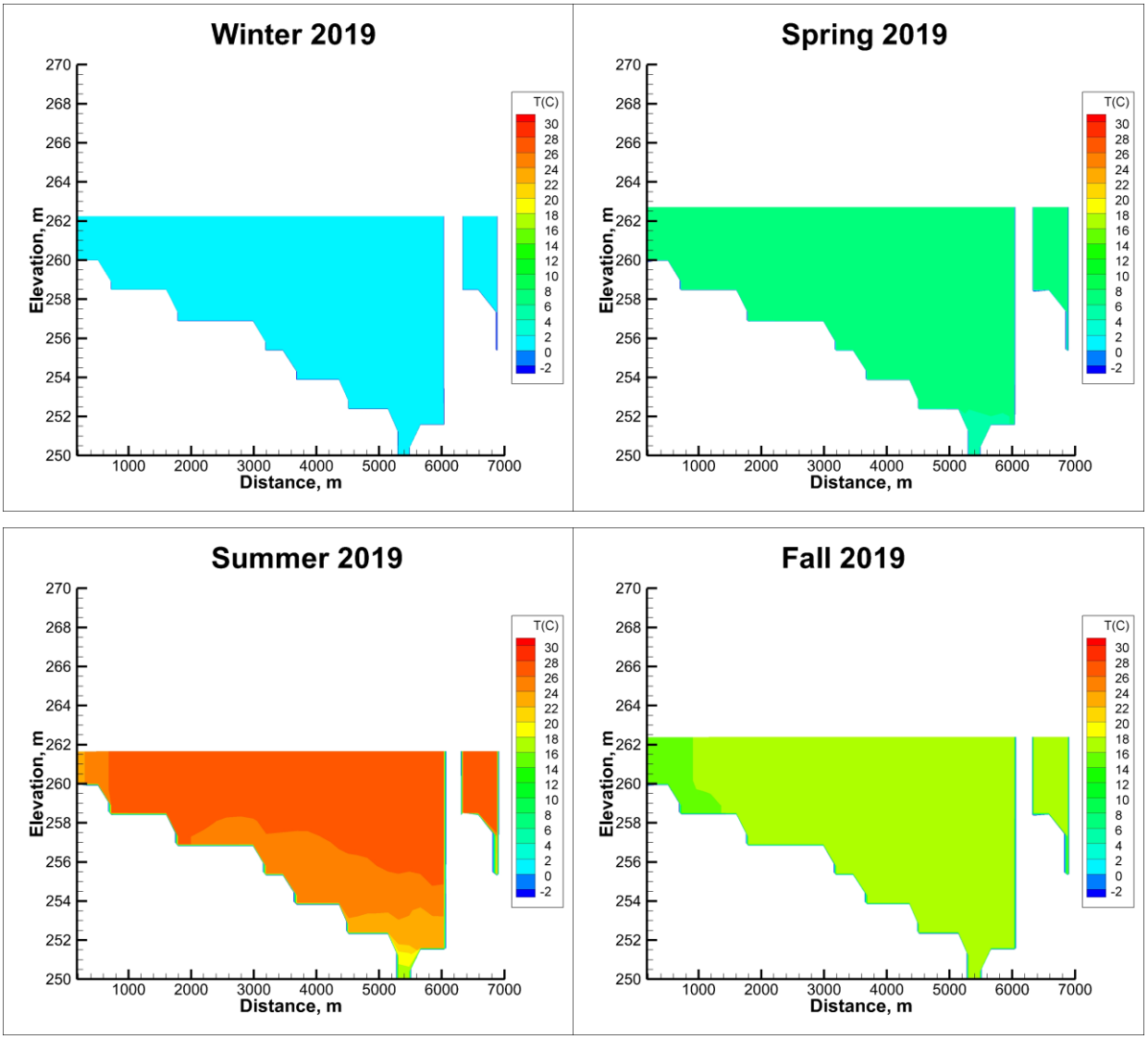

Figure 3-8. Spatial distribution of water temperature for whole Fanshawe Reservoir in different season at 2019 (Segments 2-33 were plotted from 0m to 6000m; Segments 36-38 were plotted from 6300m-7000m).

Monitoring dammed reservoirs located in high-latitude areas is significantly reduced during low temperature seasons. For example, water quality samples are not easy to take in the Fanshawe Reservoir in the winter, and therefore water quality is hard to consistently monitored. Therefore, the ice cover model may help fill in these gaps, and lead to more accurate sediment and water quality modeling results. Furthermore, the water quality model with ice cover information can help government monitor and regulate reservoirs during the wintertime, which can may improve the effectiveness of water quality management.

An ice cover model was developed in the current CE-QUAL-W2 model. The modeling results successful provided ice thickness of Fanshawe Reservoir during the modeling year (Figure 3). In the 2018 wintertime, there was 56 days that ice formed in the Fanshawe Reservoir. The maximum ice thickness was 0.25m and the average ice thickness was 0.10 m. In the 2019 wintertime, there was 87 days that ice formed in the Fanshawe Reservoir. The maximum ice thickness was 0.283m and the average ice thickness was 0.09m. Due to the weather limitation, measured data only have 5 points. The average error is 0.11m and the RMSE is 0.13m. The differences may be caused by the modeling assumption and measured errors. For instance, the meteorological data may not accurate in the winter at low temperature and extreme weather, and the assumptions of the cloud information may not accurately display the actual environment at that specific day. In additions, the measured data were measured through rule. It may not uniform for the different location. However, the current ice cover model successful simulated the ice thickness during the wintertime. It is first step for the ice cover model in the Fanshawe study. In summary, the current ice cover model provided reasonable information on the ice information in Fanshawe Reservoir. Further model calibration may be possible through the detailed measurement of ice thickness in the future.

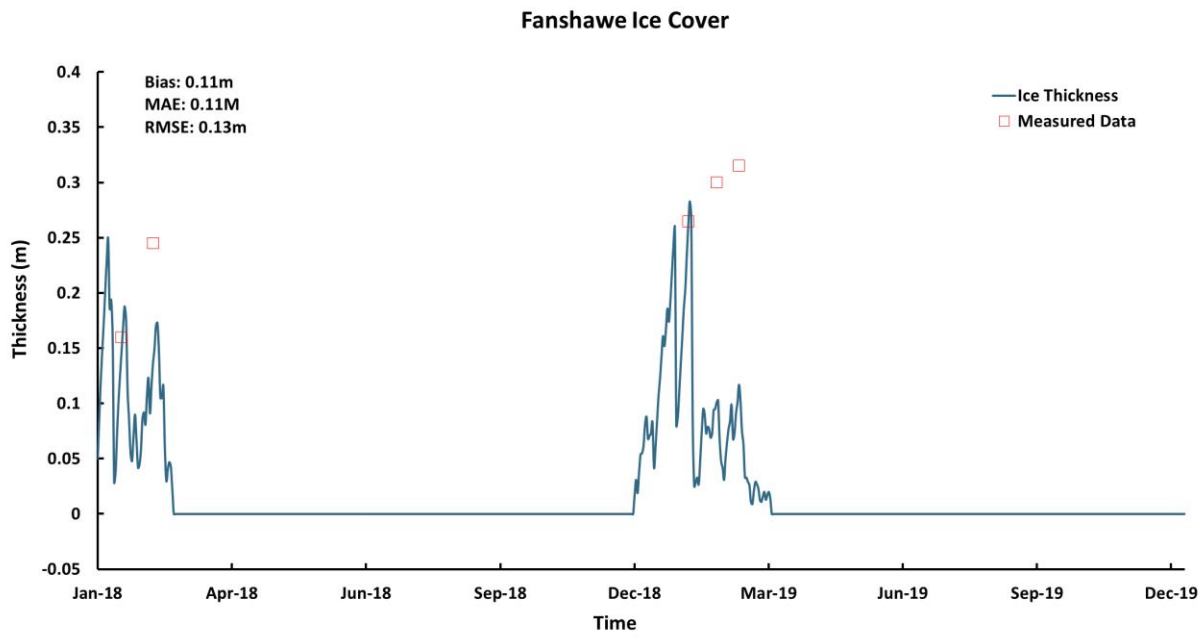

Figure 3-9. Ice cover thickness in Fanshawe Reservoir from 2018 to 2019.

3.4 Results and Discussions

3.4.1 DO Dynamics and Scenarios

3.4.1.1 DO Dynamics

Inferior water quality and the observation of blue-green algae in TRW have caused people to pay more attention to the water quality effects on the Great Lakes. The water quality has been significantly affected by the bloom of blue-green algae. For instance, harmful cyanobacterial blooms (cHABs) have significantly negative effects on water quality and management in lakes and reservoirs because cyanobacteria produce cyanotoxins(Becker et al., 2009; Carmichael & Boyer, 2016; Watson et al., 2008). Oxygen dynamics are important to determine the water quality in Fanshawe Reservoir. For example, algae and other biomass can be affected by the DO concentration in the water column through photosynthesis and respiration. In addition, the DO concentration in the bottom water has significant effects on the sediment model because of changing redox reactions. Therefore, the development, calibration and validation of the DO model are very important for detailed understanding of P transport and biomass growth in Fanshawe Reservoir. In the current model, surface and bottom time series DO concentrations, and spatial distribution of DO concentrations were simulated (Figure 3-10 to Figure 3-13).

The modeling results well captured the trend of surface and bottom DO during 2018 and 2019 modeling year. The surface DO time series modeling results and measurement data had differences between the measured data and the modeling results, which ranged from -2.28 mg L^{-1} to 0.77 mg L^{-1} and the Bias was -0.21 mg L^{-1} (Figure 3-10). The MAE and RMSE of surface DO were 0.56 mg L^{-1} and 0.81 mg L^{-1}, respectively. The negative bias value illustrated that the modeling results overestimated the surface DO concentrations. The largest error date is June 19th 2019. In the bottom DO time series modeling results, the differences between measured data and modeling results ranged from -1.4 mg L^{-1} to 9.2 mg L^{-1} (Figure 3-11). The Bias was 1.83 mg L^{-1}, the MAE was 2.10 mg L^{-1}, and the RMSE was 3.32 mg L^{-1}. The positive value of Bias reflected the modeling results underestimated the bottom DO concentrations. The largest error of bottom DO was July 10th 2019. Bottom DO measured data amount was limited by the field profile data. The measured equipment was failed in some measured days. The differences between modeling results and measured data may be caused by measurement errors and the uncertainties of the current model. For instance, the DO measured data were not directly measured after the water sampling. Bottom DO measured equipment was not available and stable; The modeling

assumptions for input biomass (algae) may not accurate, which may influence the surface and bottom DO concentrations through photosynthesis. In addition, the accuracy of water temperature modeling results also has effects on the DO modeling results because of the bioactivities, the exchange between DO and atmosphere. The spatial distribution of DO strongly suggests that anoxia develops in the deeper pats of Fanshawe Reservoir at the summertime (Figure 3-12 to Figure 3-13). The depletion of DO in summertime of 2019 was more intensive than the depletion of DO in summertime of 2018. In the spring and winter time, DO was well mixed in the whole Fanshawe Reservoir.

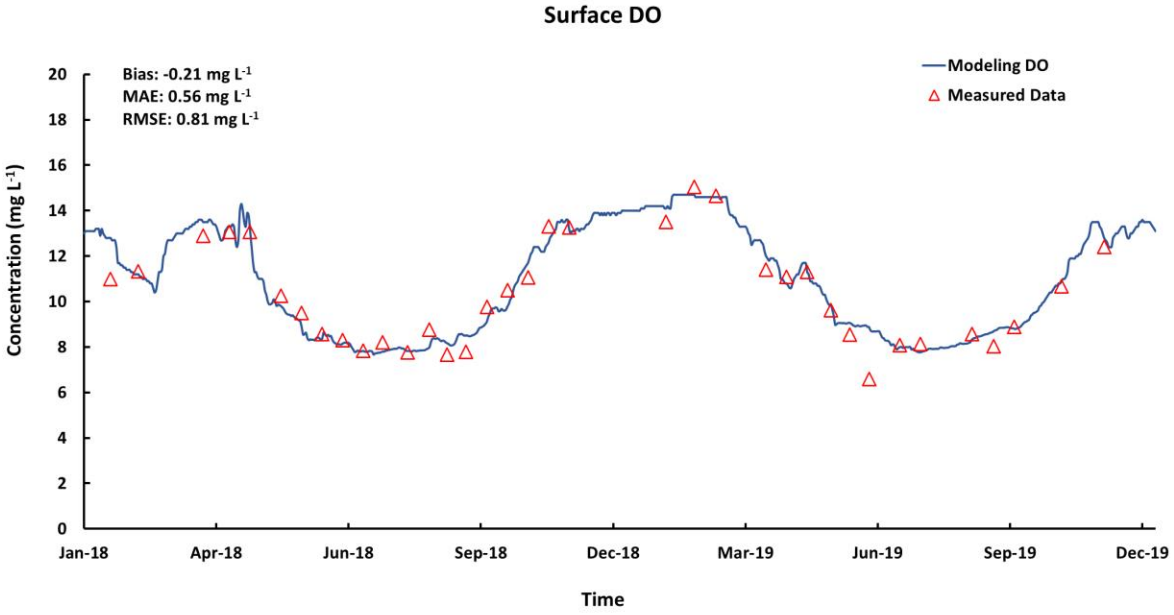

Figure 3-10. Surface DO simulation results with measured data in Fanshawe Reservoir from 2018 to 2019.

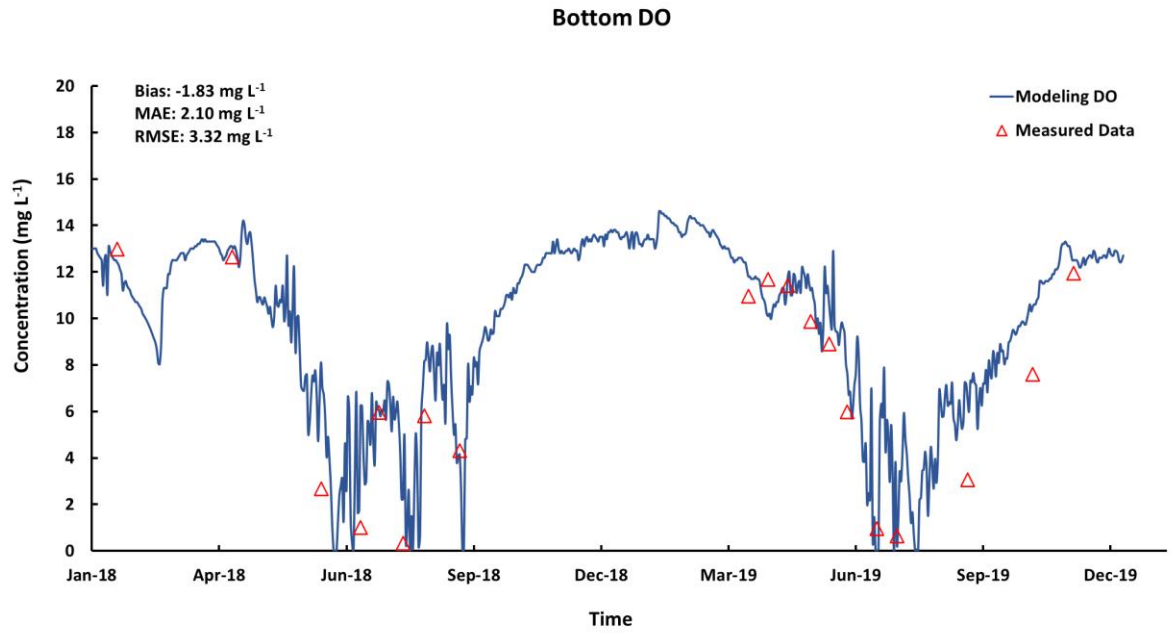

Figure 3-11. Bottom DO simulation results with measured data in Fanshawe Reservoir from 2018 to 2019.

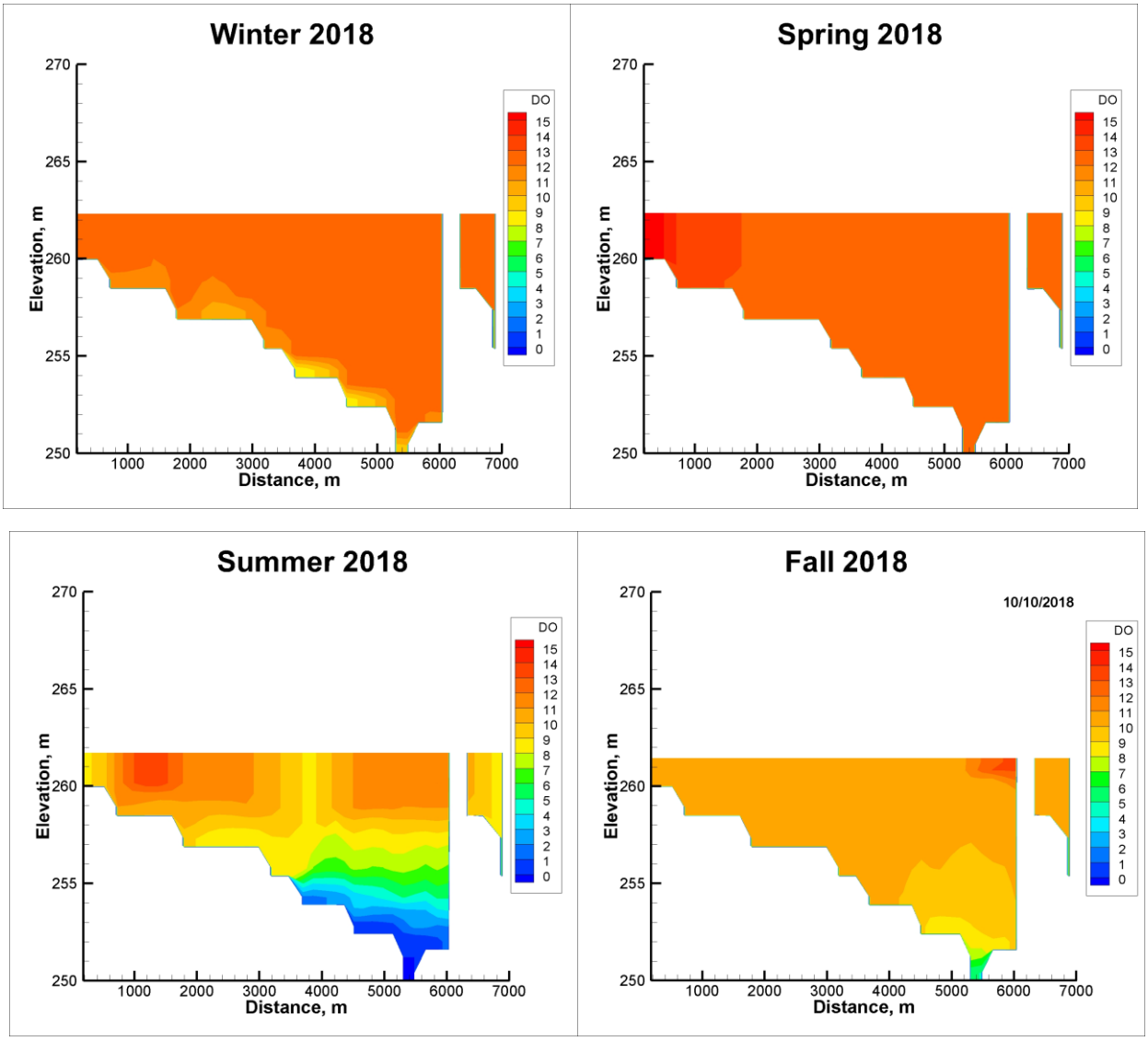

Figure 3-12. Spatial distribution of DO for whole Fanshawe Reservoir at 2018 in different season at 2018 (Segments 2-33 were plotted from 0m to 6000m; Segments 36-38 were plotted from 6300m-7000m).

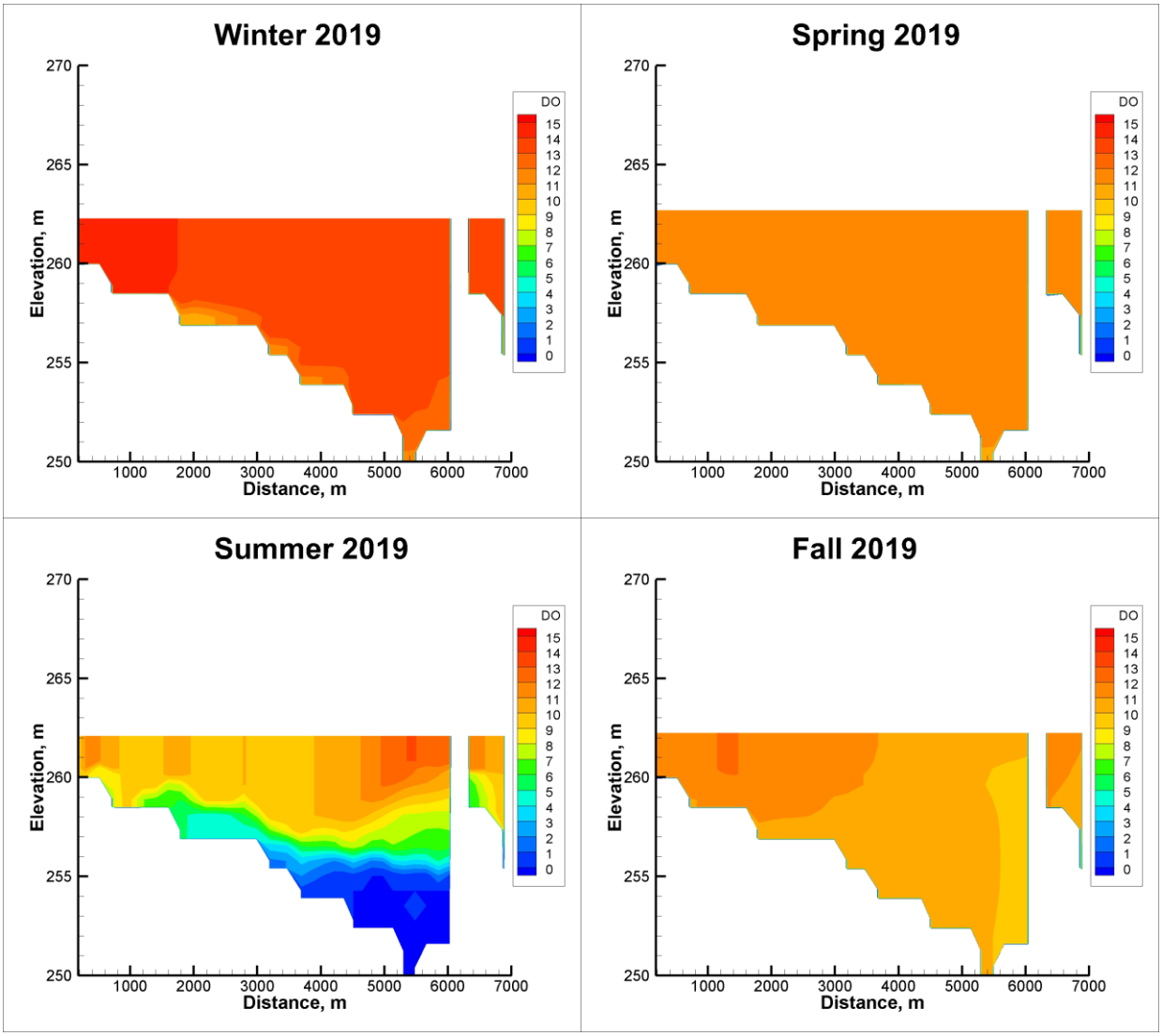

Figure 3-13. Spatial distribution of DO for whole Fanshawe Reservoir in different season at 2019 (Segments 2-33 were plotted from 0m to 6000m; Segments 36-38 were plotted from 6300m-7000m).

3.4.1.2 DO Scenarios

To examine sediment and biomass effects on DO dynamics in Fanshawe Reservoir, two different scenarios were applied in the current modeling study. The current DO scenarios focused on the DO depletion and provide discussion on the bottom DO concentration in Fanshawe Reservoir. Further algal scenarios were simulated flux dynamics. The first scenario was the DO dynamics without the effects of biomass: Input algae was set as zero, and algal growth rate was also set as zero. The bottom DO concentrations had big differences from May to September in the two modeling years (Figure 3-14). With the algal effects, depletion of DO happened from late May to late September. However, without the algal effects, bottom depletion of DO disappeared during the modeling year. At the beginning of the algal growth (early May 2018 and early May 2019), the original DO concentration is higher than the DO-NoAlgae because of the photosynthesis of the algae group produced oxygen to the water column, however, the following enrichment and death of algae in the reservoir caused the depletion of DO in the deeper part of the reservoir. The largest DO difference was 7.78 mg L^{-1} during the summertime. According to EPA regulation, all fish will dead when the DO concentration below 3 mg L^{-1}. This DO scenarios revealed that algal blooms play significant roles in the depletion of DO in reservoir systems. The second scenario was the DO dynamics without the effects of sediment. In the current model, the sediment provided P for the growth of algae. If the sediment module is removed from the current modeling study, DO concentration will increase 0.97 mg L^{-1}during the modeling period. Although the variation of DO concentrations existed in summertime and fall time, the depletion of DO did not happen during the summertime and fall time.

In summary, DO modeling study well reproduced and reasonable predict the DO distribution during different year. The depletion of DO happened in the summertime of 2018 and 2019. DO concentrations were highly controlled by the biogeochemical processing of biomass and sediment in bottom reservoir during the summertime and fall time at Fanshawe Reservoir. Sediment could provide more nutrients for the growth of algae. The enrichment and death of algae caused the depletion of DO in the deeper part of Fanshawe Reservoir.

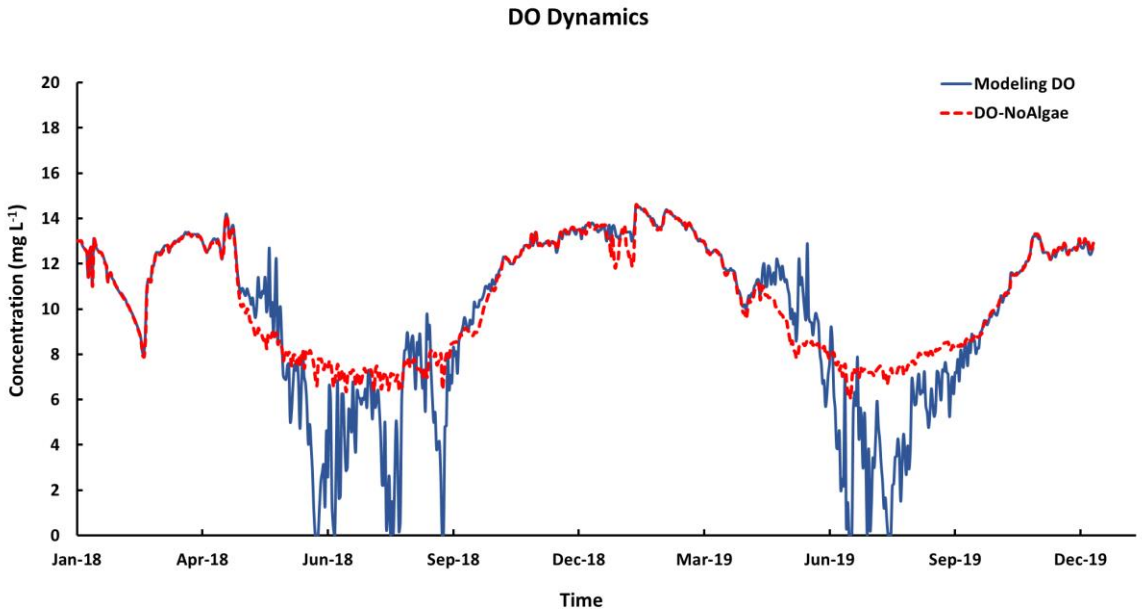

Figure 3-14. DO dynamics without algal effects.

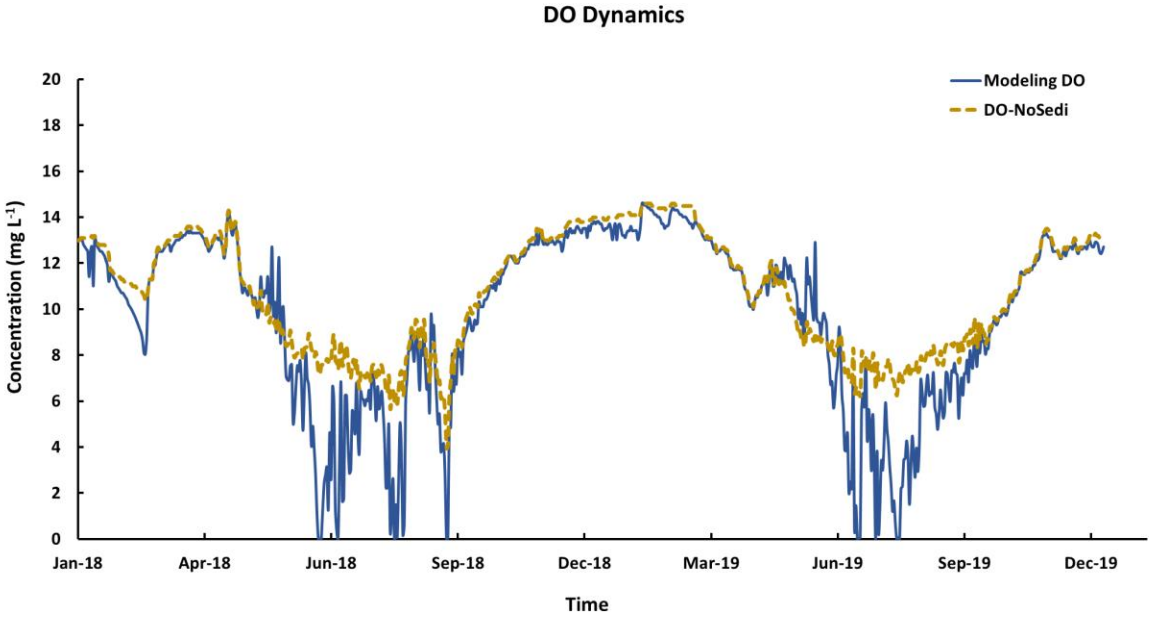

Figure 3-15. DO dynamics without sediment effects.

3.4.2 P Dynamics, Internal Loading and Scenarios

3.4.2.1 P Dynamics

The biomass of algae and other vegetation are significantly influenced by water temperature and nutrient concentrations in the waterbody. Phosphorus is the primary limiting nutrient for the biomass breeding in the lake systems (Schindler 1974, Schindler et al., 2008). The seasonal variation of dissolved reactive phosphate (DRP) and total phosphorus (TP) were simulated and analyzed in a water quality and sediment model described above (Figure 3-16 to Figure 3-18). The surface and bottom DRP and TP, and downstream DRP and TP modeling results were compared with measured data from 2018 to 2019 year (Figure 3-16 to Figure 3-18). According to Amanda Niederkorn and Nady Kao's field data, in the site 1 (before the dam), there are 36 measured DRP and TP for surface layer from 2018 to 2019, and 35 measured DRP and TP for bottom layer from 2018 to 2019. The first measurement started on January 19th, 2018 and the last measurement was on November 26th, 2019.

The modeling DRP and TP results captured most of the variation of surface and bottom DRP and TP during 2018 and 2019 modeling year. The surface DRP results had some differences between the modeling results and measured data. The error ranged from -0.075 mg L^{-1} to 0.069 mg L^{-1}, and the Bias was 0.004 mg L^{-1}. The MAE for modeling DRP and measured DRP was 0.016 mg L^{-1}. The RMSE for surface DRP was 0.024 mg L^{-1}. The surface TP results had differences between modeling results and measured data which ranged from -0.29 mg $L^{-1}$to 0.25 mg L^{-1}. The bias was 0.017 mg L^{-1}. The MAE and RMSE for modeling DRP and measured DRP were 0.054 mg L^{-1} and 0.023 mg L^{-1}, respectively. Low DRP concentration during summertime reflected that algae and biomass uptake the DRP as their growth nutrients. The modeling results overestimated the surface DRP and TP in the February 20th and March 7th 2019. On June 19th 2019 and August 28th 2019, modeling DRP and TP underestimated the concentrations in the reservoir. In bottom layer, the error of bottom DRP ranged from -0.18 mg L^{-1} to 0.11 mg L^{-1}. The Bias was -0.015 mg L^{-1}. The MAE for modeling DRP and measured DRP was 0.038 mg L^{-1}. The RMSE for bottom DRP was 0.057 mg L^{-1}. The error of bottom TP ranged from -0.39 mg L^{-1} to 0.23 mg L^{-1}. The Bias was -0.015 mg L^{-1}. The MAE for TP was 0.068 mg L^{-1}. The RMSE for bottom DRP was 0.103 mg L^{-1}. Comparing the surface and bottom DRP and TP concentrations is important for further understanding of the fate of P in the waterbody and water-sediment interface. The knowledge from

long-term modeling results may inform government decisions to implement more regulations on the reservoir for water quality management.

The downstream P loading is important for downstream water quality management and further understanding of the fate of P (Figure 3-18 to Figure 3-19). According to the current modeling results and measured data, the peak P loading to downstream usually happens during high flow season, such as spring and fall. The highest modeling loading of DRP is 3011 kgP day^{-1}, and TP is 7927 kgP day^{-1}. The average differences for DRP and TP were -10.59kgP day^{-1} and 67 kgP day^{-1}. Total TP loading to the downstream area was 241.2 tones. The average TP loading was 120.6t $year^{-1}$(Figure 3-19). These values are similar with previous report (Nürnberg & Lazerte, 2005) and Nady Kao's work, which is not published yet. According to the current modeling results, retention efficiency of P in Fanshawe Reservoir was calculated as 19.7% (Figure 3-19). Previous research demonstrated that the worldwide TP retention in dammed reservoir is about 12% from 1970 to 2000 (Maavara et al., 2015). Concentration - Discharge (CQ) relationship of DRP displayed flatterning of the trend for outflow DRP (Figure 3-20). In general, it means the concentration of DRP becomes less dependent on the discharge due to the biogeochemical processing of P in the reservoir (Godsey et al., 2009; Hunsaker & Johnson, 2017). For example, the internal P loading, and algal uptake had significant effects on the DRP concentration in the reservoir.

In summary, surface DRP and TP modeling results were able to reasonably capture most of the DRP and TP concentration trends during from 2018 to 2019 in the Fanshawe Reservoir. Water temperature was observed to have notable effects on the variation of DRP and TP concentrations because most of the growth of biomass and other chemical reactions are temperature dependent. DRP depletion occurred in the summertime because of the algae blooms. The biogeochemical processing of P in the reservoir makes C-Q relationship become more chemostatic. Due to the biomass and sediment effects during summertime, the variation of bottom DRP and TP concentrations is more inconsistent than surface DRP and TP concentrations. The bottom DRP and TP concentrations are also much higher than the surface DRP and TP concentrations. The current modeling results still have some uncertainties in the DRP and TP concentration results, which may be caused by the limitations in the input modeling data and modeling coefficients. For example, the assumptions of P species and biomass data of input data may cause differences

between modeling results and measured data. Biomass did not have measured data, and some algal input data were estimated.

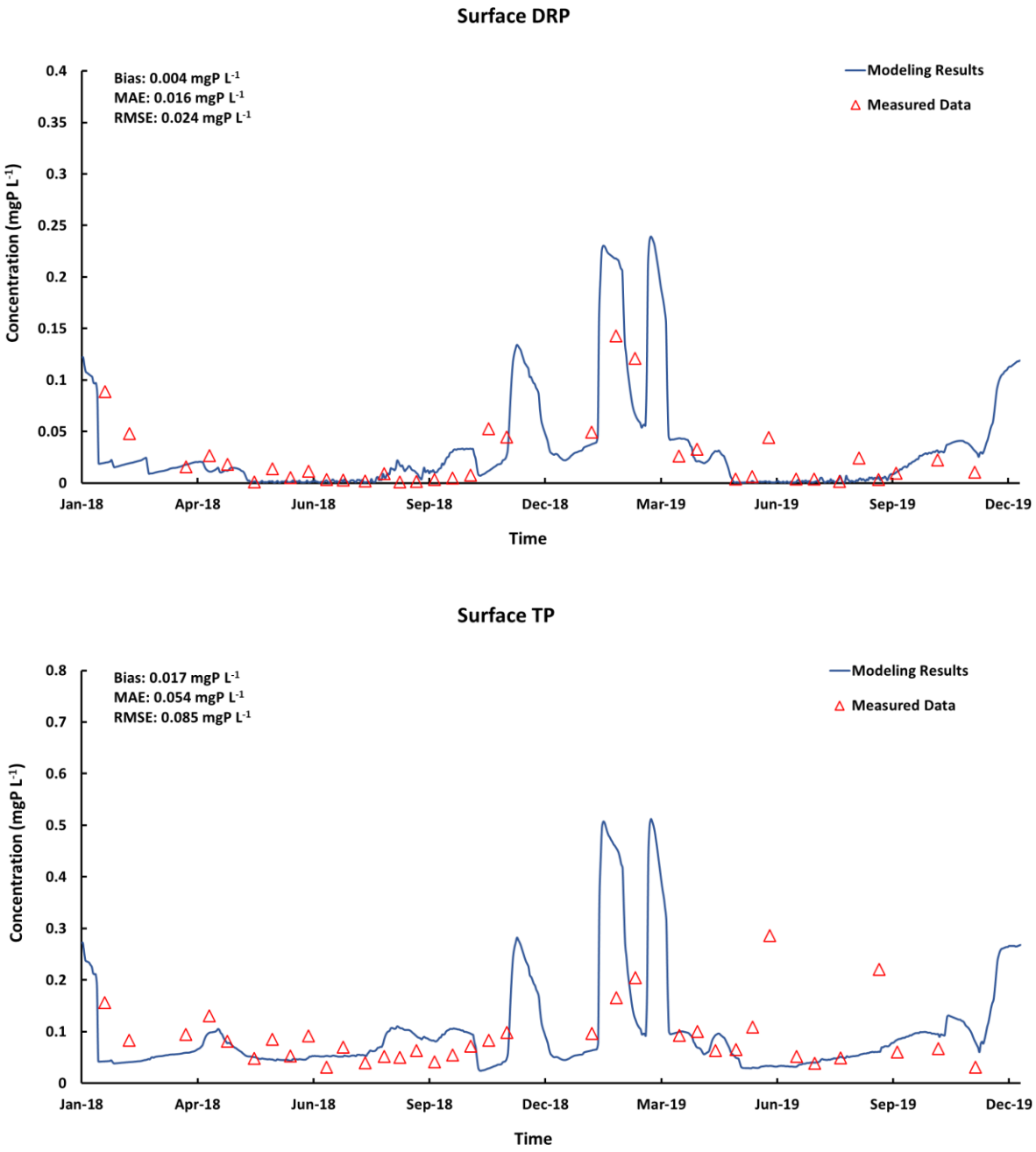

Figure 3-16. Comparison of surface DRP and TP simulation results with measured data in Fanshawe Reservoir from 2018 to 2019.

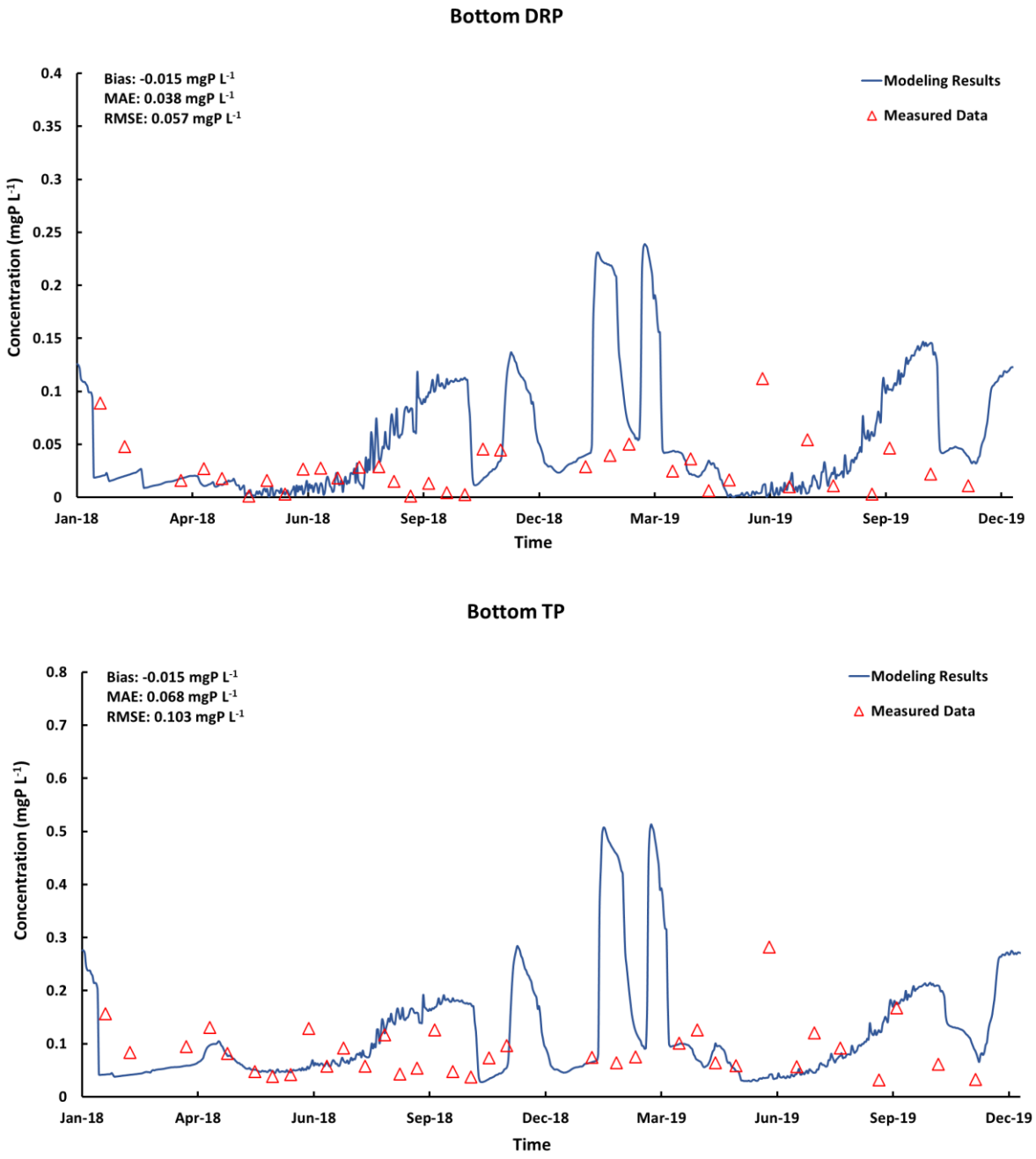

Figure 3-17. Comparison of bottom DRP and TP simulation results with measured data in Fanshawe Reservoir from 2018 to 2019.

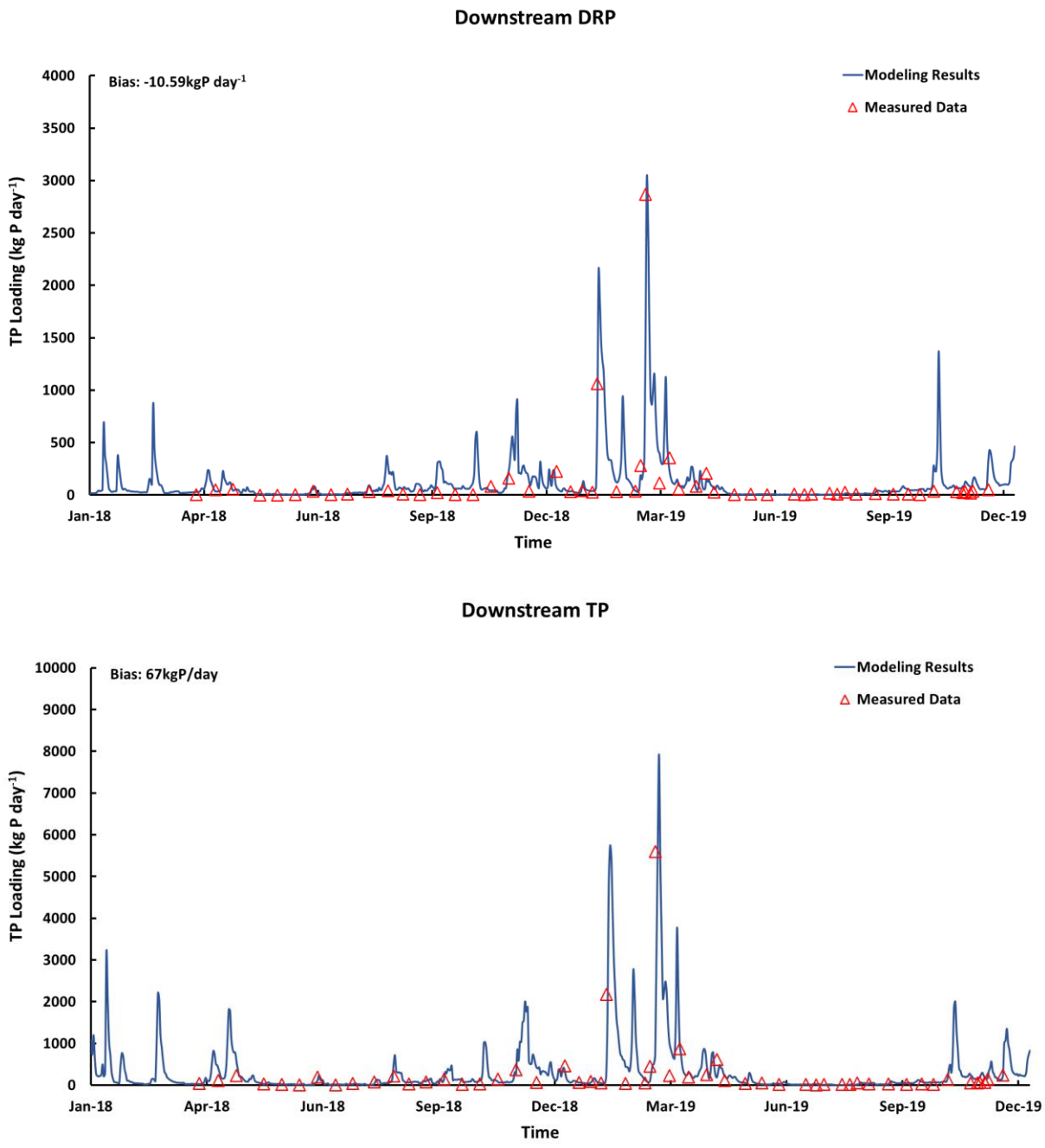

Figure 3-18. Downstream DRP and TP loading with measured data from 2018 to 2019.

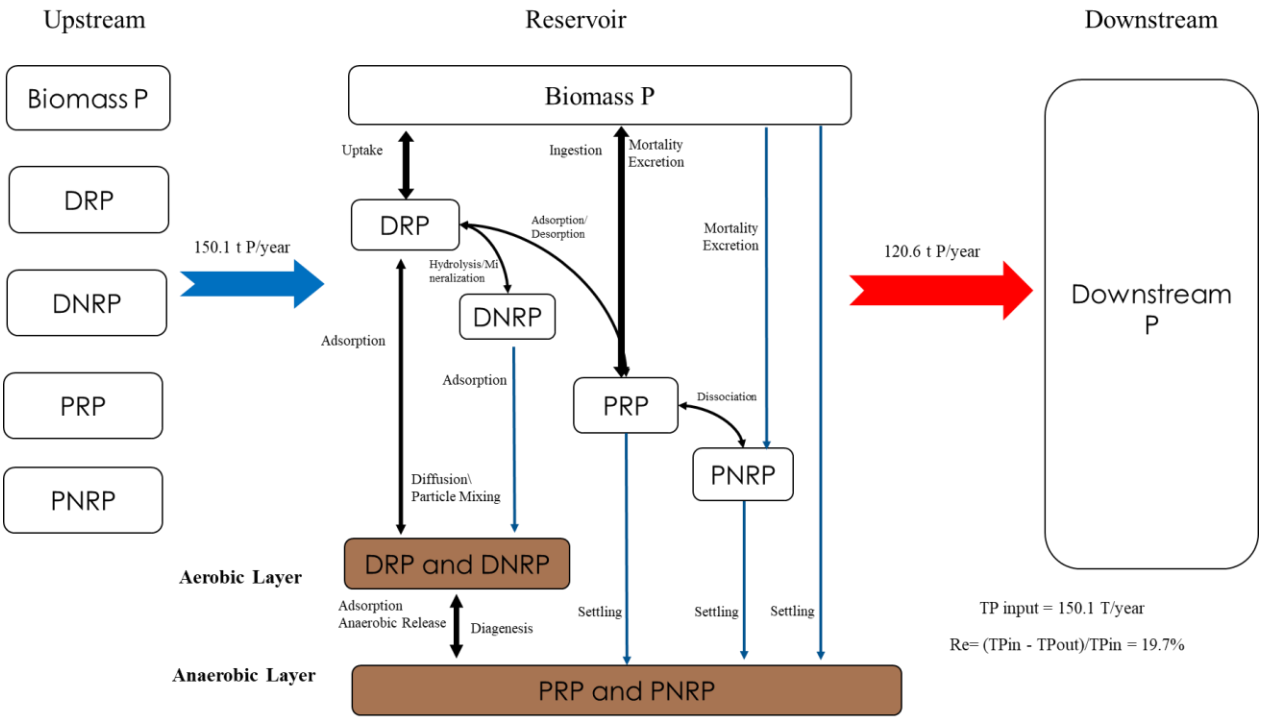

Figure 3-19. Schematic of upstream loading and downstream loading with retention efficiency of Fanshawe Reservoir.

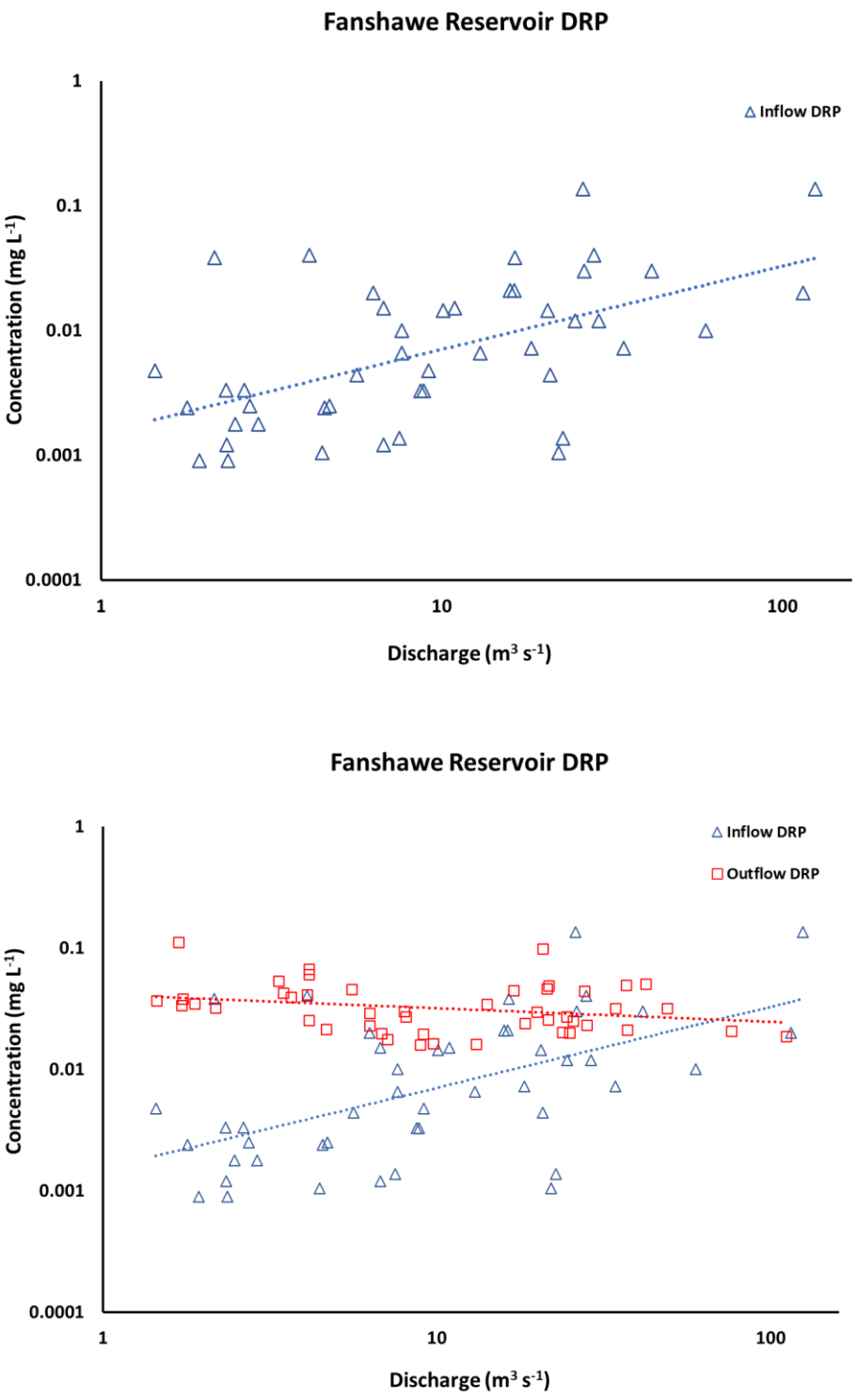

Figure 3-20. Concentration - Discharge relationship for DRP in Fanshawe Reservoir.

3.4.2.2 External Loading and Internal Loading

External loading and internal loading of P have extreme effects on the water quality in Fanshawe Reservoir and downstream ecological systems. The bottom reservoir sediment is a very important source/sink term for P internal loading. Most of previous reservoir water quality model did not apply the sediment diagenesis model and quantitative analyze the effects of sediments on P retention and release. Therefore, the quantitative description of internal P loading has essential effects on water quality management. P sediment diagenesis model were coupled with the hydrodynamic model and water quality model for providing reasonable modeling results for internal and external P loading. During the 2018 and 2019 modeling year, the contribution of internal P loading and external P loading to the Fanshawe Reservoir was simulated and compared with bottom DO concentrations (Figure 3-21). The percentage of internal P loading ranged from 0.07% to 86.7%. The average internal P loading percent was 22.3% during the modeling year. The average internal P loading percentages were 42.3% and 39.76% during the summertime and fall time in 2018 and 2019, respectively. Internal P loading dominated P loading during the summertime and early fall time and has minor effects on the high flow season (springtime). During the summertime, the decreasing of DO concentrations always accompanied by increasing of the internal P loading. The reason is that increasing of internal P loading could cause the growth of algae group. The bioactivities caused the depletion of DO during the summertime. The differences between surface DRP and bottom DRP also displayed the effects of internal P loading on the water column DRP. The average percentage difference between surface DRP and bottom DRP was 322% during the modeling year. The large differences between surface and bottom DRP most often occurs during the summertime and early fall time due to the bioactivities and thermal stratification. Another reason for high DRP concentration in the bottom layer is the sediment effects, for example, sediment releases more DRP during the summertime because the high temperature and the depletion of DO in the bottom water column.

In summary, the contribution of internal P loading and external P loading with DO variations provided reliable retention and release modeling results for the Fanshawe Reservoir. The simulation results imply a major role of internal P loading during the summertime and early fall time when the reservoir stratifies. Retention of P mainly occurs during wintertime, while the reservoir is a source of P during summertime. The annual sediment P releasing rate is 7.5mg m^{-2} day^{-1}. Previous studies of sediment releasing rate ranged from 0.5 mg m^{-2} day^{-1} to 21 mg m^{-2} day^{-}

[1].(Auer et al., 1993; L. H. Kim et al., 2003) Previous report for Fanshawe Reservoir gave a annual estimated rate as 8 mg m^{-2} day^{-1}, and the author also demonstrated the P sediment releasing rate may vary from 24 mg m^{-2} day^{-1} to 56 mg m^{-2} day^{-1} in summertime(Nürnberg & Lazerte, 2005). The current model provided reasonable work in the internal P loading. It is a high releasing rate for Fanshawe Reservoirs which means the contribution of internal P need to be considered by water quality strategies.

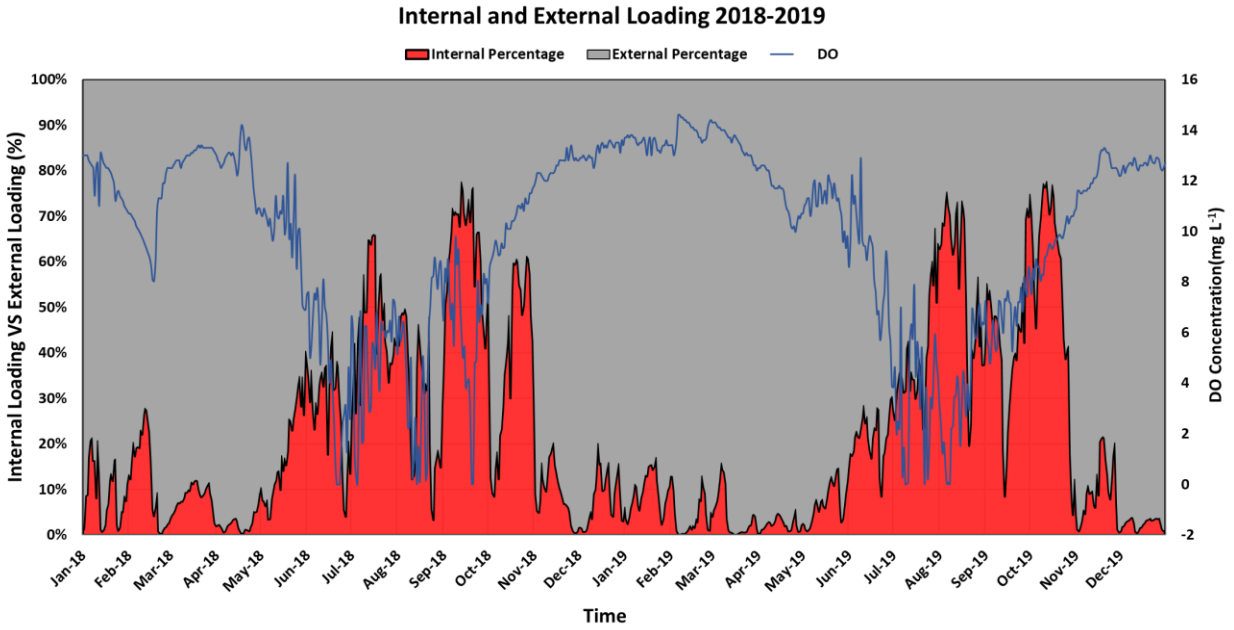

Figure 3-21.Contribution of internal P loading (red area) and external P loading (grey area) with bottom DO concentrations (blue lines) from 2018 to 2019.

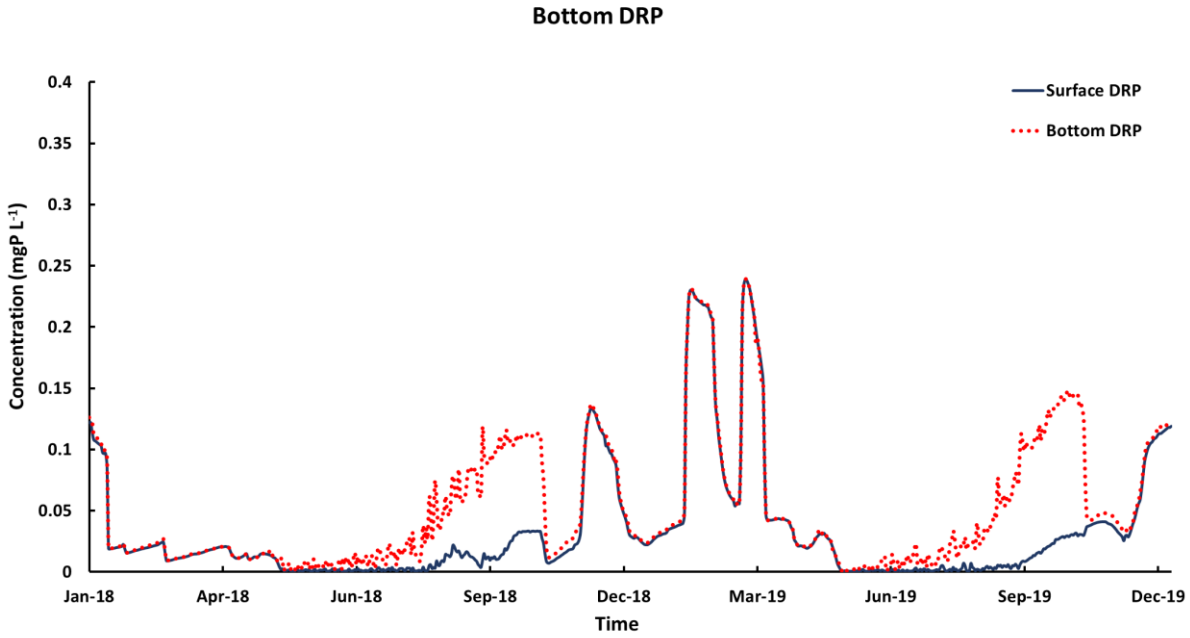

Figure 3-22. Comparison of surface DRP and bottom DRP in Fanshawe Reservoir from 2018 to 2019.

3.4.2.3 P Scenarios

To have more comprehensive understanding on the sediment effects and P future management, two different scenarios were implemented in the current modeling study. The first scenario was 40% reduction of the external P loading to the Fanshawe Reservoir. According to Canada-Ontario Lake Erie Action Plan, a 40% reduction of P loading to western basin, central basin, and nearshore areas was required. Here, the first P loading scenarios was aimed to study the long-term sediment P effects on the reservoir water quality and downstream water quality.

The cumulative downstream TP loading was simulated by the current CE-QUAL-W2 Fanshawe model (Figure 3-23). In this scenario where P input to the reservoir is instantaneously reduced by 40%, the first year downstream export of P from the reservoir only decreases by 22%, because of internal P loading from the sediments. Due to the legacy P stored in the sediments, it would take on the order of 22 years for P export from Fanshaw Reservoir to drop to 36.5% of its current value. In addition, after decreasing P input to the reservoir, the annual average percentage of the contribution of internal P loading also displayed decreasing trend during the long-term model. However, the contributions of internal P loading of the first two years (32.2% for the scenarios) were higher than the original contribution of internal P loading mentioned above (22.3% for 2018 and 2019 modeling year). The assumption of this scenario may cause this condition. This scenario assumed the upstream external P to immediately reduce 40%. However, the reduction of external P loading may reduce every year by a small percentage. This assumption may cause the high contribution of internal P loading at the beginning of the long-term model. After 22 years for the reduction of external P loading, the annual average percentage of the contribution of internal P loading dropped to 13%. Comparing with the beginning time of the reduction of external P loading. The contribution of internal P loading dropped about 20% after 22 years.

In summary, there are still limitations for the long-term P loading at the current modeling work. For instance, the long-term sediment model was developed through three measured sediment cores; The current sediment module in the CE-QUAL-W2 has simple input items for P species and not fully consider the bioactivities in the sediment module. However, the current internal P loading model provided reasonable model work for the relationship between the internal P loading and external P loading

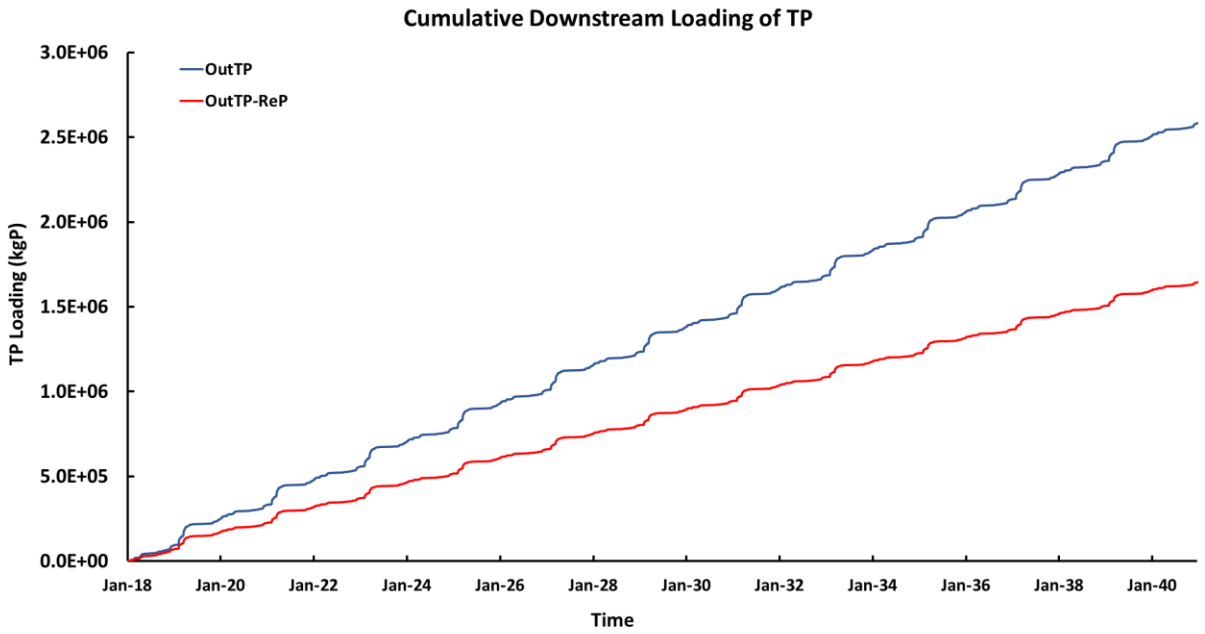

Figure 3-23. Long-term TP loading after the reduction of external P loading.

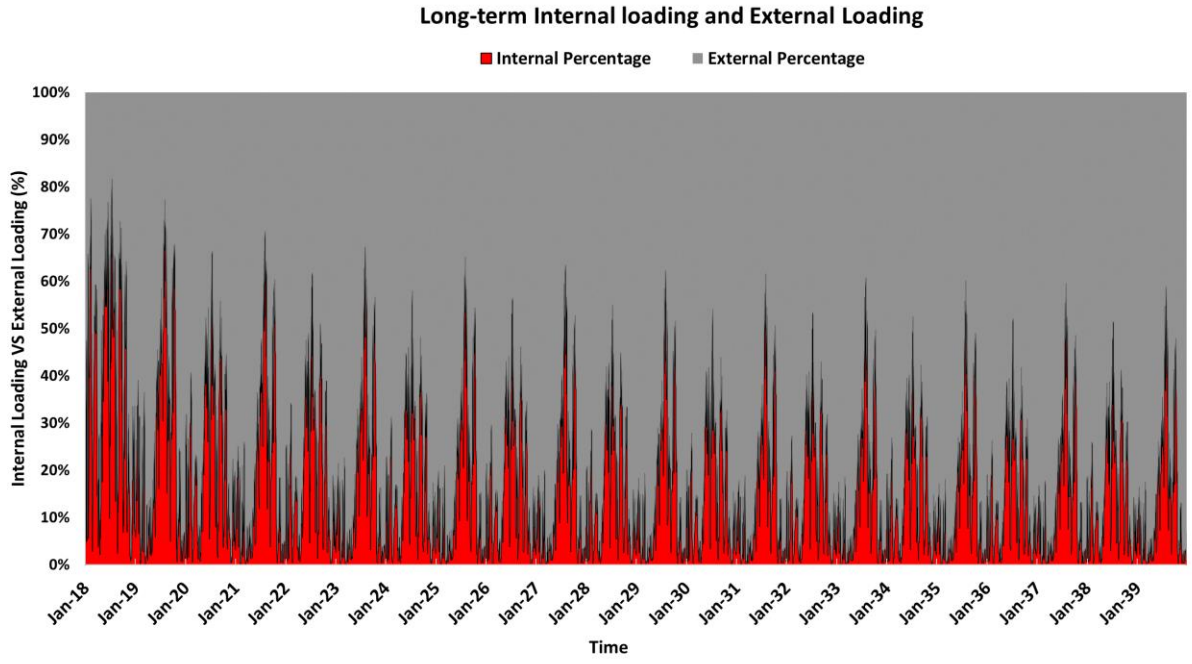

Figure 3-24. Long-term contribution of internal P loading (red area) and external P loading (grey area).

The second scenario was outflow control scenario, which aims to control P loading by modifying the dam outflow. Fanshawe Dam has three outlets which control the outflow in the Fanshawe Reservoir. Two outlets are located at the bottom of the dam (model elevation was 252.4m). One top outlet is at 262m. In this scenario, dam outflow was assumed to only come out through top outflow or bottom outflow. The modeling results reasonably displayed the differences between top outflow control and bottom outflow control (Figure 3-25 to Figure 3-26).

The simulation results well reflected the differences of DRP concentrations in the Fanshawe Reservoir. In the surface layer, the annual average percentage of differences for DRP between top outflow scenario and bottom outflow scenario was 2.1%. which means bottom outflow partly modifies the waterbody DRP concentrations in the surface layer and output more DRP to the downstream area. In the bottom layer, the annual average percentage of differences for DRP between top outflow scenario and bottom outflow scenario is 5.2%, which means bottom outflow has larger effects on the bottom layer DRP concentrations in the waterbody.

In summary, modifying the outflow water amount in different elevation would slightly change the constituent concentrations during the wintertime, and the outflow control would partly modify the constituent concentrations during the summertime and then change the constituents loading to the downstream area. Top outflow scenario has larger TP mass in the waterbody than the bottom outflow scenario. The average percentage of waterbody TP mass difference is 2.7% during the 2 modeling years. In the summertime, the waterbody TP mass difference is 8.1% during the modeling years. The modeling results of outflow application scenario descripted that the outflow may be controlled during the summertime to partly retain or release more nutrients.

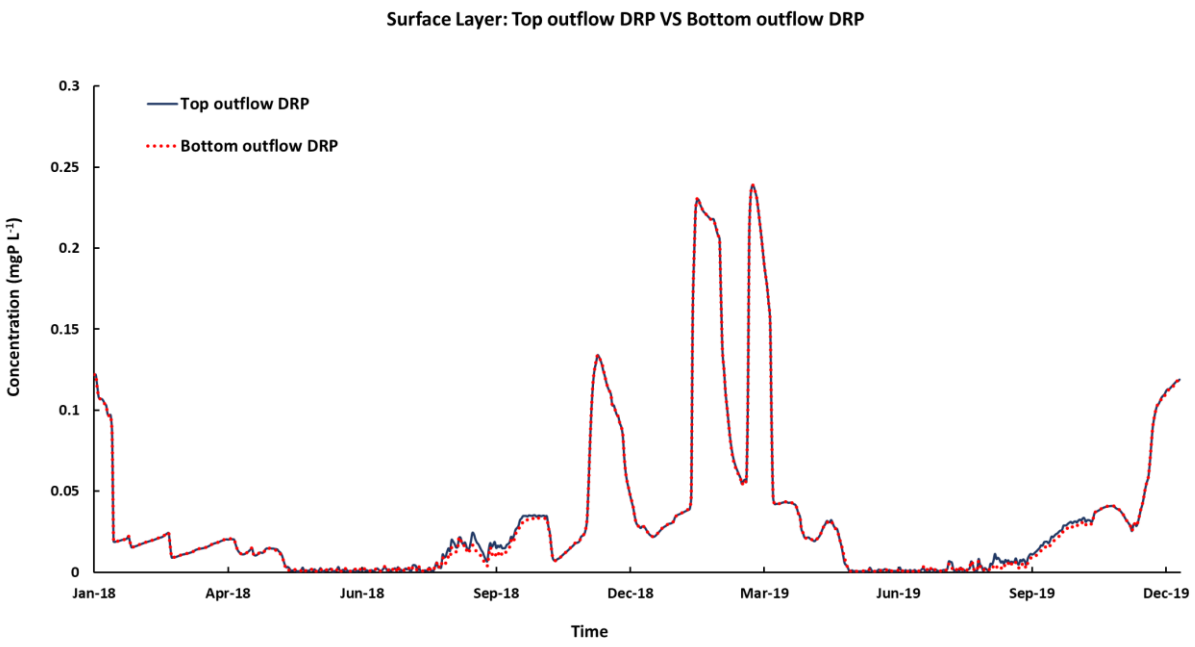

Figure 3-25. Comparison of surface DRP simulation results after managed outflow in Fanshawe Reservoir.

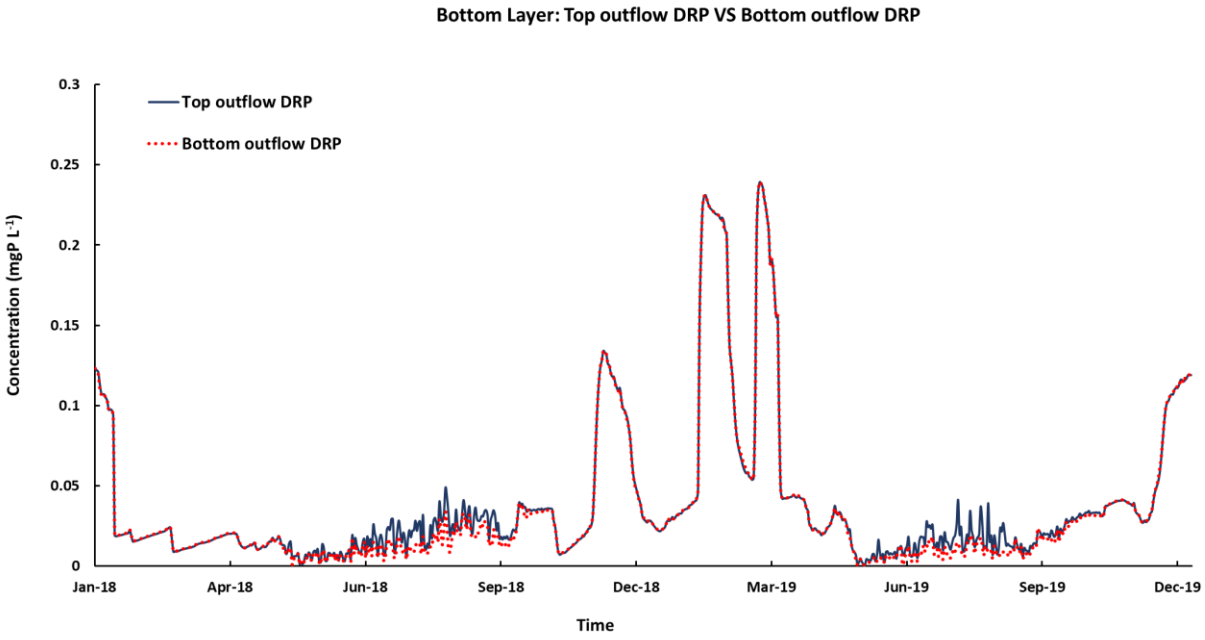

Figure 3-26. Comparison of bottom DRP simulation results after managed outflow in Fanshawe Reservoir.

3.4.3 Biomass Dynamics and Scenarios

3.4.3.1 Biomass Dynamics

To have a comprehensive understanding of the current water quality model, an algae model was developed for simulating algal concentrations, spatial distribution of algae, and algal growth. cHABs cause the depletion of the DO and the bad water quality in the reservoirs (Becker et al., 2009; Carmichael & Boyer, 2016; Watson et al., 2008). Due to the limitation of measured data for algae, default coefficients, such as algae growth rate and mortality rate, were recommended and implemented in the current algal model(Cole & Wells, 2017). The 2018 input upstream algae data were estimated and calibrated from chlorophyll-a in the profiler data. Due to the 2019 measured data did not have chlorophyll-a information, the input of 2019 algal data was estimated from 2018 data.

The current algal model is the first step for modeling the algal group in Fanshawe Reservoir. Although there are limited measured data and some estimated input modeling data, the algal modeling scenarios provided useful and interesting simulation results for the relationship between algal growth and internal and external P loading. According to the modeling results, the algal blooms happened in the late springtime, summertime, and early fall season (Figure 3-27). The average difference between input algal concentrations with modeling results is 1.18 mg L^{-1}. The average percentage differences between input algal concentrations and modeling reservoir algal concentrations was 178% during the whole modeling years, which means algae grew very well through the uptake of the nutrients in the water column. The highest input value was 2.3 mg L^{-1}, however, the highest algal concentration in reservoir was 5.4 mg L^{-1}. According to the modeling algal results, the algal growth had lag times comparing with the input data. There are several reasons may cause this condition: The first reason is the variation of water temperature may delay the growth of algae in the reservoir; The second reason is the variation of the water column DRP may also have significant effects on the growth of algal. The effects of P were discussed in the following Algal Scenarios section. Spatial distribution of algal concentration in the whole reservoir provided reasonable modeling algal concentration for the Fanshawe Reservoir during the 2018 and 2019 year. Algal blooms happened during the summertime of 2018 and 2019. Even in the early fall time of 2018, there was still visible algae in the reservoir, especially before the dam area.

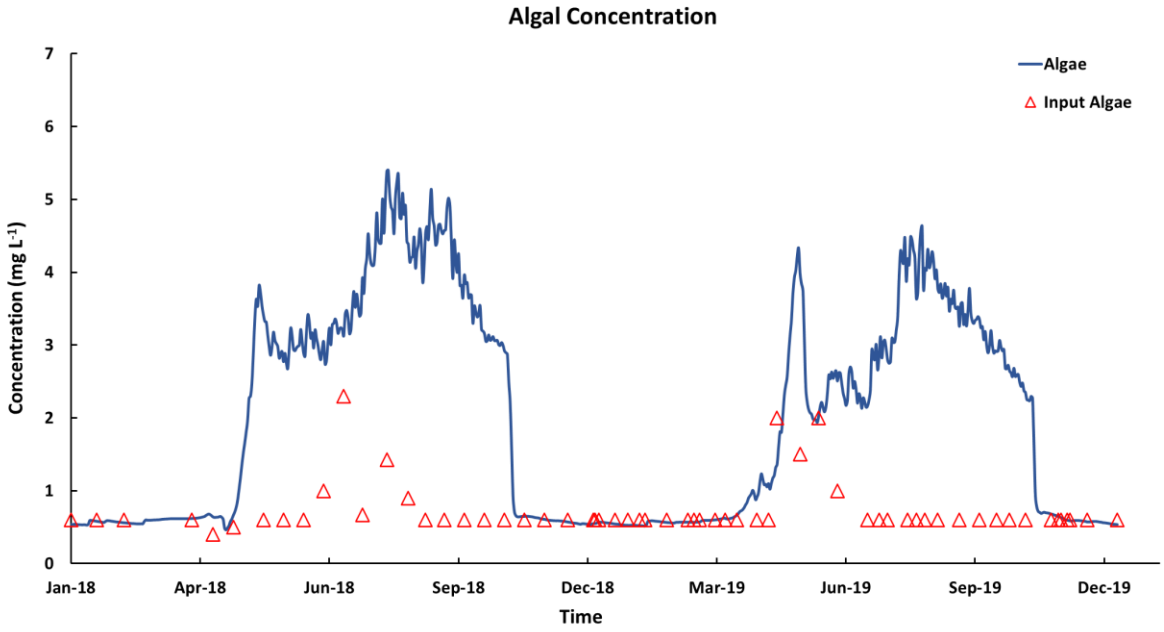

Figure 3-27. Algal concentration with input algal data in the Fanshawe Reservoir from 2018 to 2019.

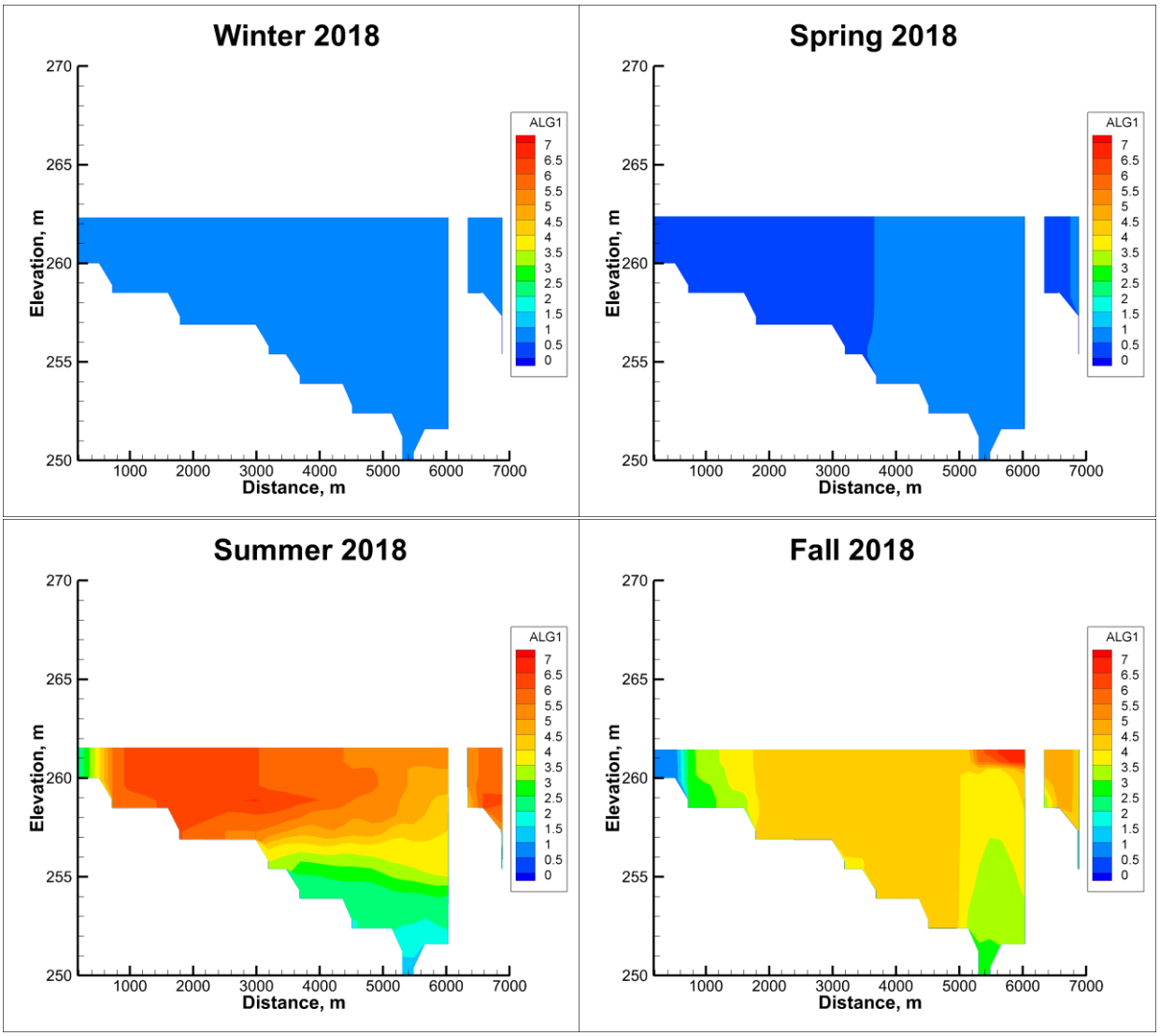

Figure 3-28. Spatial distribution of algae for whole Fanshawe Reservoir in different season at 2018 (Segments 2-33 were plotted from 0m to 6000m; Segments 36-38 were plotted from 6300m-7000m).

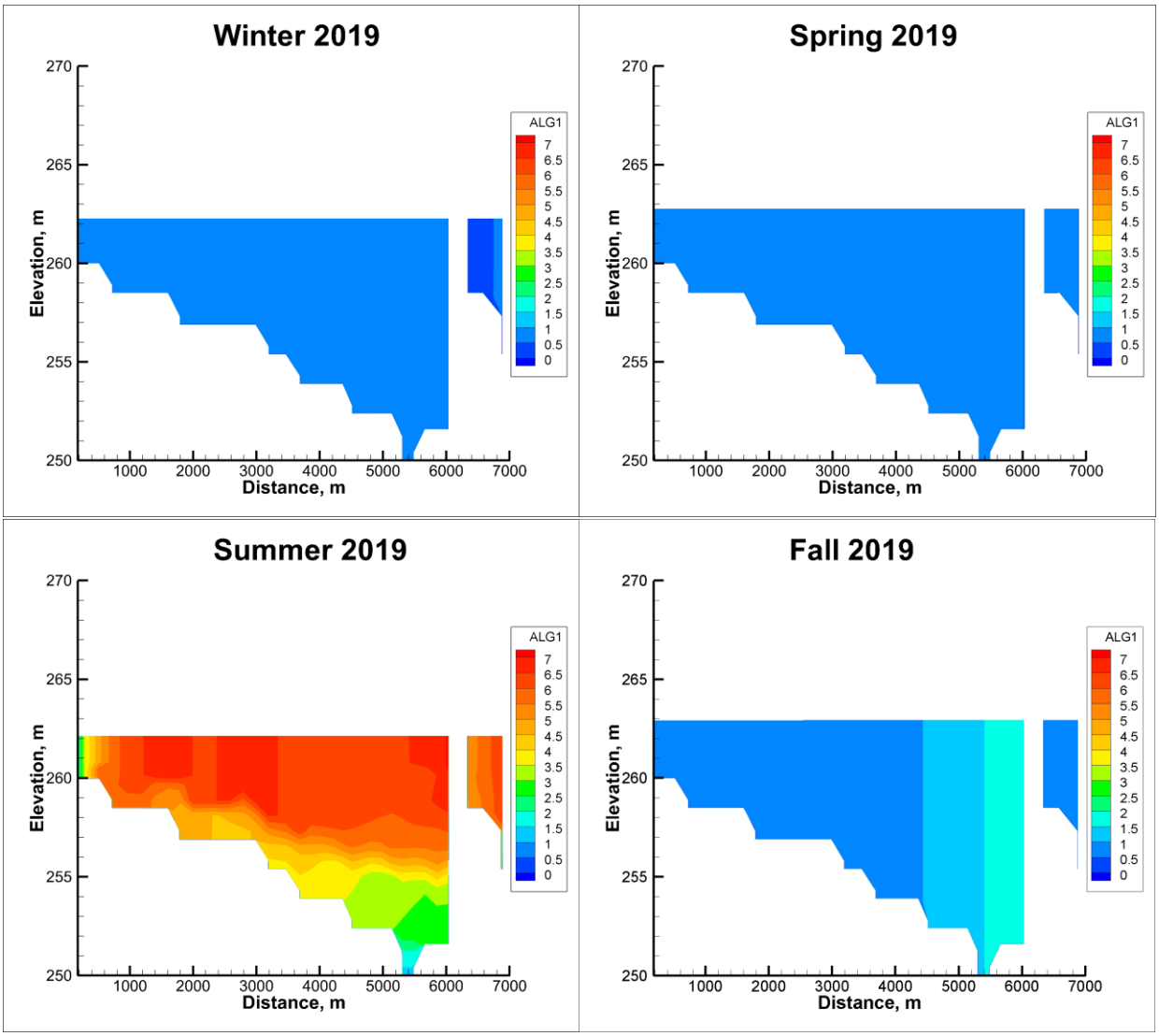

Figure 3-29. Spatial distribution of algae for whole Fanshawe Reservoir in different season at 2019 (Segments 2-33 were plotted from 0m to 6000m; Segments 36-38 were plotted from 6300m-7000m)

3.4.3.2 Biomass Scenarios

To test effects of external and internal P loading on algal concentration and algal growth, two different scenarios were implemented and compared with the original algal modeling information. The first scenario was the effects of sediment on algal information (No sediment P loading: NoSedi). The second scenario was the effects of reducing of external P on algal information (ReP). Here, 40% reduction of external P loading was implemented into the model. The reason for using 40% reduction of P was mentioned in above P subtitle.

The simulation results of algal concentration clearly displayed the differences among different scenarios (Figure 3-30). The reduction of external P loading has less effects than the sediment P loading on the algal growth in the modeling scenarios. The yearly average differences of original algal concentrations with No-Sedi algal concentrations and ReP algal concentrations was 12.5% and 5.4%, respectively. These differences were larger from June to late August (summertime), the average differences of original algal concentrations with No-Sedi algal concentrations and ReP algal concentrations was 36.1% and 15.9%, respectively. According to algal concentrations simulation results, the sediment P loading have more positive effects (40.1% in summertime and 13.5% for two years average) on algal concentrations than the reduction of external P loading. In addition, the fluxes of DRP for algal growth are another indicator for studying the effects of sediment P loading and external P loading on algal growth. DRP fluxes for algal growth in different scenarios have been simulated and plotted as monthly variations (Figure 3-31). During these two modeling years, the highest difference between original group and No-Sedi group was 60.1% at August 2019. The highest difference between original group and ReP group was 23.9% at May 2018. According to DRP fluxes simulation results, the sediment P loading have more positive effects on algal growth than the reduction of external P loading. During summertime, sediment P loading plays an important role for the algal blooms because the external P loading is usually very low at this time period.

In summary, although the input upstream data were very small values, sharply growth of algae occurred because the nutrients level, photosynthesis and high temperature in the summer and fall season. In wintertime and early spring season, although nutrients were loaded in the reservoir, algae did not grow because of the low water temperature. Although there are limitations of the current measured data, the current algal model reasonably and successfully simulated the growth

processing of algae in the whole reservoir system. Scenarios revealed that the sediment P loading has significant effects on algal growth than external P loading in the summertime. Algal blooms management strategies may pay more attention on the sediment nutrients loading during the summertime.

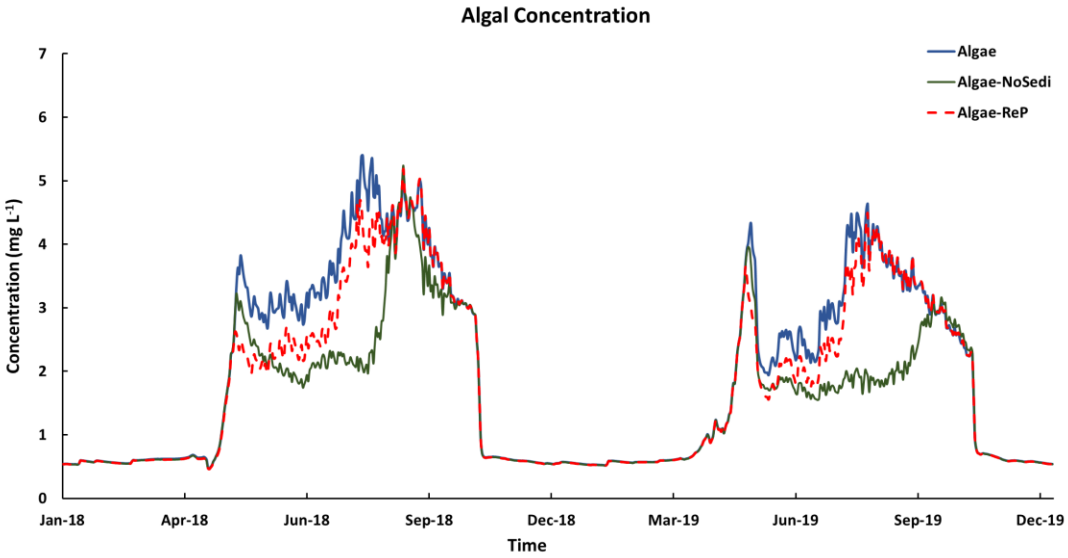

Figure 3-30. Algal Concentration after modifying sediment P loading and external P loading.

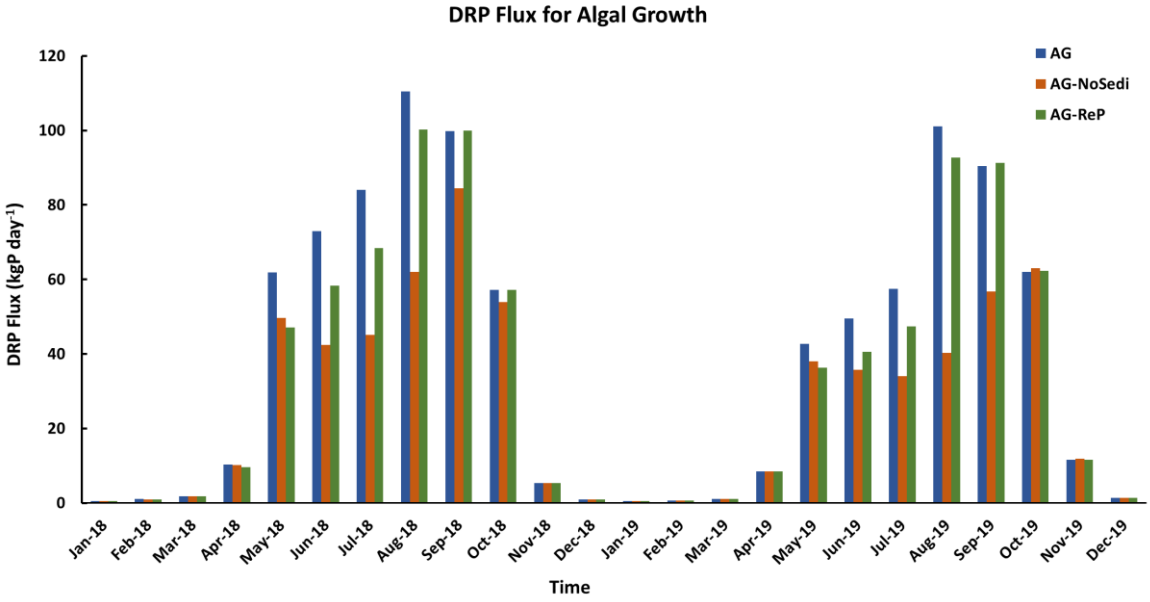

Figure 3-31. DRP flux for algal growth in different scenarios (Blue bars are original algal growth DRP; Orange bars are algal growth without sediment P; Green lines are algal growth with reduction of external P loading).

Chapter 4 Model Application – Coupling with BP-ANN Model

4.1 Introduction and Research Method

In the current modeling study, a BP-ANN model was developed and calibrated through CE-QUAL-W2 modeling results. The original code was developed in MATLAB software. The ANN models have been widely implemented into different research area, such as rainfall-runoff forecasting, water temperature and water quality forecasting etc. (Demirel et al., 2009; Kişi, 2008; Maier and Dandy, 2000; Ömer Faruk, 2010; Singh et al., 2009). The BP-ANN model has been extensively and commonly used in the data driven modeling works (Kişi, 2008; Maier and Dandy, 2000; Ömer Faruk, 2010; Yang et al., 2018). The current modeling work is the first time that combine the CE-QUAL-W2 modeling results with a BP-ANN model. The combination of these two methods provides high-efficiency and reliable model for future prediction and application. For example, the CE-QUAL-W2 model need lots of parameters and measured data for simulating constituents in different year. After calibrating BP-ANN model with validated CE-QUAL-W2 modeling results, BP-ANN model could forecast these constituents only through changing the inflow or climate data. It may not be an accurate or perfect way to obtain water quality information, however, it would be a very fast way to predict water quality information.

In the current BP-ANN model, the model consists of a data input layer which includes the number of the input data as the number of nodes, hidden layers which contains different nodes, and an output layer (Figure 4-1). In the BP-ANN model, the modeling signal is feedforward and the modeling errors are back propagation. The BP-ANN model adjusts the weight values and threshold values through the comparison between the modeling results and input data until the errors of the whole network are minimized (Demirel et al., 2009; Maier & Dandy, 2000; Yang et al., 2018). The BP-ANN model in the current Fanshawe Reservoir study used the sigmoid transfer functions which have been developed in MATLAB software, and the Levenberg-Marquardt BP method was applied as the training algorithm. The following steps and equations described the modeling processes of BP-ANN model:

The first step is the organization and initialization of the input data and the network. Input data, weight values (W_{ij}, W_{jk}) and threshold values for hidden layers (a) and output layer (b) are initialized. The training parameters, such as the training performance goal, the learning rate, and momentum constant etc., are set.

The second step is the calculation and simulation of the hidden layers results (H) and output layer results (O).

$$\mathrm{H}_j = f\left(\sum_{i=1}^{n} \omega_{ij} X_i - a_j\right) \qquad j = 1,2,\dots l$$

$$f(x) = \frac{1}{1+e^{-x}}$$

$$\mathrm{O}_k = \sum_{j=1}^{l} H_j \omega_{jk} - b_k \qquad k = 1,2,\dots,m$$

Where X is the input data; w is the weight values; n is the node in the input layer; l is the node in the hidden layers; a and b is the threshold values for hidden layer and output layer; f is the hidden layer transmission functions; O is the output results.

The third step is the calculation of the errors (e) between output results (O) and expected results (Y) and the update of the weight values and threshold values.

$$e_k = Y_k - O_k \; k = 1,2,\dots,m$$

$$\omega_{ij} = \omega_{ij} + \eta H_j\left(1 - H_j\right) x(i) \sum_{k=1}^{m} \omega_{jk} e_k \qquad i = 1,2,\dots,n; j = 1,2,\dots,l$$

$$\omega_{jk} = \omega_{jk} + \eta H_j e_k \qquad j = 1,2,\dots,l; k = 1,2,\dots,m$$

$$a_j = a_j + \eta H_j (1 - H_j) \sum_{k=1}^{m} \omega_{jk} e_k \; j = 1,2,\dots,l$$

$$b_k = b_k + e_k \qquad k = 1,2,\dots,m$$

where e is the errors; Y is the expected results; O is the output results; w is the weight values; a and b are the threshold values for hidden layer and output layer; η is the coefficient for learning rate, which is very small value.

The fourth step is the judgment of the degree of completion of the iteration. If the errors are expected values, the iteration will stop; otherwise, the modeling signals are transmitted to the second step.

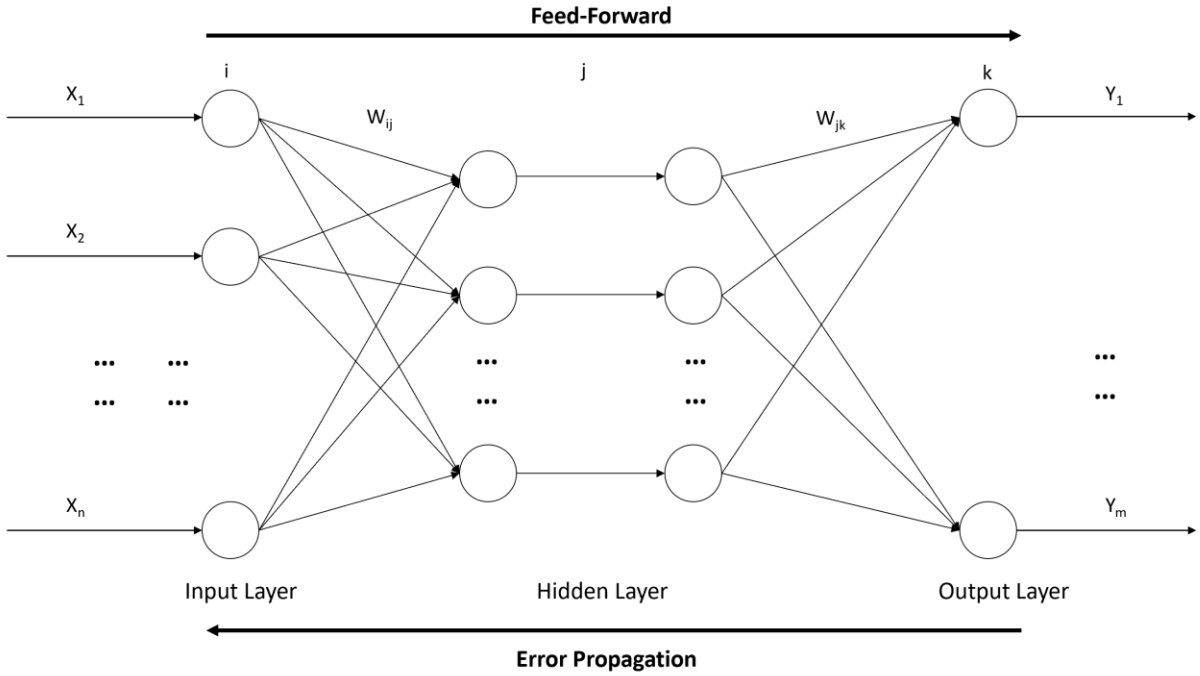

Figure 4-1. Schematic of BP-ANN model.

4.2 BP-ANN Modeling Results and Discussions

The current hydrodynamic and chemical model were well reproduced and predicted the hydrodynamic and chemical properties of the Fanshawe Reservoir in 2018 and 2019. The 2018 CE-QUAL-W2 modeling results were used as calibration data and the BP-ANN model were validated by 2019 data. The prediction of future constituents in watersheds and reservoirs is a very complex progress. However, the limitations of measurement data may not feasible for the prediction of the current CE-QUAL-W2 model. A BP-ANN model was developed and coupled with CE-QUAL-W2 modeling results for further understanding and applications. The BP-ANN modeling results successful predicated ice thickness, DO concentrations and algae concentrations.

The DO concentrations were simulated through the BP-ANN model (Figure 4-2). The input data of DO in BP-ANN model were related to the CE-QUAL-W2 DO modeling results CE-QUAL-

W2 input conditions. The DO BP-ANN modeling results well matched with CE-QUAL-W2 modeling results. The R^2 between CE-QUAL-W2 modeling DO and BP-ANN modeling DO was 0.967. In the current BP-ANN model, there are some errors in the beginning of 2019 modeling results. These errors may be caused by the coefficients that calibrated by 2018 data. If more CE-QUAL-W2 modeling results can be used for calibration. These errors could be minimized.

The algal concentrations were also calibrated and validated through the current BP-ANN model (Figure 4-3). The BP-ANN algae modeling results capture most of the trend of algae in 2019. The R^2 between CE-QUAL-W2 modeling algae and BP-ANN modeling algae was 0.895. The 2019 BP-ANN modeling results was overestimated the algal concentrations during the summertime and early fall time. The BP-ANN modeling results has 28% differences in the algal concentrations for 2019 modeling results. This errors may be caused by the sample size of the calibration for the BP-ANN model and the DO errors may also be magnified in the algal modeling results because the DO modeling results were input data for the algal modeling results.

In the ice thickness ANN modeling results, the ice thickness was dynamic related to time, water inflow, water elevation, and metrological input files. The ice thickness BP-ANN modeling results well reproduced the 2018 ice thickness and matched most of the ice thickness with the 2019 CE-QUAL-W2 modeling results. The R^2 is 0.905.

In summary, the current BP-ANN modeling work reasonably reproduced CE-QUAL-W2 modeling result in Fanshawe Reservoir. The inputs of BP-ANN model only have upstream and reservoir information of CE-QUAL-W2 model. The dam outflow data and downstream P loading information did not include in the BP-ANN model. However, the current BP-ANN model successfully captured the trend of DO concentrations, algal concentrations, and ice thickness in the reservoir and downstream. The R^2 between BP-ANN model and CE-QUAL-W2 results were higher than 0.8, which means the correlation was good and acceptable. The current BP-ANN model is the first step to combine the water quality modeling results with data driving results. The BP-ANN model could be a prediction tools for future water quality applications.

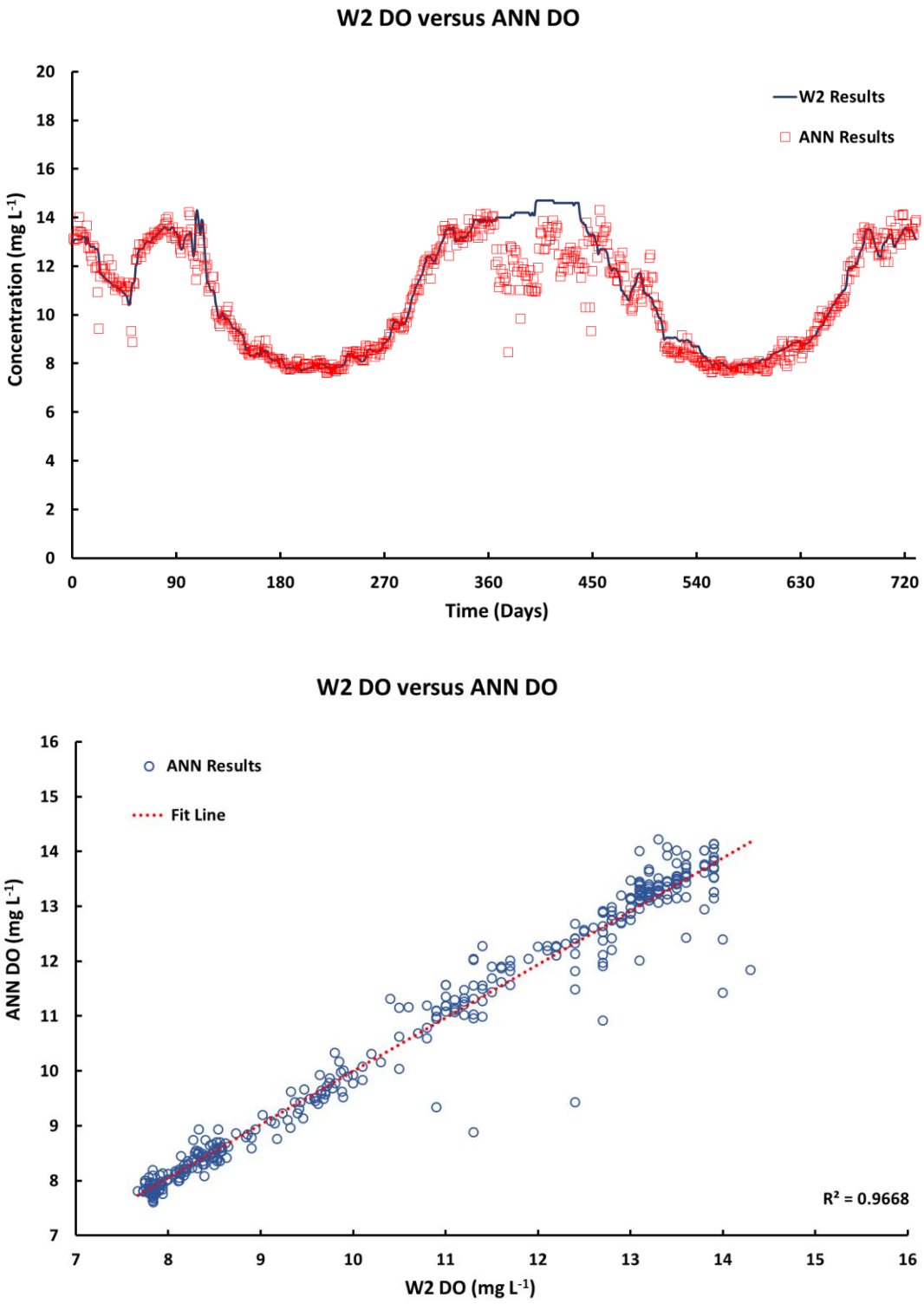

Figure 4-2. Comparison of DO simulation results with BP-ANN modeling results in Fanshawe Reservoir from 2018 to 2019.

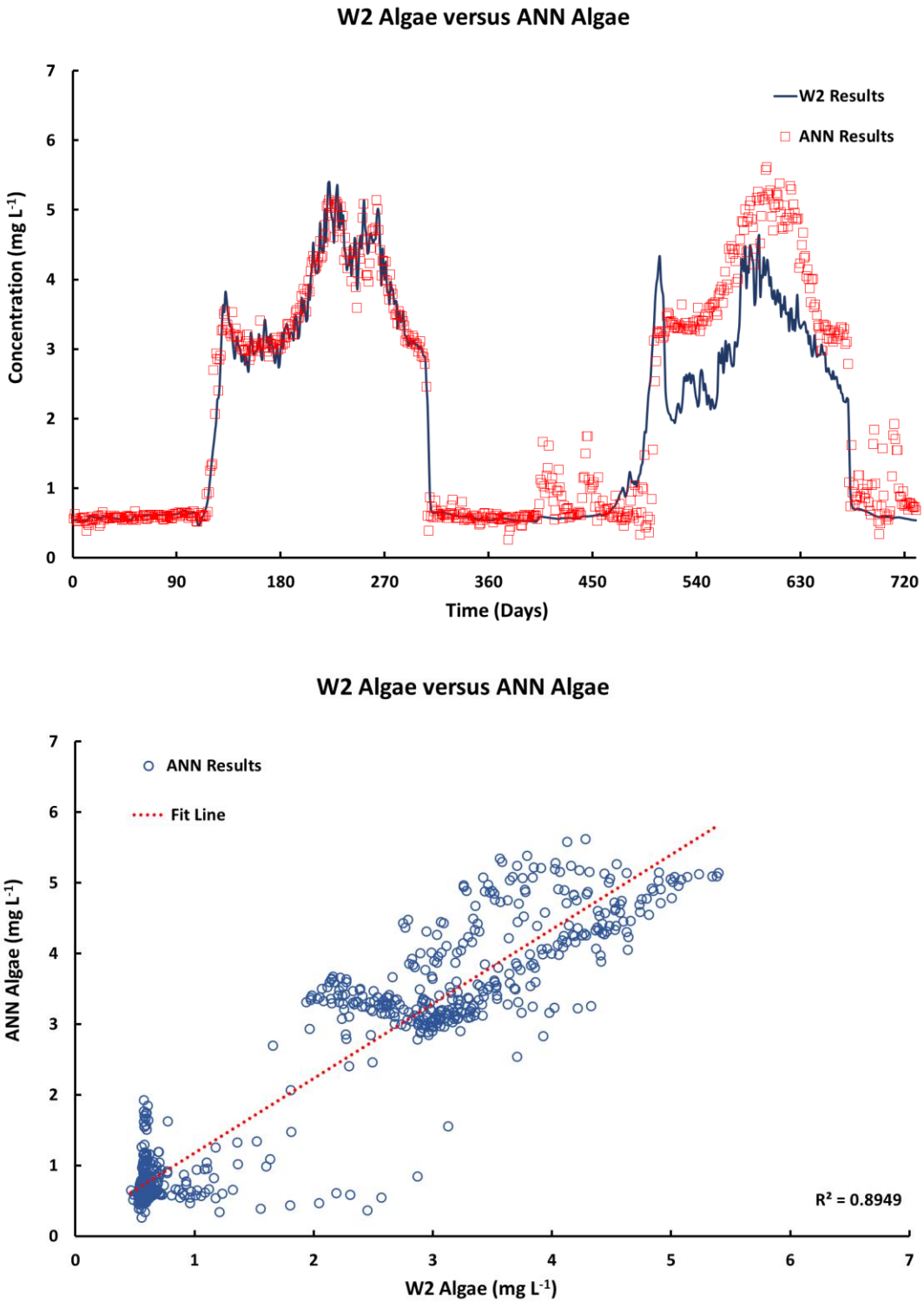

Figure 4-3. Comparison of algae simulation results with BP-ANN modeling results in Fanshawe Reservoir from 2018 to 2019.

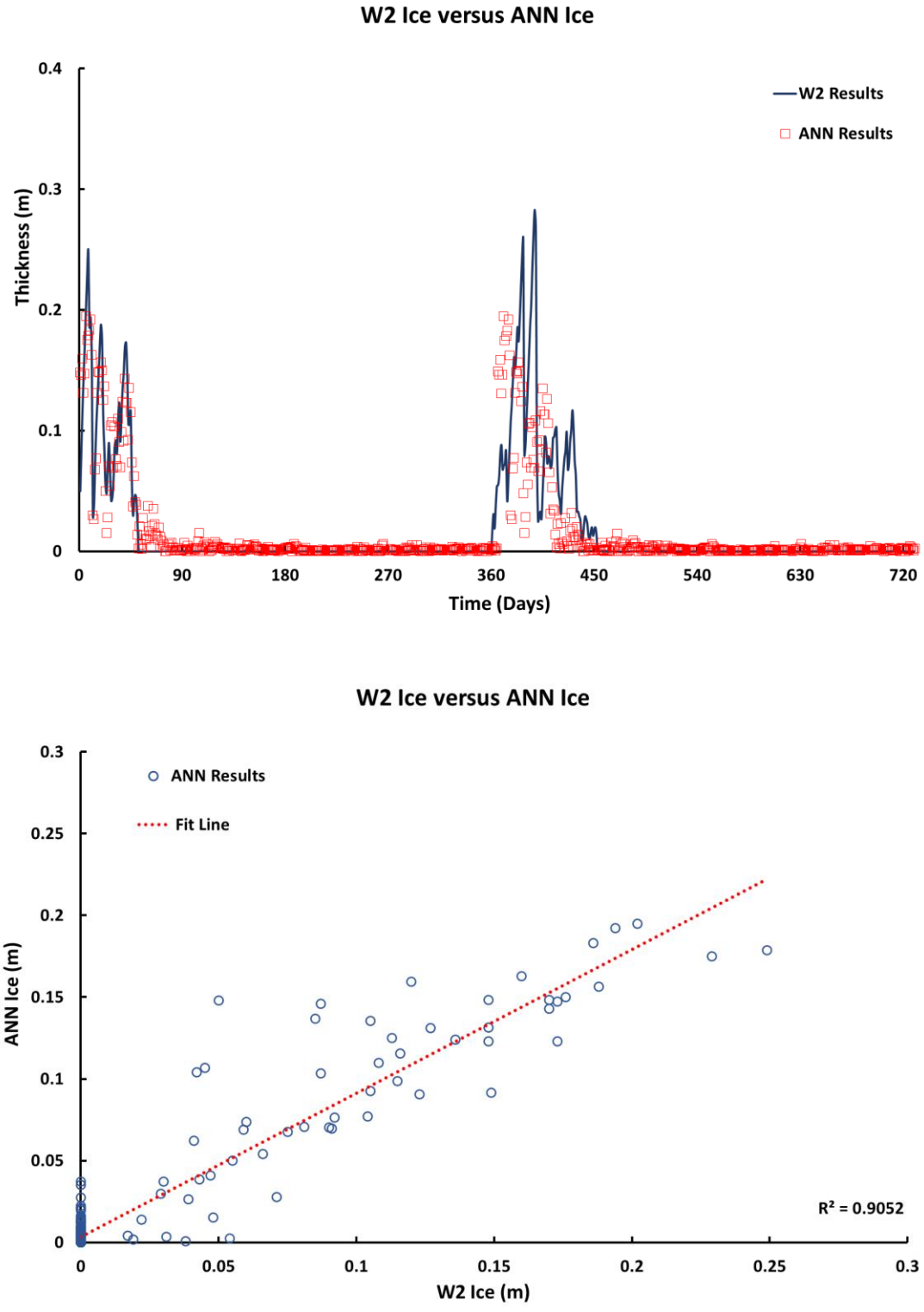

Figure 4-4.Comparison of Ice cover simulation results with BP-ANN modeling results in Fanshawe Reservoir.

Chapter 5 Conclusions and Perspectives

5.1 Summary

The Fanshawe Reservoir model provided good modeling viewpoints of the water quality – sediment model, which may have feasible applications for the legacy nutrients issues in reservoirs, watersheds, and lakes. The simulation results of this water quality – sediment model reasonably fit the hydrodynamic and chemical property data for the Fanshawe Reservoir. The water quality and sediment model may also be affected by assumptions and uncertainties during the modeling processes. All assumptions, results and future work are summarized in this chapter.

5.2 Assumptions and Limitations

This modeling method has several assumptions that may cause some uncertainties in the simulation results. The main limitation in the CE-QUAL-W2 model is that the governing equations are laterally, and layer averaged, which means the lateral variations in flow velocities, water temperatures, and water constituents are being neglected during the modeling processes. This limitation may not fully consider the wind effects on the water flow in the waterbody. Another limitation is that vertical momentum is not included in the model. Therefore, if there is significant vertical acceleration in the waterbody, the modeling results may not very accurate.

In the initial and boundary conditions, the first assumption is the shape of the layer and segment. At this step, due to the precision of the measured data, segments length and layer heights may not very accurate in the current model. This assumption may cause some uncertainties in the transport processes and the fluxes of the constituents. In addition, the number of the layer is limited by the topographical data. The simulation results may be affected by the number of the vertical layers. For example, the vertical simulation results may not capture enough small variations in the water column due to the number of vertical layers. If more layers and segments are created in the system, the uncertainties could be minimized. However, the current topographical data cannot support the development of more layers. The second assumption is the input water flow and water temperature in the boundary conditions. In branch 1, the measured station is not located directly upstream of the first segment in the model (the station is located 15km at upstream). Therefore, some missing inflow water may not be accounted for in the input data. Additionally, branch 2 (Wye Creek) does not have daily flow data. The input branch 2 data were calculated from the linear regression relationship of previous branch 1 flow data. The linear regression relationship was based on Wye

Creek and main branch (Upper Thames River) flow data from 1953 to 1991. Those missing water was balanced through CE-QUAL-W2 model to build a better hydrodynamic system for other constituents modeling. Water temperature input data are measured once per two weeks and the measured water temperature were limited in wintertime. Here, 0 ℃ was assumed to be the water inflow temperature for the missing values in wintertime. The third assumption involves the input meteorological data. The description of cloud cover was descriptive information and discrete number values (0 to 10) were applied to the meteorological file. The input meteorological file also required solar radiation data; however, the solar radiation data are not available in the Fanshawe Reservoir. This limitation may have caused some uncertainties in the surface heat of waterbody in the model.

In addition, due to the limitations of the measurement data, such as biomass detailed information, the water quality model and sediment diagenesis model were calibrated based on the default coefficients. The default coefficients may differ in the Fanshawe Reservoir, which may have led to some errors in the modeling results. The P scenario model used in this thesis ran a scenario that imposed a immediately 40% decrease of TP upstream loads to the Fanshawe Reservoir. The original government action plan was 40% decrease of TP loads until 2025. However, the CE-QUAL-W2 modeling input data required concentrations of DRP, biomass, and P in labile and refractory organic matter. The measurement data did not include detailed information on biomass and P concentration in labile and refractory organic matter. Therefore, the modeling input data assumed P species based on the measured data we have. These estimations may have caused some uncertainties and modeling errors in the model.

In the ice cover formation model, ice cover does not include the gravity effects of the snow accumulation and the ice ablation. The formation of the ice does not contain the dissolved substances, which means only pure ice was formed, and the constituents may be accumulating in the waterbody.

The performance of the BP-ANN model is highly related to the accuracy of the current CE-QUAL-W2 model. Long-term BP-ANN prediction results may be limited by the accuracy of the modeling results from CE-QUAL-W2 model. In addition, the coefficients in BP-ANN model, such as the frequency of training and learning rate etc., may also cause some uncertainties and errors in the BP-ANN modeling results.

5.3 Conclusions

Water quality in the TRW has been significantly affected by the intensive inputs of P and other nutrients. These polluted waters could have significant and chronic negative effects on the downstream and nearby aquatic environment, such as Lake St. Clair and Lake Erie. Dammed reservoirs are built for flood control and hydropower services. However, excess nutrients could stagnate in the reservoirs and slowly release over a long period, posing significant difficulties for water quality management.

In this thesis, the primary objectives were to develop a feasible and reliable model for the quantitative analysis of the hydrodynamic characteristics, water quality, and the sediment effects on P retention and release in the Fanshawe Reservoir. The 2-D water quality and sediment model, and BP-ANN model were able to reasonably simulate the hydrodynamic characteristics, water quality, and sediment P effects in the Fanshawe Reservoir. Modeling applications provided insightful and valuable simulation results for water quality management, such as the external and internal loading of P effects on the algae blooms and DO dynamics.

The current work on the Fanshawe Reservoir model provided complex hydrodynamic, water quality - sediment results that were applicable to BP-ANN model. In the hydrodynamic part of the model, although modeling results have different values in limiting time points, the simulation results of Fanshawe Reservoir model reproduced the waterbody volume, surface water temperature and vertical thermal structures in Fanshawe Reservoir. In the water quality and sediment modeling results, the DO and biomass concentrations, the DRP and TP concentrations, and the retention and release of sediment P were simulated well. The DO depletion happens during the summertime in the deeper layer of the Fanshawe Reservoir. Due to the growth of algae, the DO concentrations during the summertime are lower than they are during the wintertime. The simulation results of the internal loading of P suggested an annual sediment P releasing rate as 7.5mg m^{-2} day^{-1}, which is a considerable issue for Fanshawe Reservoir. the Fanshawe Reservoir. High flux of P between the water column and sediment happens during the summertime and the variations of P concentrations are very high in the bottom of the reservoir during this time. The scenario where a 40% decrease of upstream P was imposed did not immediately decrease the downstream P and the P concentrations in the reservoir, which may be because of the legacy P in the reservoir sediments. Knowledge regarding the sediment P effects on algal concentrations in reservoirs are valuable for

water quality management. Algae blooms occur during summertime and early fall seasons with the depletion of DO in the deep layer of the waterbody. A 40% reduction of upstream P only caused a 5.4% decrease of the algal concentration in the summertime. In addition, in the algal dynamics scenarios, the results highly recommend people should pay more attention on the effects of internal P loading on the algal growth than the external P loading during the summertime. The applications of CE-QUAL-W2 model provided valuable reservoir outflow control methods and the ice over model provided reasonable ice thickness modeling results. The BP-ANN modeling results provided a reliable modeling method between CE-QUAL-W2 modeling results and BP-ANN modeling work. The BP-ANN modeling showed good correlation and prediction modeling results with the CE-QUAL-W2 model.

5.4 Perspectives

The CE-QUAL-W2 and BP-ANN models provided useful, flexible, and insightful modeling results and applications for future water quality models and water quality management. Due to the increasing world population, increased agricultural nutrient usage, and the construction of dams, the water quality in the dammed reservoirs may be at risk, negatively affecting the aquatic environments and human lives. The modeling used in this thesis may be applied in different areas for monitoring the water quality. Future application and research work can be descripted in three parts:

The first perspective is the extension of CE-QUAL-W2 water quality and sediment model, which could be extended to a large-scale area, such as different watersheds with dammed reservoirs. The dam cascade could be applied into the CE-QUAL-W2 model. Water quality factors, such as DO, the fate of contaminants, nutrients concentrations, and the biomass algae etc., could be simulated and predicted for the future. Additionally, due to the original limitation in the CE-QUAL-W2 code, the CE-QUAL-W2 model did not simulated the iron effects on P retention and release well. Including large-scale sediment retention and release of nutrients with iron effects in the future would aid in future regulations. For example, the simulation results would provide information about external and internal nutrient loading at a watershed scale, including the detailed iron information. The government could regulate different reservoirs to retain or release nutrients based on the simulation results. This application would very helpful for decreasing the nutrients input to the downstream area, such as the nutrients in the Great Lakes.

The second application involves coupling the CE-QUAL-W2 model and BP-ANN model. The ice, DO, TP, and algae information may be influenced by the runoff season. In the future, different runoff scenarios can be applied into the BP-ANN model such as wet and dry season. In addition, after building the watershed CE-QUAL-W2 model, the BP-ANN modeling method could very useful for predication research over a long time period.

The third perspective is the calibration, improvement, and application of the BP-ANN model. The BP-ANN model is a type of data driven model and it could provide simulation results at a very fast speed. The future development of the BP-ANN model could help governments monitor and regulate the water quality in real-time. According to the previous large databases, a BP-ANN modeling tool may be developed for a specific watershed or lake. The BP-ANN modeling results may easily and quickly predict the variation of water quality in any waterbody.

References

Canada-Ontario Lake Erie Action Plan. (2018). Retrieved from https://www.canada.ca/content/dam/eccc/documents/pdf/great-lakes-protection/dap/action_plan.pdf

Afshar, A., Kazemi, H., & Saadatpour, M. (2011). Particle Swarm Optimization for Automatic Calibration of Large Scale Water Quality Model (CE-QUAL-W2): Application to Karkheh Reservoir, Iran. *Water Resources Management*, *25*(10), 2613–2632. https://doi.org/10.1007/s11269-011-9829-7

Ashley, K., Cordell, D., & Mavinic, D. (2011). A brief history of phosphorus: From the philosopher's stone to nutrient recovery and reuse. *Chemosphere*, *84*(6), 737–746. https://doi.org/10.1016/j.chemosphere.2011.03.001

Auer, M. T., Johnson, N. A., Penn, M. R., & Effler, S. W. (1993). Measurement and verification of rates of sediment phosphorus release for a hypereutrophic urban lake. *Hydrobiologia*, *253*(1–3), 301–309. https://doi.org/10.1007/BF00050750

Becker, R. H., Sultan, M. I., Boyer, G. L., Twiss, M. R., & Konopko, E. (2009). Mapping cyanobacterial blooms in the Great Lakes using MODIS. *Journal of Great Lakes Research*, *35*(3), 447–453. https://doi.org/10.1016/j.jglr.2009.05.007

Bennett, E. M., Carpenter, S. R., & Caraco, N. F. (2001). Human Impact on Erodable Phosphorus and Eutrophication: A Global Perspective. *BioScience*, *51*(3), 227. https://doi.org/10.1641/0006-3568(2001)051[0227:hioepa]2.0.co;2

Berger, C., & Wells, S. (2014). *Updating the CEMA Oil Sands Pit Lake Model*. *August*.

Canadian Weather - Environment Canada. (n.d.). Retrieved from https://weather.gc.ca/canada_e.html

Carmichael, W. W., & Boyer, G. L. (2016). Health impacts from cyanobacteria harmful algae blooms: Implications for the North American Great Lakes. *Harmful Algae*, *54*, 194–212. https://doi.org/10.1016/j.hal.2016.02.002

Carpenter, Caraco, N. F., Correll, D. L., Howarth, R. W., Sharpley, A. N., & Smith, V. H. (1998). Nonpoint pollution of surface waters with phosphorus and nitrogen. In *Ecological Applications* (Vol. 8, Issue 3).

Carpenter, S. R. (2005). Eutrophication of aquatic ecosystems: Bistability and soil phosphorus.

Proceedings of the National Academy of Sciences of the United States of America, *102*(29), 10002–10005. https://doi.org/10.1073/pnas.0503959102

Cole, T. M., & Wells, S. A. (2017). *CE-QUAL-W2 : A Two-Dimensional , Laterally Averaged , Hydrodynamic and Water Quality Model , Version 4.1*. *March*.

Cordell, D., Drangert, J., & White, S. (2009). *The story of phosphorus : Global food security and food for thought*. *19*, 292–305. https://doi.org/10.1016/j.gloenvcha.2008.10.009

Correll, D. L. (1998). The Role of Phosphorus in the Eutrophication of Receiving Waters: A Review. *Journal of Environmental Quality*, *27*(2), 261–266. https://doi.org/10.2134/jeq1998.00472425002700020004x

Demirel, M. C., Venancio, A., & Kahya, E. (2009). Flow forecast by SWAT model and ANN in Pracana basin, Portugal. *Advances in Engineering Software*, *40*(7), 467–473. https://doi.org/10.1016/j.advengsoft.2008.08.002

Elçi, Ş. (2008). Effects of thermal stratification and mixing on reservoir water quality. *Limnology*, *9*(2), 135–142. https://doi.org/10.1007/s10201-008-0240-x

Elser, J., & Bennett, E. (2011). A broken biogeochemical cycle. *Nature*, *478*, 29–31. https://doi.org/978-3-540-87644-1

Fanshawe Reservoir Water Levels | UTRCA: Inspiring A Healthy Environment. (n.d.). Retrieved July 2, 2020, from http://thamesriver.on.ca/water-management/thames-river-levels/fanshaweres-levels-startpage/

Filippelli, G. M. (2002). *The Global Phosphorus Cycle*. https://doi.org/10.2138/rmg.2002.48.10

Filippelli, G. M. (2008). The global phosphorus cycle: Past, present, and future. *Elements*, *4*(2), 89–95. https://doi.org/10.2113/GSELEMENTS.4.2.89

Godsey, S., Kirchner, J., & Clow, D. (2009). Concentration-discharge relashionships reflect chemostatic characteristics of US catchments. *Hydrological Processes*, *23*, 1844–1864. https://doi.org/10.1002/hyp

Gorham, E., & Boyce, F. M. (1989). Influence of Lake Surface Area and Depth Upon Thermal Stratification and the Depth of the Summer Thermocline. *Journal of Great Lakes Research*, *15*(2), 233–245. https://doi.org/10.1016/S0380-1330(89)71479-9

Goyette, J. O., Bennett, E. M., & Maranger, R. (2018). Low buffering capacity and slow recovery of anthropogenic phosphorus pollution in watersheds. *Nature Geoscience*, *11*(12),

921–925. https://doi.org/10.1038/s41561-018-0238-x

Hunsaker, C. T., & Johnson, D. W. (2017). Concentration-discharge relationships in headwater streams of the Sierra Nevada, California. *Water Resources Research*, *53*(9), 7869–7884. https://doi.org/10.1002/2016WR019693

Indicators: Dissolved Oxygen | National Aquatic Resource Surveys | US EPA. (n.d.). Retrieved from https://www.epa.gov/national-aquatic-resource-surveys/indicators-dissolved-oxygen

J.Berger, C., & Wells, S. A. (2008). Modeling the Effects of Macrophytes on Hydrodynamics. *Journal of Environmental Engineering*, *134*(July 2008), 778–788. https://doi.org/10.1061/(ASCE)0733-9372(2008)134

Jarvie, H. P., Sharpley, A. N., Scott, J. T., Haggard, B. E., Bowes, M. J., & Massey, L. B. (2012). Within-river phosphorus retention: Accounting for a missing piece in the watershed phosphorus puzzle. *Environmental Science and Technology*, *46*(24), 13284–13292. https://doi.org/10.1021/es303562y

Jarvie, H. P., Sharpley, A. N., Spears, B., Buda, A. R., May, L., & Kleinman, P. J. A. (2013). Water quality remediation faces unprecedented challenges from "legacy Phosphorus." *Environmental Science and Technology*, *47*(16), 8997–8998. https://doi.org/10.1021/es403160a

Katsev, S., Tsandev, I., L'Heureux, I., & Rancourt, D. G. (2006). Factors controlling long-term phosphorus efflux from lake sediments: Exploratory reactive-transport modeling. *Chemical Geology*, *234*(1–2), 127–147. https://doi.org/10.1016/j.chemgeo.2006.05.001

Kim, L. H., Choi, E., & Stenstrom, M. K. (2003). Sediment characteristics, phosphorus types and phosphorus release rates between river and lake sediments. *Chemosphere*, *50*(1), 53–61. https://doi.org/10.1016/S0045-6535(02)00310-7

Kim, Y., Kim, B., Soyang, R. L., Kim, Y., & Kim, B. (2009). *Lake and Reservoir Management Application of a 2-Dimensional Water Quality Model (CE-QUAL-W2) to the Turbidity Interflow in a Deep Reservoir (Lake Soyang , Korea) Application of a 2-Dimensional Water Quality Model (CE-QUAL-W2) to the Turbidity Inter*. *2381*. https://doi.org/10.1080/07438140609353898

Kirillin, G., & Shatwell, T. (2016). Generalized scaling of seasonal thermal stratification in lakes. *Earth-Science Reviews*, *161*, 179–190.

https://doi.org/10.1016/j.earscirev.2016.08.008

Kişi, Ö. (2008). River flow forecasting and estimation using different artificial neural network techniques. *Hydrology Research*, *39*(1), 27–40. https://doi.org/10.2166/nh.2008.026

Maavara, T., Chen, Q., Van Meter, K., Brown, L. E., Zhang, J., Ni, J., & Zarfl, C. (2020). River dam impacts on biogeochemical cycling. *Nature Reviews Earth & Environment*, *1*(2), 103–116. https://doi.org/10.1038/s43017-019-0019-0

Maavara, T., Parsons, C. T., Ridenour, C., Stojanovic, S., Dürr, H. H., Powley, H. R., & Van Cappellen, P. (2015). Global phosphorus retention by river damming. *Proceedings of the National Academy of Sciences of the United States of America*, *112*(51), 15603–15608. https://doi.org/10.1073/pnas.1511797112

Maier, H. R., & Dandy, G. C. (2000). Neural networks for the prediction and forecasting of water resources variables: A review of modelling issues and applications. *Environmental Modelling and Software*, *15*(1), 101–124. https://doi.org/10.1016/S1364-8152(99)00007-9

Meals, D. W., Dressing, S. A., & Davenport, T. E. (2010). Lag Time in Water Quality Response to Best Management Practices: A Review. *Journal of Environmental Quality*, *39*(1), 85–96. https://doi.org/10.2134/jeq2009.0108

Nowlin, W. H., Davies, J. M., Nordin, R. N., & Mazumder, A. (2004). Effects of water level fluctuation and short-term climate variation on thermal and stratification regimes of a British Columbia reservoir and lake. *Lake and Reservoir Management*, *20*(2), 91–109. https://doi.org/10.1080/07438140409354354

Nürnberg, G. K., & Lazerte, B. (2015). Water Quality Assessment in the Thames River Watershed Draft- Nutrient and Sediment Sources. *Freshwater Research*, *March*, 1–95.

Nürnberg, G. K., & Lazerte, B. D. (2005). *Reservoir Water Quality Treatment Study Includes Water Quality Assessment and Modeling for the reservoirs Fanshawe Lake, Wildwood, and Pittock*. *February 2005*, Freshwater Research: 58. http://thamesriver.on.ca/wp-content/uploads/SurfaceWater/ReservoirWaterQualityTreatmentStudy1-GertrudNurnberg.pdf

Nürnberg, G. K., & Lazerte, B. D. (2006). *Reservoir Water Quality Treatment Study, II Water Quality Assessment and Modeling for the North Thames River watershed, including its major reservoirs and Pittock Lake on the Thames River*. *June 2006*.

Ömer Faruk, D. (2010). A hybrid neural network and ARIMA model for water quality time series prediction. *Engineering Applications of Artificial Intelligence*, *23*(4), 586–594. https://doi.org/10.1016/j.engappai.2009.09.015

Orihel, D. M., Baulch, H. M., Casson, N. J., North, R. L., Parsons, C. T., Seckar, D. C. M., & Venkiteswaran, J. J. (2017). *Internal phosphorus loading in Canadian fresh waters : a critical review and data analysis*. *25*(September), 1–25.

Paytan, A., & McLaughlin, K. (2007). The oceanic phosphorus cycle. *Chemical Reviews*, *107*(2), 563–576. https://doi.org/10.1021/cr0503613

Petticrew, E. L., & Gregor, D. J. (1982). *The Bioavailability of Phosphorus in the Avon River. December*, 46.

Powers, S. M., Bruulsema, T. W., Burt, T. P., Chan, N. I., Elser, J. J., Haygarth, P. M., Howden, N. J. K., Jarvie, H. P., Lyu, Y., Peterson, H. M., Sharpley, A. N., Shen, J., Worrall, F., & Zhang, F. (2016). Long-term accumulation and transport of anthropogenic phosphorus in three river basins. *Nature Geoscience*, *9*(5), 353–356. https://doi.org/10.1038/ngeo2693

Prakash, S., Vandenberg, J. A., & Buchak, E. M. (2015). Sediment Diagenesis Module for CE-QUAL-W2 Part 2: Numerical Formulation. *Environmental Modeling and Assessment*, *20*(3), 249–258. https://doi.org/10.1007/s10666-015-9459-1

Quinlan, C. (2013). *The Thames River , Ontario Prepared by*.

Ruttenberg, K. C. (2014). The Global Phosphorus Cycle. In *Treatise on Geochemistry: Second Edition* (2nd ed., Vol. 10, Issue 2). Elsevier Ltd. https://doi.org/10.1016/B978-0-08-095975-7.00813-5

Schindler, D. W. (1974). *Eutrophication and Recovery in Experimental Lakes : Implications for Lake Management*. *184*(4139), 897–899.

Schindler, D. W., Hecky, R. E., Findlay, D. L., Stainton, M. P., Parker, B. R., Paterson, M. J., Beaty, K. G., Lyng, M., & Kasian, S. E. M. (2008). Eutrophication of lakes cannot be controlled by reducing nitrogen input: Results of a 37-year whole-ecosystem experiment. *Proceedings of the National Academy of Sciences of the United States of America*, *105*(32), 11254–11258. https://doi.org/10.1073/pnas.0805108105

Shabani, A., Zhang, X., & Ell, M. (2017). Modeling Water Quantity and Sulfate Concentrations in the Devils Lake Watershed Using Coupled SWAT and CE-QUAL-W2. *Journal of the*

American Water Resources Association, *53*(4), 748–760. https://doi.org/10.1111/1752-1688.12535

Sharpley, A., Jarvie, H. P., Buda, A., May, L., Spears, B., & Kleinman, P. (2013). Phosphorus Legacy: Overcoming the Effects of Past Management Practices to Mitigate Future Water Quality Impairment. *Journal of Environmental Quality*, *42*(5), 1308–1326. https://doi.org/10.2134/jeq2013.03.0098

Sharpley, A. N., Smith, S. J., Jones, O. R., Berg, W. A., & Coleman, G. A. (1992). The Transport of Bioavailable Phosphorus in Agricultural Runoff. *Journal of Environmental Quality*, *21*(1), 30–35. https://doi.org/10.2134/jeq1992.00472425002100010003x

Singh, K. P., Basant, A., Malik, A., & Jain, G. (2009). Artificial neural network modeling of the river water quality-A case study. *Ecological Modelling*, *220*(6), 888–895. https://doi.org/10.1016/j.ecolmodel.2009.01.004

Smith, V. H., & Schindler, D. W. (2009). Eutrophication science: where do we go from here? *Trends in Ecology and Evolution*, *24*(4), 201–207. https://doi.org/10.1016/j.tree.2008.11.009

Søndergaard, M., Bjerring, R., & Jeppesen, E. (2013). Persistent internal phosphorus loading during summer in shallow eutrophic lakes. *Hydrobiologia*, *710*(1), 95–107. https://doi.org/10.1007/s10750-012-1091-3

Søndergaard, M., Jensen, J. P., & Jeppesen, E. (2003). Role of sediment and internal loading of phosphorus in shallow lakes. *Hydrobiologia*, *506–509*(1), 135–145.

Van Meter, K., Van Cappellen, P., & Basu, N. B. (2018). Legacy nitrogen may prevent achievement of water quality goals in the Gulf of Mexico. *Science*, *360*(6455), 427–430. https://doi.org/10.1126/science.aau8401

Vandenberg, J. A., Prakash, S., & Buchak, E. M. (2015). Sediment Diagenesis Module for CE-QUAL-W2. Part 1: Conceptual Formulation. *Environmental Modeling and Assessment*, *20*(3), 239–247. https://doi.org/10.1007/s10666-014-9428-0

Water Level and Flow - Environment Canada. (n.d.). Retrieved from https://wateroffice.ec.gc.ca/

Watson, S. B., Ridal, J., & Boyer, G. L. (2008). Taste and odour and cyanobacterial toxins: Impairment, prediction, and management in the Great Lakes. *Canadian Journal of Fisheries and Aquatic Sciences*, *65*(8), 1779–1796. https://doi.org/10.1139/F08-084

Yang, K., Yu, Z., Luo, Y., Yang, Y., Zhao, L., & Zhou, X. (2018). Spatial and temporal variations in the relationship between lake water surface temperatures and water quality - A case study of Dianchi Lake. *Science of the Total Environment*, *624*, 859–871. https://doi.org/10.1016/j.scitotenv.2017.12.119

Yuan, Z., Jiang, S., Sheng, H., Liu, X., Hua, H., Liu, X., & Zhang, Y. (2018). Human Perturbation of the Global Phosphorus Cycle: Changes and Consequences. *Environmental Science and Technology*, *52*(5), 2438–2450. https://doi.org/10.1021/acs.est.7b03910

Appendix A Topographical input files

Table A-1. Fanshawe Bathymetry Input File

DLX (Segment Length m)									
356.3	356.3	232.6	206.5	220.9	249.6	206	231	156.2	223.3
205.7	164.2	174.1	229.7	223.7	174.2	238.9	296	160.4	184.8
202.8	120	162	143.3	134.3	179.6	160.4	160.4	174.5	174.3
187	187	174.8	174.8	270.1	270.1	482	124	124	
ELWS (Initial water surface elevation m)									
262.128	262.128	262.128	262.128	262.128	262.128	262.128	262.128	262.128	262.128
262.128	262.128	262.128	262.128	262.128	262.128	262.128	262.128	262.128	262.128
262.128	262.128	262.128	262.128	262.128	262.128	262.128	262.128	262.128	262.128
262.128	262.128	262.128	262.128	262.128	262.128	262.128	262.128	262.128	
PHI0 (Orientation angle in radians)									
0	1.43	0.87	0.35	5.95	5.93	5.84	5.81	5.74	5.61
5.49	5.36	5.36	5.28	5.2	5.13	5.13	5.29	5.76	5.92
6.07	0.01	0.19	0.35	0.52	0.7	0.98	0.98	1.15	1.15
1.15	1.15	1.15	0	0	0.54	0.54	0.45	0	
FRIC (Friction Factor)									
0.035	0.035	0.035	0.035	0.035	0.035	0.035	0.035	0.035	0.035
0.035	0.035	0.035	0.035	0.035	0.035	0.035	0.035	0.035	0.035
0.035	0.035	0.035	0.035	0.035	0.035	0.035	0.035	0.035	0.035
0.035	0.035	0.035	0.035	0.035	0.035	0.035	0.035	0.035	
Layer Height (m)									
0.45	0.45	0.45	0.3	0.3	0.75	0.75	0.8	0.8	0.75
0.75	0.75	0.75	0.75	0.75	0.8	0.8	0.8	0.8	
Width of Segment #1									
0	0	0	0	0	0	0	0	0	0
0	0	0	0	0	0	0	0	0	
Width of Segment #2									
0	241.125	112.375	39.475	22.425	0	0	0	0	0
0	0	0	0	0	0	0	0	0	

Width of Segment #3

0	342.1	176.5	81.275	56.425	0	0	0	0	0
0	0	0	0	0	0	0	0	0	

Width of Segment #4

0	425.55	263.05	150.275	87.225	0	0	0	0	0
0	0	0	0	0	0	0	0	0	

Width of Segment #5

0	419.95	412.65	375	307	240.925	176.775	0	0	0
0	0	0	0	0	0	0	0	0	

Width of Segment #6

0	621.25	584.35	495.15	353.65	249.225	181.875	0	0	0
0	0	0	0	0	0	0	0	0	

Width of Segment #7

0	570.325	519.775	454.65	374.95	318.15	284.25	0	0	0
0	0	0	0	0	0	0	0	0	

Width of Segment #8

0	595.7	559.7	526.2	495.2	454.375	403.725	0	0	0
0	0	0	0	0	0	0	0	0	

Width of Segment #9

0	621.95	607.05	573.925	522.575	456.8	376.6	0	0	0
0	0	0	0	0	0	0	0	0	

Width of Segment #10

0	476.375	391.325	342.3	329.3	307.675	277.425	251.925	231.175	0
0	0	0	0	0	0	0	0	0	

Width of Segment #11

0	432.225	414.275	386.9	350.1	313.95	278.45	247.3	220.5	0
0	0	0	0	0	0	0	0	0	

Width of Segment #12

0	578.35	546.65	510.075	468.625	413.4	344.4	303.675	291.225	0
0	0	0	0	0	0	0	0	0	

Width of Segment #13

0 667.925 638.775 614.25 594.35 569.9 540.9 475.175 372.725 0
0 0 0 0 0 0 0 0 0

Width of Segment #14

0 623.275 617.825 607.175 591.325 569 540.2 435.4 254.6 0
0 0 0 0 0 0 0 0 0

Width of Segment #15

0 549.7 545.1 533.6 515.2 491.425 462.275 376.725 234.775 0
0 0 0 0 0 0 0 0 0

Width of Segment #16

0 473.05 457.15 439.625 420.475 403.125 387.575 344.3 273.3 0
0 0 0 0 0 0 0 0 0

Width of Segment #17

0 434.55 414.65 395.65 377.55 353.075 322.225 276.475 215.825 166.125
127.375 0 0 0 0 0 0 0 0

Width of Segment #18

0 482.275 472.425 461.85 450.55 438.025 424.275 402.275 372.025 288.925
152.975 0 0 0 0 0 0 0 0

Width of Segment #19

0 408.45 407.15 406.5 406.5 406.5 406.5 384.375 340.125 294.075
246.225 180.075 95.625 0 0 0 0 0 0

Width of Segment #20

0 927.35 918.65 904.45 884.75 861.2 833.8 808.125 784.175 701.7
560.7 396.425 208.875 0 0 0 0 0 0

Width of Segment #21

0 804.875 784.625 762.25 737.75 713.2 688.6 624.65 521.35 443.725
391.775 335.425 274.675 0 0 0 0 0 0

Width of Segment #22

0 500.375 483.925 469 455.6 433.65 403.15 359.55 302.85 263.875
242.625 216.75 186.25 0 0 0 0 0 0

Width of Segment #23

0 399.2 370.6 344.375 320.525 301.025 285.875 265.875 241.025 216.7

192.9 165.275 133.825 0 0 0 0 0 0

Width of Segment #24

0 531.2 503.4 477.55 453.65 431.8 412 391.85 371.35 351.4

332 305.75 272.65 219.85 147.35 0 0 0 0

Width of Segment #25

0 488.875 451.625 424.125 406.375 386.85 365.55 348.025 334.275 317.7

298.3 272.05 238.95 189.35 123.25 0 0 0 0

Width of Segment #26

0 396.475 360.025 330.325 307.375 287.525 270.775 249.6 224 202.4

184.8 165.375 144.125 110.9 65.7 0 0 0 0

Width of Segment #27

0 295.1 267.3 242.275 220.025 198.825 178.675 162.325 149.775 133.6

113.8 100.025 92.275 79 60.2 0 0 0 0

Width of Segment #28

0 291.275 265.825 242.65 221.75 203 186.4 170.75 156.05 140.35

123.65 108.275 94.225 80.575 67.325 0 0 0 0

Width of Segment #29

0 314.375 297.125 280.1 263.3 245.15 225.65 206.2 186.8 170.425

157.075 143.05 128.35 114.025 100.075 86.9 74.5 37 0

Width of Segment #30

0 311.825 301.475 282.475 254.825 230.125 208.375 187.525 167.575 150.675

136.825 122.625 108.075 94.2 81 67 52.2 26 0

Width of Segment #31

0 244.7 213.7 187.425 165.875 147.75 133.05 115.575 95.325 77.975

63.525 49.875 37.025 25.575 15.525 10 0 0 0

Width of Segment #32

0 249.5 225.3 204.325 186.575 171.25 158.35 144.5 129.7 116.475

104.825 92.45 79.35 63.65 45.35 30 0 0 0

Width of Segment #33

0 258.275 244.225 229.675 214.625 190.45 157.15 128.625 104.875 75.675

41.025 22.625 20.475 18 15 12 0 0 0

Width of Segment #34

0	0	0	0	0	0	0	0	0	0
0	0	0	0	0	0	0	0	0	

Width of Segment #35

0	0	0	0	0	0	0	0	0	0
0	0	0	0	0	0	0	0	0	

Width of Segment #36

0	126.425	101.475	72.675	40.025	17.775	5.925	0	0	0
0	0	0	0	0	0	0	0	0	

Width of Segment #37

0	144.325	136.775	121.725	99.175	65.925	21.975	0	0	0
0	0	0	0	0	0	0	0	0	

Width of Segment #38

0	186	177.2	167.15	155.85	144.95	134.45	117.7	94.7	73.025
52.675	0	0	0	0	0	0	0	0	

Width of Segment #39

0	0	0	0	0	0	0	0	0	0
0	0	0	0	0	0	0	0	0	

Table A-2. Segment Rotation Angle.

Segments (4 blank segment)	Rotation degree based on CE-QUAL-W2	Rotation angle(radian)
1	0.00	0.00
2	81.93	1.43
3	49.85	0.87
4	20.05	0.35
5	340.91	5.95
6	339.76	5.93
7	334.61	5.84
8	332.89	5.81
9	328.88	5.74
10	321.43	5.61
11	314.55	5.49
12	307.11	5.36
13	307.11	5.36
14	302.52	5.28
15	297.94	5.20
16	293.93	5.13
17	293.93	5.13
18	303.09	5.29
19	330.02	5.76
20	339.19	5.92
21	347.79	6.07
22	0.57	0.01
23	10.89	0.19
24	20.05	0.35
25	29.79	0.52

26	40.11	0.70
27	56.15	0.98
28	56.15	0.98
29	65.89	1.15
30	65.89	1.15
31	65.89	1.15
32	65.89	1.15
33	65.89	1.15
34	0.00	0.00
35	0.00	0.00
36	30.94	0.54
37	30.94	0.54
38	25.78	0.45
39	0.00	0.00

Appendix B Support Materials for Modeling conditions and Parameters

Initial Conditions

To build the water quality and sediment model of Fanshawe Reservoir, geometric data, hydraulic parameters, kinetic parameters, initial conditions, boundary conditions and calibration data of Fanshawe Reservoir were carefully prepared, organized and simulated.

The initial and boundary conditions were based on the organization and calibration of measured data and long year modeling results. There are five different data types, default values (D), literature values (L), calibration values (C), measured data (M) and fitting values (F). Default values were obtained from CE-QUAL-W2 model manual, literature values were collected from literature review, field measurement data, calibration values were modified and verified from modeling results and measurement data, and fitting values were estimated from measured data and previous modeling examples.

Table B-1. Waterbody location and initial conditions.

Parameters Name and Units	Values	Description	Sources
Latitude	43.0326	L	Google Earth Pro
Longitude	81.1028	L	Google Earth Pro
Bottom Elevation (m)	250	L, C	UTRCA
Initial Temperature (°C)	0	C	Calibration Data
Ice Thickness (m)	0.05	D, C	Default and Calibration
Water Type	Fresh	D	Cole and Wells (2017)

Table B-2. Constituent initial concentrations in waterbody.

Species Name (g/m^3)	Value	Description
TDS	241	C
Phosphate (DRP)	0.03	M, C
Algae	0.5	C, F
Dissolved oxygen	13.0	C
DNRP	0.005	C
PRP	0.005	C
PNRP	0.005	C

Table B-3. Initial conditions of sediment diagenesis model.

Parameters Name and Units	Values	Description
Initial sediment bed thickness (m)	0.70	M, C
Initial sediment bed porosity (-)	0.60	M, C
Initial temperature for each region (℃)	20.00	M, C
Initial particulate organic carbon concentration for each region (mgC/l)	951.00	C
Initial particulate organic nitrogen concentration for each region (mgN/l)	152.16	C
Initial particulate organic phosphorus concentration for each region (mgP/l)	60.00	M, C
Initial total phosphate concentration for each region (mgP/l)	0.03	C
Initial ferrous iron concentration for each region (mgFe/l)	1	C
Initial iron oxyhydroxide concentration for each region (mgFe/l)	1	C

Boundary Conditions:

(1) Water flow boundary conditions:

Missing values are removed from the raw data. The current CE-QUAL-W2 model was calibrated from 2018 measured data and validated through 2019 data. The upstream inflows consist of the water inflow from branch 1 and branch 2. The inflow boundary conditions of the main branch were measured by the Government of Canada – Water office at station 02GD015. The Wye Creek inflow (Branch 2) input data were based on the linear regression analysis with previous main branch inflow data. The relationship between two branches is: $Branch\,1\;inflow = 18.093 \times Branch\,2\;inflow + 10.816$. Wye Creek (Branch 2) inflow water was more than 20 times less than main branch, so its influence on the hydrodynamics of the whole waterbody is limited. The dam outflow data in 2018 and 2019 were obtained from UTRCA. Three outlets were built for Fanshawe Reservoir model: The first outlet is the high flow surface outlet at elevation 262m. Another two outlets, which have same elevations, are develop at the bottom outlets (elevation is 252.4m). Different outlet has different outflow input data. During the whole year, the outflow that discharged through top spillway is related to the inflow water amount, and the bottom outflow that discharged through hydropower vane and valve are controlled by UTRCA.

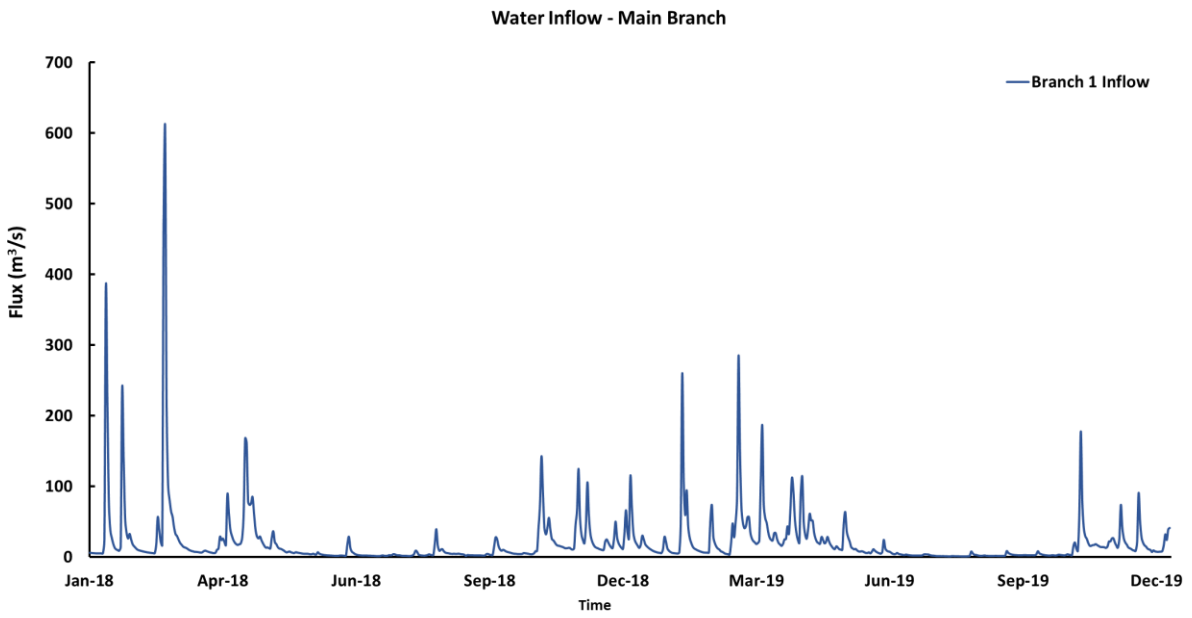

Figure B-1. Upstream water inflow at branch 1 from 2018 to 2019 (Main branch: North Thames River) (Data Sources: ECCC).

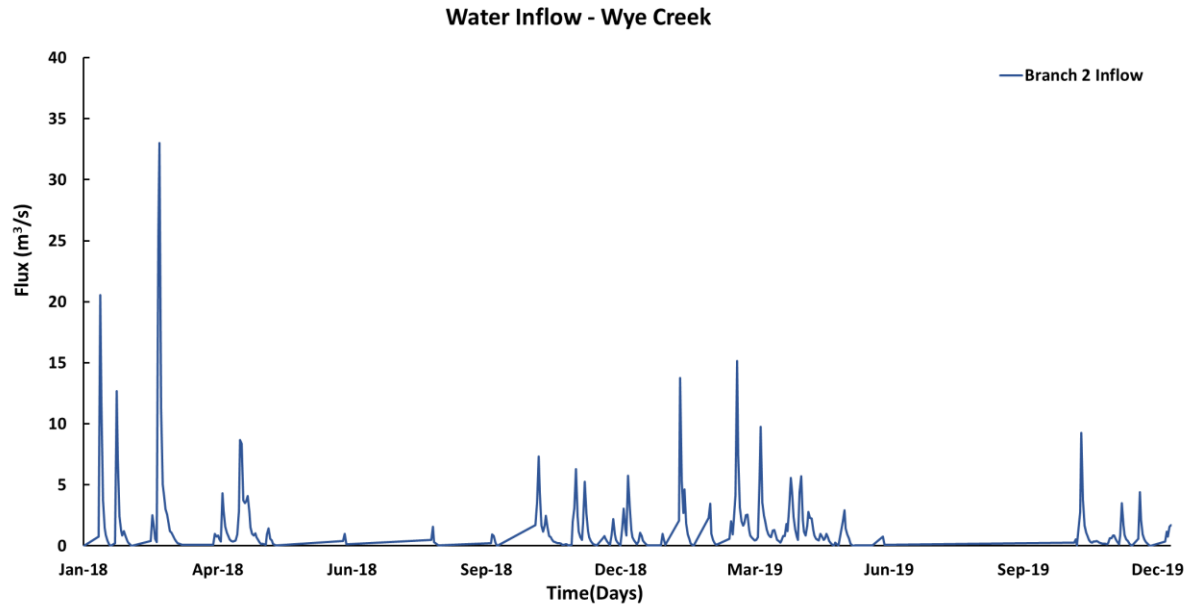

Figure B-2. Upstream water inflow from branch 2 from 2018 to 2019 (Wye Creek).

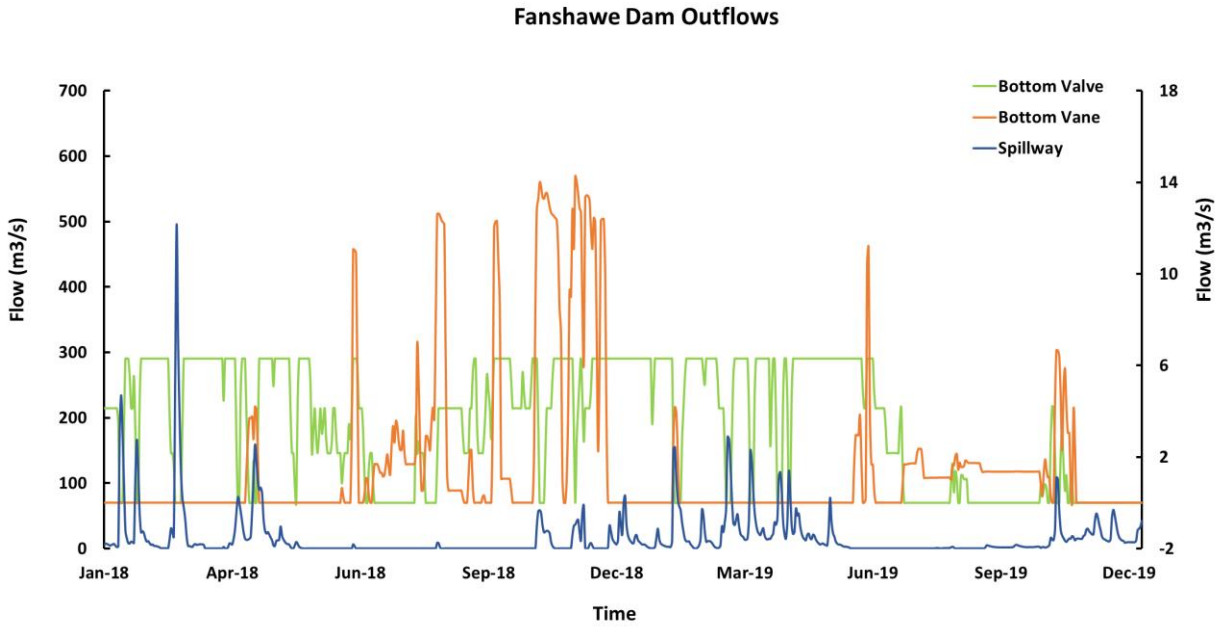

Figure B-3. Downstream water outflow. (Outlets of Fanshawe Dam: Blue line is the top outlet and plotted on the left axis; green and orange lines are bottom outflows and plotted on the right axis) (Data Sources: UTRCA).

To have a better water level for simulating the water quality in the Fanshawe Reservoir, the water inflow was also calibrated by the input distributed tributary inflow files. The hourly distributed tributary inflows were added as water flow boundary conditions for the whole waterbody Distributed tributary inflows was calibrated by a dynamic water balance program in CE-QUAL-W2 model and represented the missing data of water in the waterbody, such as the groundwater discharge and recharge, and the missing water in the input inflow files. This input flow was distributed throughout the whole waterbody and it is weighted and computed by the surface area of whole waterbody (Cole and Wells, 2017).

In addition, precipitation daily input data were obtained and organized from ECCC station in London, Ontario (London CS). The unit of input precipitation data converted from mm/day to m/s for applying in the CE-QUAL-W2 model. According to the input precipitation data and Nürnberg and Lazerte's study (2005, 2015), water comes from precipitation less than 0.1% of the annual branch inflow in Fanshawe Reservoir and the TP loading through precipitation is also insignificant. Therefore, the precipitation has limited effects on the current study.

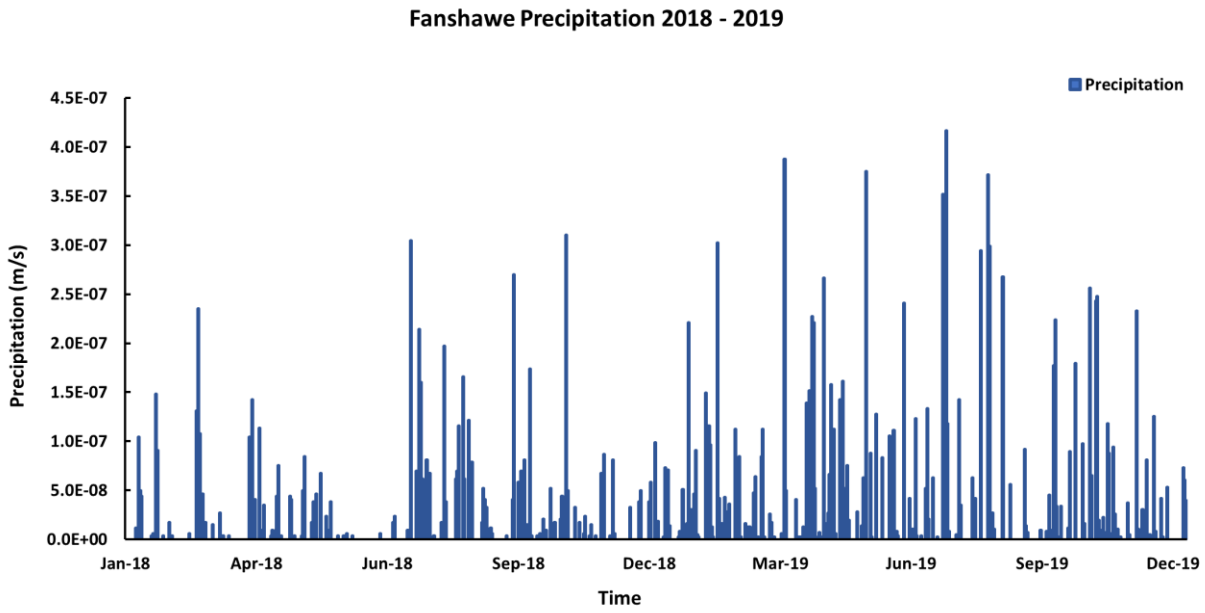

Figure B-4. Daily precipitation input data in Fanshawe Reservoir from 2018 to 2019 (Data sources: ECCC)

(2) Meteorological boundary conditions:

In the CE-QUAL-W2 model, the observation data of air temperature, dewpoint temperature, wind speed, wind direction and cloud cover are necessary for the input meteorological file. The input meteorological data were obtained and organized from Environment and Climate Change Canada – London A meteorological station, which is the nearest meteorological station for the Fanshawe Reservoir(3.2km).

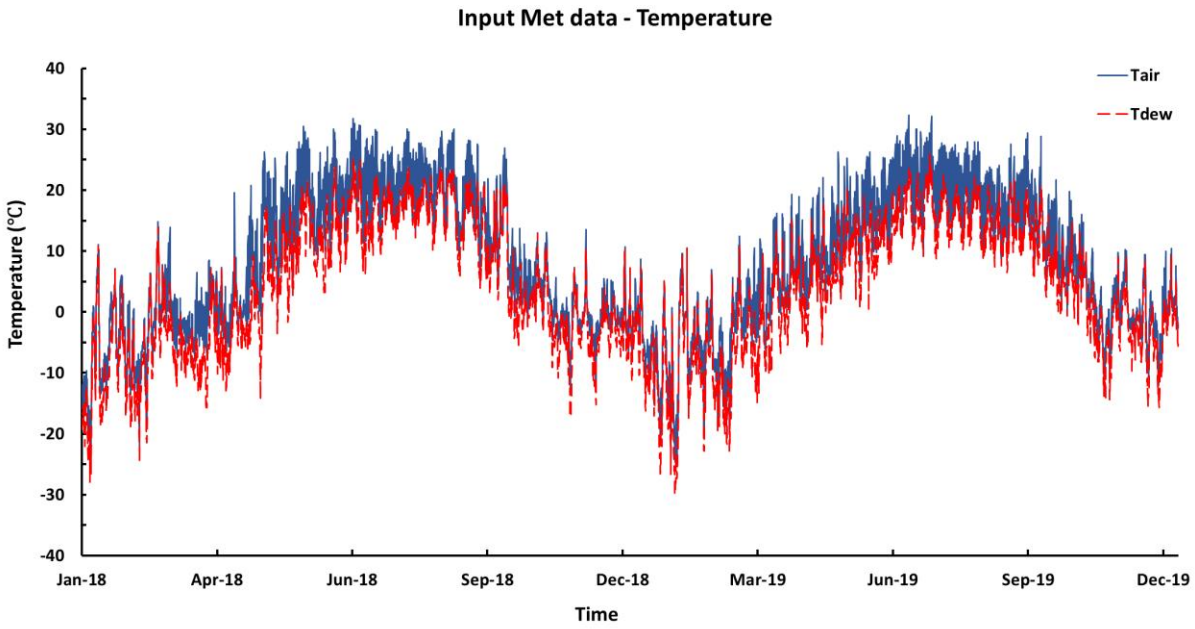

Figure B-5. Input data of air temperature and dewpoint temperature at London A station (Data sources: ECCC).

The wind speed (m/s) and wind direction (radian) hourly data were also applied in the current CE-QUAL-W2 model. Wind speed and wind direction information is significant in the CE-QUAL-W2 model because they have important effects on the water temperature and the extent of water mixing in the Fanshawe Reservoir. In the whole year wind input data, most of the wind come from northwest (NW). The wind speed ranged from 0m/s to 16.1 m/s. 49.9% of the wind speed was between 0m/s – 4m/s, 42.8% of the wind speed was between 4m/s – 8m/s, and only 7.3% of the wind speed was larger than 8m/s.

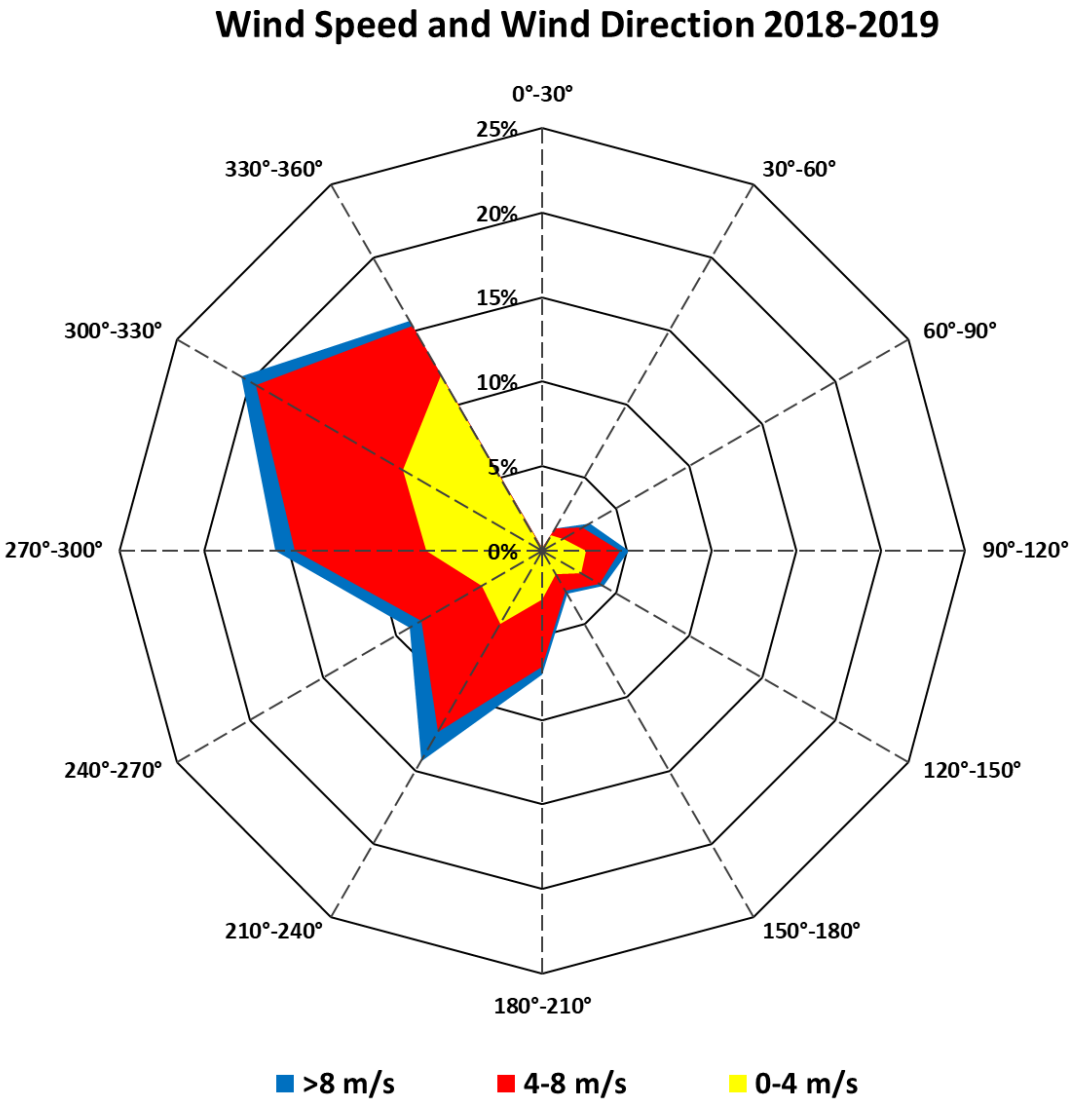

Figure B-6. Wind rose diagram for input wind information in Fanshawe Reservoir (Data sources: ECCC).

The cloud cover input data were also obtained and organized from London A station. The cloud modeling input information is significant for the surface heat exchange calculation. In the weather description file, the cloud part was described as different weather condition. For example, heavy raining, snowing, drizzle etc. In the CE-QUAL-W2 model, number 0 to 10 were used as input cloud data, where 0 is no cloud and 10 is fully cloudy. The following descriptions of the cloud data were obtained based on the instruction from Environment and Climate Change Canada: Clear is 0, mainly clear is 1 to 4, mostly cloudy is 5 to 9, and cloudy is 10. In the model developed for the

study, clear was applied as 0, mainly clear was 2.5, mostly cloudy was 5, cloudy was 10, and other raining and snowing descriptions were assumed to be 6.

Appendix C Parameters

Modeling Parameters and Coefficients

In the current model, most of the hydraulic coefficients, wind coefficient, ice coefficient and time weighting values were given default values that were obtained from literature review and previous modeling calibrations. Some parameters were calibrated through the comparison between simulation results and measured data. For example, the wind sheltering coefficients (WSC) calibrated by water temperature modeling results and the magnitude of wind effects in different reservoir areas.

Fanshawe wind sheltering calibration file

In each row, the value is applied in each segment from right to left. According to the filed environment, segments 1-9 and 34-39 were assumed to have same wind effects. Segment 10-27 were assumed to have same wind effects. In addition, segment 28-33 were assumed to have same wind effect.

Table C-1. Fanshawe wind sheltering calibration file.

DAY	WSC	WSC	WSC	WSC	WSC	WSC	WSC	WSC	WSC
1	1	1	1	1	1	1	1	1	1
	1.2	1.2	1.2	1.2	1.2	1.2	1.2	1.2	1.2
	1.2	1.2	1.2	1.2	1.2	1.2	1.2	1.2	1.2
	0.3	0.3	0.3	0.3	0.3	0.1	1	1	1
	1	1	1						
135	1.1	1.1	1.1	1.1	1.1	1.1	1.1	1.1	1.1
	1.1	1.1	1.1	1.1	1.1	1.1	1.1	1.1	1.1
	1.2	1.2	1.2	1.2	1.2	1.2	1.2	1.2	1.2
	0.15	0.15	0.15	0.15	0.15	0.15	1	1	1
	1	1	1						

163	1	1	1	1	1	1	1	1	1
	1	1	1	1	1	1	1	1	1
	1	1	1	1	1	1	1	1	1
	0.15	0.15	0.15	0.15	0.15	0.15	1	1	1
	1	1	1						
177	0.8	0.8	0.8	0.8	0.8	0.8	0.8	0.8	0.8
	1	1	1	1	1	1	1	1	1
	1	1	1	1	1	1	1	1	1
	0.15	0.15	0.15	0.15	0.15	0.15	1	1	1
	1	1	1						
204	1.2	1.2	1.2	1.2	1.2	1.2	1.2	1.2	1.2
	1.2	1.2	1.2	1.2	1.2	1.2	1.2	1.2	1.2
	1.2	1.2	1.2	1.2	1.2	1.2	1.2	1.2	1.2
	0.05	0.05	0.05	0.05	0.05	0.05	1	1	1
	1	1	1						
236	0.7	0.7	0.7	0.7	0.7	0.7	0.7	0.7	0.7
	1.2	1.2	1.2	1.2	1.2	1.2	1.2	1.2	1.2
	1.2	1.2	1.2	1.2	1.2	1.2	1.2	1.2	1.2
	0.05	0.05	0.05	0.05	0.05	0.05	1	1	1
	1	1	1						
365	1	1	1	1	1	1	1	1	1
	1	1	1	1	1	1	1	1	1

1	1	1	1	1	1	1	1	1
0.2	0.2	0.2	0.2	0.2	0.1	1	1	1
1	1	1						

Table C-2. Coefficient for hydrodynamic modeling. Modified from Cole and Wells, (2017).

Name and Units	Values	Description
Longitudinal eddy viscosity (m^2s^{-1})	1	D
Longitudinal diffusivity viscosity (m^2s^{-1})	1	D
Bottom heat exchange (W m^{-2} °C^{-1})	0.3	D
Interfacial friction factor	0.015	D
Heat lost to sediments	1.0	D
Water surface roughness height (m)	0.001	D
a in the wind speed formulation (Wm^{-2} mm Hg^{-1})	9.2	D
b in the wind speed formulation (Wm^{-2} mm Hg^{-1} (ms^{-1})-^{cfw}	0.46	D
c in the wind speed formulation (cfw) (-)	2.0	D
Albedo of ice	0.25	D
Water-ice heat exchange (W m^{-2} °C^{-1})	10.0	D
Fraction of solar radiation absorbed in the ice surface	0.6	D
Solar radiation extinction coefficient (m^{-1})	0.07	D
Minimum ice thickness (m)	0.03	D
Temperature threshold (°C)	3.0	D
Time-weighting for vertical advection	0.5	D

Due to limitations of current water and sediment measurement data (sediment only has three cores in summertime, no algal information), the default values of coefficients for water quality and sediment modeling were also applied in the current model. The algal growth information and nutrients modeling coefficient were simulated based on the CE-QUAL-W2 default values, which were calibrated through literature review (Cole and Wells, 2017)

Table C-3. Coefficient of water quality and sediment model. Modified from Cole and Wells, (2017).

Parameters Name and Unit	Values	Description
Water extinction coefficients (m^{-1})	0.25	D
Algal extinction (m^{-1}/ (g/m^3))	0.2	D
Algal growth rate (d^{-1})	2	D
Algal dark respiration rate (d^{-1})	0.04	D
Algal excretion rate (d^{-1})	0.04	D
Algal mortality rate (d^{-1})	0.1	D
Algal settling rate (d^{-1})	0.1	D
Algal half-saturation P limited algal growth (g m^{-3})	0.003	D
Fraction of algae in P	0.005	D
Lower temperature for algal growth (℃)	5	D
Lower temperature for maximum algal growth (℃)	25	D
Upper temperature for maximum algal growth (℃)	35	D
Upper temperature for algal growth (℃)	40	D
Sediment bulk density (kg m^{-3})	1376	C
Sediment particle settling velocity (m d^{-1})	5	D
Pore water diffusion coefficient (m^2 d^{-1})	0.0005	D,C
DO threshold for aerobic layer oxidation rates (mgO_2 L^{-1})	2	D
Temperature coefficient for port water diffusion between layers (-)	1.08	D
Mineralization rate for labile POP (d^{-1})	0.035	D
Mineralization rate for refractory POP (d^{-1})	0.035	D
Mineralization rate for inert/slow refractory POP (d^{-1})	0.035	D
Temperature coefficient for labile POP (-)	1.1	D
Temperature coefficient for refractory POP (-)	1.15	D
Temperature coefficient for inert/slow refractory POP (-)	1.17	D
Phosphorus Sorption Coefficient in Aerobic Layer (m^3g^{-1})	0.00005	D
Phosphorus Sorption Coefficient in Anaerobic Layer (m^3 g^{-1})	0.01	D
Particle Mixing Velocity between Aerobic and Anaerobic layer (m d^{-1})	0.05	D
Burial velocity of sediment (m d^{-1})	0.001	D
Half-saturation constant for O2 for FeOOH reduction to Fe (II) (g m^{-3})	0.2	D
Reduction rate, FeOOH to Fe (II) (d^{-1})	4	D

Oxidation rate, Fe (II) to FeOOH (m^3 $d^{-1}g^{-1}$)	1	D
FeOOH settling velocity (m d^{-1})	0.001	D

The modeling parameters in BP-ANN model were used from the default values in MATLAB functions and calibrated through the current CE-QUAL-W2 modeling results.

Table C-4. Parameters for BP-ANN model.

Parameter Name	**Values**	**Descriptions**
Maximum number of epochs to train	5000	C
Minimum performance gradient	1×10^{-7}	D
Performance goal	1×10^{-6}	C